STUDIES ON THE STABILITY OF THIN FILMS IN BUBBLE-PARTICLE ADHESION

by

Jorge Luis Yordan Hernandez

Dissertation submitted to the Faculty of the
Virginia Polytechnic Institute and State University
in partial fulfillment of the requirements for the degree of

DOCTOR OF PHILOSOPHY

in

Mining and Minerals Engineering

APPROVED:

R. H. Yoon, Chairman

M. E. Karmis, Department Head

G. T. Adel

G. H. Luttrell

M. S. Celik

February, 1989

Blacksburg, Virginia

STUDIES ON THE STABILITY OF THIN FILMS IN BUBBLE-PARTICLE ADHESION

by

Jorge Luis Yordan Hernandez

Committee Chairman: Roe-Hoan Yoon
Department of Mining and Minerals Engineering

(ABSTRACT)

The critical rupture thicknesses (H_c) of thin liquid films between air bubbles and solid surfaces have been measured using an optical interferometry technique. The results of the measurements show that H_c increases with the increasing hydrophobicity of a solid and varies inversely with the work of adhesion (W_A) of water on the solid. The relationship between H_c and W_A has, therefore, been used to estimate the values of H_c for the systems in which direct measurement is not possible.

Thermodynamic calculations have been carried out for the bubble-particle adhesion process using the DLVO theory modified to include interaction energies due to structural forces. The calculations required knowledge of the values of various parameters such as, H_c, zeta potentials and Hamaker constants for both bubbles and particles. The results of the calculations conducted on methylated silica and coal show that the thin film ruptures mainly due to the attractive structural force (i.e., hydrophobic interaction). For silica and mica immersed in dodecylamine hydrochloride solutions, the major driving force for film rupture is either the attractive electrostatic force or the hydrophobic interaction force, depending on the pH and the amine concentration.

ACKNOWLEDGMENTS

The author wishes to express his sincere gratitude and appreciation to Dr. Roe-Hoan Yoon for his guidance, support and useful suggestions throughout the course of this investigation. Special thanks are also given to Dr. Gregory Adel, Dr. Gerald Luttrell and for their helpful suggestions, to Dr. Jerzy Mielczarski for his help with the FTIR and to Dr. Janusz Laskowski for the help provided during his visit to Virginia Tech in the summer of 1987.

The author is also grateful for the financial support he received from the U.S. Department of Energy (Contract No. DE-AC22-86PC91221) and the Universidad Catolica Madre y Maestra (UCMM) in The Dominican Republic.

The author also expresses his gratitude to his fellow graduate students in the department for their friendship, particularly

and

Additional gratitude is expressed to

and for their technical assistance.

Finally, the author wishes to express his deep appreciation to his parents for their continued support, and especially to his unconditional and most loyal fans, his wife, , and two daughters, and for their support, understanding and love.

TABLE OF CONTENTS

LIST OF FIGURES

LIST OF TABLES

CHAPTER I.

INTRODUCTION

1.1 General

Froth Flotation is a physico-chemical process commonly used for beneficiating a wide variety of ores, coal, oil shale, tar sand, industrial waste and other biological substances. The importance of this process to the economy of the whole industrial world is enormous; approximately $2x10^9$ tonnes of crushed rock is treated annually by flotation and the proportion of base-metals won by this process is about 95% (Kitchener, 1984).

The majority of minerals required by man occur in complex aggregates (ores) of different minerals of which only one or two will be of value and, consequently, it is necessary to physically remove the undesired minerals prior to metallurgical processing. This involves fine grinding of the ore in order to liberate the various minerals from each other, and then separating them, almost always by flotation.

The success of the flotation process depends on rendering selected minerals in a pulp hydrophobic and hence floatable while keeping or making all the other minerals hydrophilic. In the simplest case, this is achieved by adding a surface-active agent called collector which has selectivity for the mineral to be floated. Normally, however, additional reagents are required to accentuate the differences in the surface chemical properties of the minerals. Depressants are added to

prevent flotation of unwanted minerals and activators are used to promote the adsorption of collector on a given mineral. Air bubbles blown into the pulp and stabilized by the addition of a frother, most commomly a nonionic surfactant, collect the hydrophobic particles and carry them to the froth layer at the top of the slurry, where they concentrate and overflow into a launder. The hydrophylic minerals or tailings are rejected from the bottom of the flotation cell.

From the fundamental viewpoint, it is well recognized that for successful flotation to take place both thermodynamic and kinetic criteria must be satisfied. (Laskowski, 1986).

Thermodynamically, flotation occurs when the contact angle between an air buble and a solid is greater than zero. The contact angle is given by the Young-Dupre equation:

$$\text{Cos}\theta = (\gamma_{sv} - \gamma_{sl}) / \gamma_{lv} \qquad [1.1]$$

where γ_{sl}, γ_{sv}, and γ_{lv} are the surface tensions at the solid/liquid, solid/gas, and the liquid/gas interfaces, respectively. A maximum contact angle is obtained when γ_{sv} is minimum, indicating that the surfactant adsorption must take place at the solid-gas interface to have the maximum effect. The driving force for the process of bubble-particle adhesion is given by

$$\Delta G = \gamma_{sv} - (\gamma_{sl} + \gamma_{lv}) \qquad [1.2]$$

From Equations [1.1] and [1.2], one can obtain

$$\Delta G = \gamma_{lv} (Cos\theta - 1) \qquad [1.3]$$

which suggests that for any finite value of θ, ΔG is negative. In practice, however, a certain minimum contact angle is required for flotation to occur, and this minimum depends on the nature of the mineral and its hydration state.

From a dynamic viewpoint, the events leading to flotation are usually considered to occur in three main stages (Derjaguin and Dukhin, 1961; Laskowski, 1975).

a) Bubble-particle collision with the formation of a thin wetting film, which is sometimes known as disjoining film.
b) Thinning of the disjoining film which separates the colliding bubble and particle, and film rupture at the critical thickness under the influence of interfacial surface forces.
c) Formation of a stable bubble-particle aggregate capable of withstanding considerable disruptive forces operating in the cell.

The first of these stages is controlled by the hydrodynamic conditions in the cell and related solution chemistry that determines the production of bubbles of suitable size while the other two, which deal with the attachment efficiency and contact angle formation, depend mainly on the physico-chemical conditions, particularly the degree of hydrophobicity of the surfaces of the mineral particles.

The second stage, the thinning and rupture of the wetting film, is regarded as the most important stage in flotation (Derjaguin and

Shukakidse, 1961; Rao, 1974; Laskowski, 1974; Finch and Smith, 1979 ; to name a few) because it is a slow process and, therefore, is the rate-determining step. It is well known that on the approach of a bubble to a mineral particle the intervening film undergoes thinning and, usually, after a definite length of time, it becomes unstable and subsequently ruptures under the influence of interfacial surface forces. The lifetime of the disjoining film from the onset of bubble deformation to film rupture is known as the induction time. When this time is greater than the bubble-particle contact time, the particle adhesion would be impossible during the contact even if the contact angle is large.

Most of the early research in froth flotation was concerned with the chemistry and mode of action of the collectors, activators, depressants and frothers, which are added to render the desired mineral hydrophobic. In the last few decades, however, there has been an increasing interest in the physical and chemical aspects of the adhesion process such as the hydrodynamic interaction between bubbles and particles and the thinning and rupture of the disjoining film.

The approach developed by Sutherland (1948) has provided a convenient framework for quantifying the probability of bubble-particle flotation. In his view, the overall probability of particle flotation (P) can be expressed as follows:

$$P = P_a P_c (1-P_d) \qquad [1.4]$$

where P, P_c, P_a and P_d are the probabilities of flotation, collision,

adhesion and detachment, respectively. Analysis of each of the subprocess, makes it possible to gain a better understanding of the factors influencing the overall flotation process. Recently, Al Taweel et al (1986) have pointed out that the probability of particle flotation, P, is a compromise between P_c on the one hand and $P_a(1-P_d)$ on the other so there is a size range where the recovery reaches a maximum. For strongly hydrophobic material such as coal that is floated under mildly turbulent or laminar condition, $P_a(1-P_d)$ will approach unity and the flotation rate will be determined primarily by P_c, which increases with particle size. On the other hand, for relatively large particles of less hydrophobic nature the recovery is expected to be mainly determined by $P_a(1-P_d)$, and is therefore strongly affected by the surface characteristics and decreases with increasing particle size.

Of all the terms in the Equation [1.4], the probability of particle collision (P_c) has been by far the most extensively investigated. Many researchers have derived analytical expressions, and in general P_c is related to particle and bubble sizes, particle and liquid densities, liquid viscosity and relative particle-bubble velocity. The chemical nature of the flotation system exerts no influence on collision probabilities except indirectly through its effect on bubble size and population densities. The most prominent work in this area may be the review paper by Yoon and Luttrell (1988).

Because of the difficulties involved in the quantification of the probability of adhesion in terms of induction time, a different

methodology was developed by Luttrell (1986). In his approach, the probability of particle collection, which is defined as the fraction of particles directly ahead of the bubble that actually become attached, was determined using a numerical simulation technique which allows the trajectory of a particle to be determined as it sweeps past a rising air bubble (Figure 1.1). The trajectory was calculated by taking into account the forces due to i) streamline flow of the fluid, ii) gravity, and iii) hydrodynamic resistance to film thinning (Yoon, et al, 1987). Using an equation of motion which contained all of these forces, the distance of closest approach between a bubble and a particle was determined. The criterion for particle attachment employed was whether or not the particle approaches close enough to the bubble so that the intervening film becomes unstable and ruptures, i.e. if the closest approach distance is smaller than the critical film thickness (H_c), then the particle will become attached. The critical film thickness designated as H_c was assumed to be a measure of the thermodynamics of the system or the hydrophobicity of the mineral to be floated.

Typical results obtained from such an analysis are presented in Figure 1.2 and 1.3 for different simulation conditions. In Figure 1.2, the probability of collection is shown versus H_c for a bubble of 100 microns in diameter and a range of particle diameters (D_p). As shown, the probability of collection (P) increases with H_c, indicating that particle collection increases with increasing hydrophobicity. Figure 1.3, shows the probability of collection as a

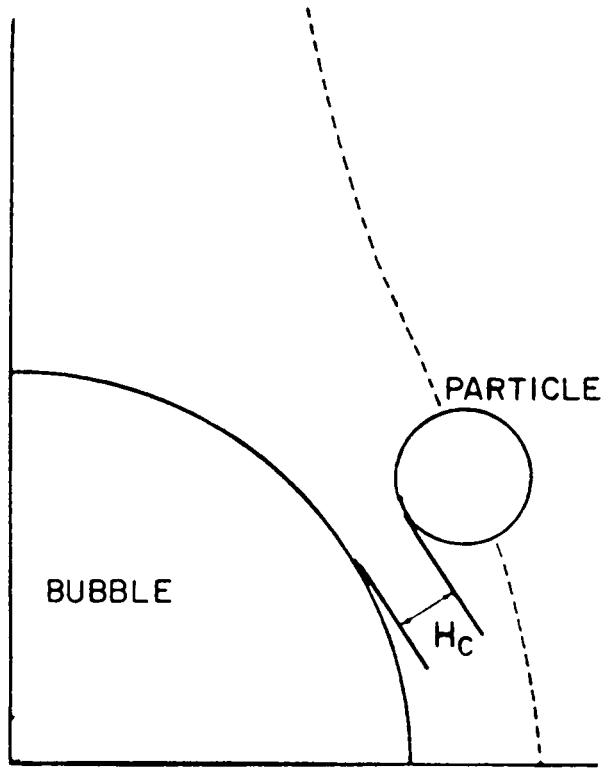

Figure 1.1 Schematic representation of a particle approaching a bubble surface under the influence of streamline flow (Luttrell, 1986)

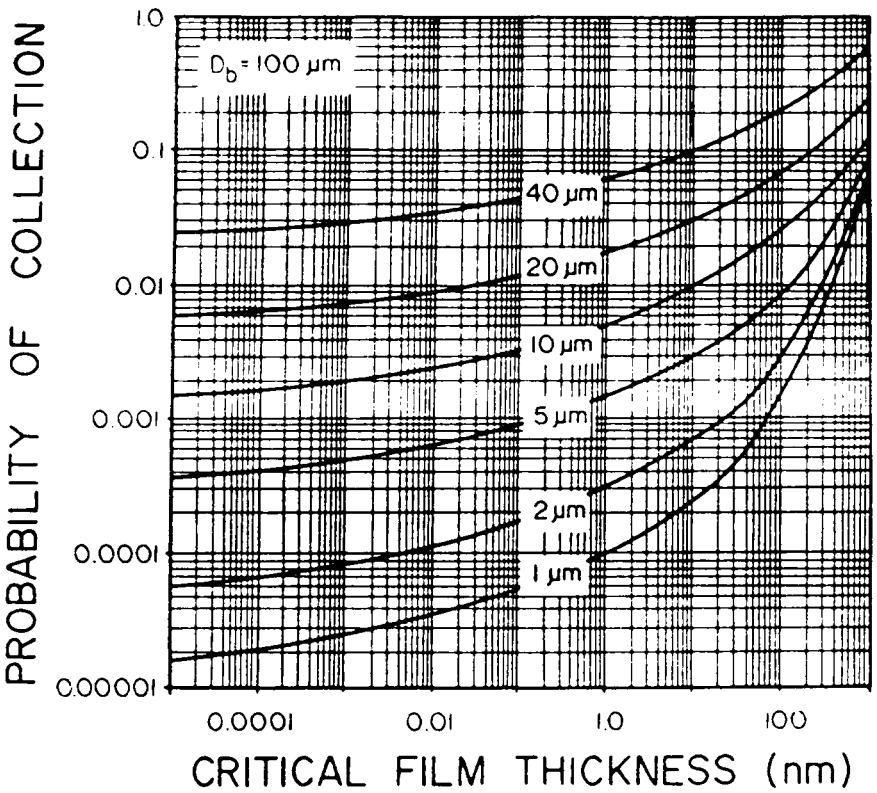

Figure 1.2 Theoretical relationship between the probability of collection (P) and the critical film rupture thickness (H_c) for a bubble diameter of 100 microns and particle diameters of 1, 2, 5, 10, 20 and 40 microns (Luttrell, 1986)

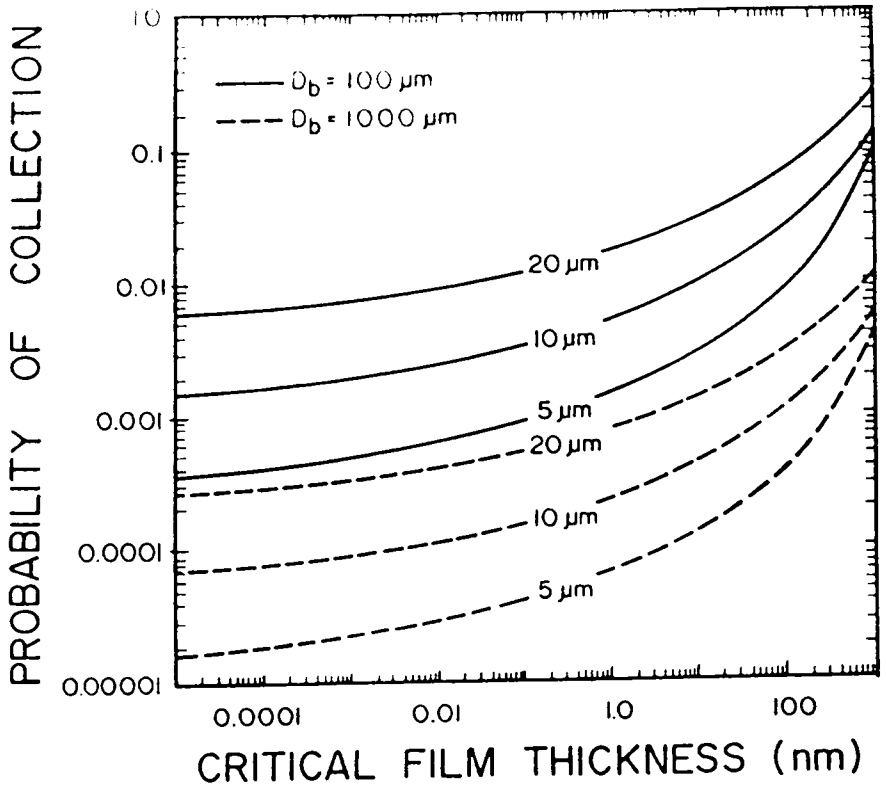

Figure 1.3 Effect of bubble size on the relationship between the probability of collection (P) and critical rupture film thickness (H_c) for particle diameters of 5, 10 and 20 microns (Luttrell, 1986)

function of H_c for three different particle sizes and two different bubbles sizes. For a given particle size and bubble size, P is shown to increase with increasing H_c, which simply means that it is easier to float more hydrophobic particles. The most important feature of this analysis is that P could be predicted should the critical film thickness, bubble size and particle size be known. This improved probability of collection model was successfully developed assuming that the H_c values for coal and quartz are 150 and 5 nm, respectively. It is, therefore, one of the major objectives of the present work to develop a technique to experimentally determine H_c, and to establish a relationship between H_c and particle hydrophobicity.

The utility of this analysis is that once P is known from the first principles, it is possible to calculate the first-order rate constant for bubble-particle attachment (K) using the following expression (Yoon, et al 1987)

$$K = \frac{6PQ}{\pi D_b D_c^2} \qquad [1.5]$$

in which Q is the volumetric gas flow rate, D_b the diameter of the bubble and D_c the cell diameter. Note that K includes physico-chemical parameters through P as well as purely physical ones like D_c and D_b. It has been pointed out by Luttrell (1986) that it is with the determination of K that the fundamental bubble-particle phenomena begin to be related to flotation parameters.

Perhaps the only disadvantage of the methodology discussed above

is that all the chemistry parameters have been lumped into one parameter, H_c. It is well recognized that interfacial surface forces are responsible for the behavior of thin films. Under the influence of repulsive surface forces, thin films remain stable and do not rupture, whereas under attractive surface forces thin films become unstable and rupture at the critical thickness. Derjaguin and co-workers examined the stability of thin films in terms of the disjoining pressure.

The concept of disjoining pressure arose from the classical experiments of Derjaguin and Kussakov (1939) who observed that when an air bubble is pressed against a hydrophilic glass plate immersed in water as schematically shown in Figure 1.4, the intervening liquid slowly thin to leave a uniform equilibrium film of considerable thickness. The film behaves as though there were an excessive pressure, Π , acting normal to the film and opposing further reductions in film thickness (h). This excess pressure, originally termed by Derjaguin as the wedging apart or disjoining pressure, represents the difference between the pressure within the bubble, p^b, and that in the bulk liquid adjacent to the solid surface, p^l, i.e.,

$$\Pi = p^b - p^l \qquad [1.6]$$

A rigorous definition of the disjoining pressure may be obtained using the concepts of equilibrium thermodynamics in the following manner (Yoon, 1988). For the water film in between the air bubble and a solid surface depicted in Figure 1.4, a small reversible change in

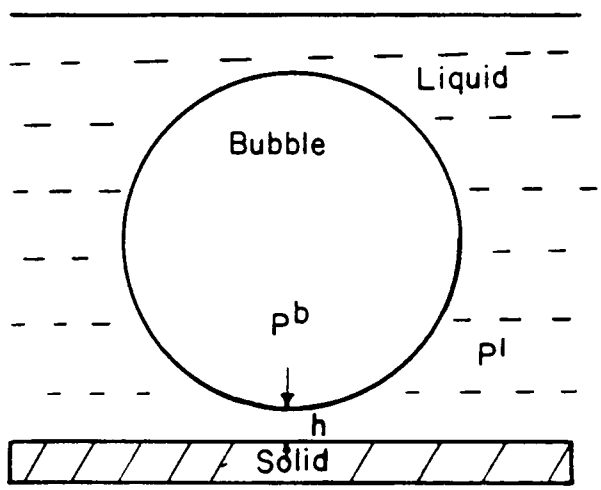

Figure 1.4 Schematic representation of the formation of a wetting film between a bubble and a plate

the internal energy (dU^{σ}) is given by:

$$dU^{\sigma} = TdS^{\sigma} - PdV^{\sigma} + \sum \mu_i dn_i^{\sigma} \qquad [1.7]$$

where T is the absolute temperature, S^{σ} the entropy, μ_i the chemical potential of species i, n the number of moles, P the pressure and V^{σ} the surface volume. Since T, P are constant for all the elements of the interface and S, n and U are extensive variables, it is possible to say that the whole interface will have a volume V obtained by summing the elemental volumes (dV) and thus, its chemical potential will be obtained by adding the dn_i^{σ}. Similarly $S^{\sigma} = \sum dS^{\sigma}$ and $U^{\sigma} = \sum dU^{\sigma}$. Therefore, the internal energy of the interface is:

$$U^{\sigma} = TS^{\sigma} + \sum \mu_i n_i^{\sigma} - PV^{\sigma} \qquad [1.8]$$

Differentiating Equation [1.8]

$$dU^{\sigma} = TdS^{\sigma} + S^{\sigma}dT + \sum \mu_i dn_i^{\sigma} + \sum n_i^{\sigma} d\mu_i - PdV^{\sigma} - V^{\sigma}dP \qquad [1.9]$$

Substration of Equation [1.7] from Equation [1.9] yields:

$$S^{\sigma}dT - V^{\sigma}dP + \sum n_i^{\sigma} d\mu_i = 0 \qquad [1.10]$$

For pure water, the free energy of the system is given by:

$$\sum n_i^{\sigma} d\mu_i = n^{\sigma}_{H_2O} d\mu_{H_2O} \qquad [1.11]$$

At constant temperature, combining Equations [1.11] and [1.10] one obtains:

$$dP = \frac{n^{\sigma}_{H_2O}}{V^{\sigma}} d\mu_{H_2O} \qquad [1.12]$$

Equation [1.12] indicates that a change in the chemical potential of water may cause a change in interface pressure. Note that $V^{\sigma}/n^{\sigma}_{H_2O}$ is the partial molar volume of water, denoted $\overline{V}^{\sigma}$. In Equation [1.12], the absolute value of dP is the disjoining pressure. Consequently, the disjoining pressure is given by:

$$\Pi = \frac{d\mu_{H_2O}}{\overline{V}^{\sigma}} \qquad [1.13]$$

Thus, Π results from the difference in chemical potential of water in the bulk and at the interface.

The chemical potential μ_{H_2O} of water, is not constant across the interface. Rather it is a function of the distance h from the surface. Noting that $n_{H_2O}\mu^{\sigma}_{H_2O} = G^{\sigma}$, one finds that:

$$\Pi(h) = \frac{1}{A}\left[\frac{\partial G^{\sigma}}{\partial h}\right]_{A,T,V} \qquad [1.14]$$

where A is the surface area.

The phenomenon of disjoining pressure is believed to result from three types of interactions: electrical, dispersion and structural. The summation of the three components constitutes the disjoining pressure (Churaev and Derjaguin, 1985):

$$\Pi(h) = \Pi_{electric}(h) + \Pi_{dispersion}(h) + \Pi_{structural}(h) \qquad [1.15]$$

Depending upon the individual contribution of these components, a particle surface may or may not acquire a stable film in an aqueous environment. Air bubbles cannot attach to the particles if the overall disjoining pressure is positive. This leads to the description of hydrophilic solids such as quartz, gypsum, etc as having indefinitely stable aqueous wetting layers attached to their surface. However, if the particle surface is such that it offsets the attractive forces between solid and the liquid, the surface is referred to as hydrophobic and, hence, floatable. The liquid films on such surfaces are characterized by a net negative disjoining pressure.

1.2 Objectives of the proposed work

The primary objectives of this dissertation have been i) to experimentally determine the critical film rupture thickness (H_c) as a function of hydrophobicity of mineral surfaces, ii) to develop a general procedure for estimating H_c from information concerning surface chemistry of minerals and iii) to identify the interfacial forces responsible for the behavior of thin wetting films using the disjoining pressure concept.

The results of the present work are presented in a sequence of independent Chapters. In Chapter 2, the optical interferometry technique of measuring H_c is described, and the results obtained with hydrophilic and hydrophobic silica and mica surfaces are given. In Chapter 3, a general method for estimating H_c from the principles of

surface chemistry has been developed. In Chapter 4, a thermodynamic model has been developed which describes the process of film rupture based on the concept of disjoining pressure. In Chapter 5, the findings of Chapter 1-4 have been applied to study the flotation behavior of fresh and oxidized coal.

Since the topics covered in the five chapters are to some degree independent of each other, they have been written with self-contained formats; each chapter have its own Introduction, Experimental, Results, Discussion and Conclusion sections.

CHAPTER 2

MEASUREMENT OF CRITICAL FILM THICKNESS OF RUPTURE ON FLAT MINERAL SURFACES

2.1 Introduction

As discussed in the previous chapter, bubble-particle attachment in flotation depends on the rupture of the intervening wetting film. The thin film ruptures when the disjoining film is thinned to certain critical thickness. At this critical thickness, the film becomes unstable and spontaneously ruptures to form a finite contact angle. In the present work, the critical rupture thicknesses (H_c) of wetting films on silica and mica specimens have been measured under different experimental conditions. The effects of solution pH, collector concentration and mineral hydrophobicity on H_c have been investigated. The optical micro-interferometric technique developed by Derjaguin and Kussakov (1939) has been employed. The apparatus used is similar in design to that of others (Read and Kitchener, 1969; Blake and Kitchener, 1972). However, in this study, film thicknesses have been measured using an image processing system rather than by photographic means. This approach has increased the speed of data acquisition and has reduced the errors involved in the measurements.

2.2 Literature Review

The bubble-against-plate technique originally introduced by Derjaguin and Kussakov (1939) has been almost exclusively the only

technique used to measure critical rupture thickness. In this technique, a film is obtained by pressing an air bubble in a liquid onto a plate substrate and the interference observed upon reflection of light by the thin film is used for the determination of its thickness. Although initially used to study the properties of equilibrium films existing between air bubbles and clean mineral surfaces by Derjaguin and Kussakov (1939), this technique has been modified to measure the critical thickness of rupture of unstable wetting films. Platikanov (1964) was probably the first investigator that employed this technique to measure H_c. The interference patterns obtained were photographed and their intensity measured with a photomultiplier. Besides measuring H_c, this author studied film thickness as a function of time and using various types of liquids the role of viscosity in the film drainage process was studied.

Blake and Kitchener (1972) also employed interferometry to measure H_c of methylated quartz as a function of electrolyte concentration. The instrument used by these investigators employed a small gas laser as a light source, which enhanced the intensity of the interference patterns. The reported results indicated that depending on the electrolyte concentration, films became unstable at thickness ranging from 60 nm up to 220 nm on a surface of hydrophobic methylated quartz. Changes in the magnitude of repulsive electrostatic forces associated with electrolyte concentration were considered the cause of the observed variations in film thickness. Recently, however Derjaguin (1987) pointed out that these films probably ruptured under

the influence of hydrophobic interaction.

Schulze (1975) measured critical rupture thickness of wetting films of aqueous solutions of dodecylamine hydrochloride on quartz as a function of DAH concentration. At a given DAH concentration and pH, the reported values of H_c range from 50 nm up to approximately 140 nm depending on the amount of electrolyte used. Attractive electrostatic forces were considered to be responsible for film rupture. H_c was also shown to be pH dependent.

Using a modified data acquisition system, Aronson and Princen (1978) studied the effect of the length of the hydrocarbon chain in a cationic surfactant on the critical rupture thickness. In their instrument, the reflectance from the liquid films was measured in-situ by means of a small fiber optics probe which was appropriately inserted in the eyepiece of the microscope. The probe was coupled to a photomultiplier and photometer. With this device, the authors were able to simultaneously view the microscopic film and to determine its reflectance photometrically. The values of H_c obtained ranged between 80 nm and 175 nm. One of the interesting findings of this research was that the critical surfactant concentration required to turn a stable thin film into an unstable one decreases with increasing surfactant chain length. Furthermore, good correlation between H_c and contact angles were reported.

2.3 Experimental

2.3.1 Equipment and Materials

a) Bubble against the Plate Apparatus

Figure 2.1 shows the bubble-against-plate apparatus used for the measurement of H_c. It consists of a capillary tube (a) with an inverted cup at the bottom which holds a 4 mm. air bubble in place; a capillary tube that can be lowered or raised by the precision micrometer (b); and an all glass cylindrical cell (c) which contains the optically smooth solid sample (d) and the solution under investigation (e). The whole unit is placed on a Zeiss inverted microscope (f) used to observe the concentric circular interference patterns that results when monochromatic light passes through the thin wetting film between the approaching bubble and the plate. The interference pattern images obtained are analyzed on-line with a computerized optical Image Processing System (Zeiss Kontron IPS). The details of the Image Processing System have been described by Choi (1986). The apparatus and the microscope are mounted on a stone table to avoid problems associated with vibration.

b) Samples

Optically-smooth fused silica plates (0.5" in diameter and 1/16" thick) were obtained from Heraues-Amersil, NJ, and used in some of the experiments. These plates were sufficiently smooth as received and no further polishing was required. Since cleanliness of the specimen's surface was of vital importance for this study, the plates

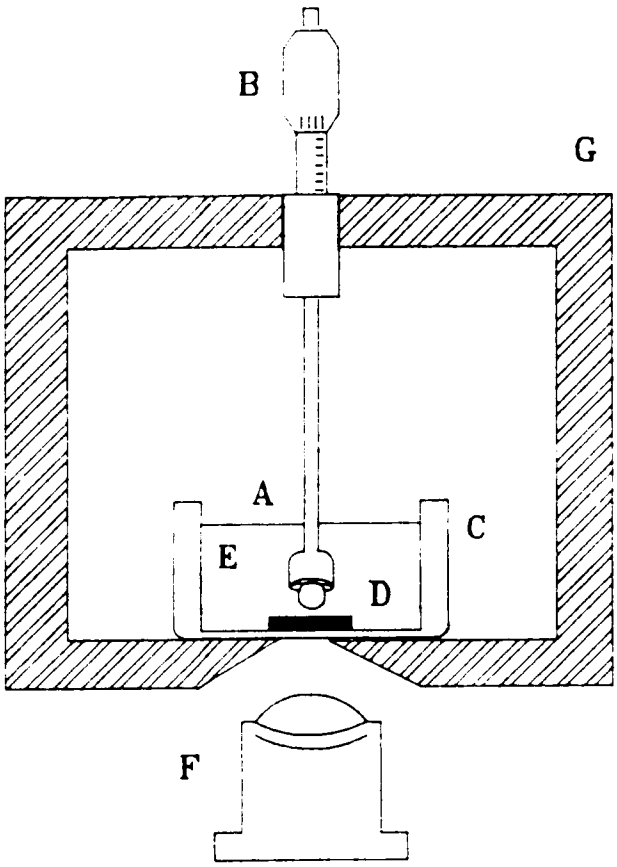

Figure 2.1 Schematic representation of the bubble-against-Plate apparatus employed in the critical fi'm rupture thickness (H_c) measurements

were thoroughly clean before any measurement following the procedure described by Laskowski and Kitchener (1969) which involved cleaning with chromic acid and repeated washing with double distilled water. After cleaning, the plates were stored under pure water in a c an pyrex beaker. Prior to an experiment, the plates were subjected to ultrasonic cleaning to dislodge particles of dust and dried with a jet of ultrapure nitrogen. With the clean fused silica plates, three different set of experiments were performed. In the first set of experiments, the plates were used immediately after drying. In the second set, the clean plates were exposed to aqueous solutions of different concentrations of dodecylamine hydrochloride (DAH). In the final series, the silica surfaces were methylated with solutions of various concentrations of trimethylchlorosilane (TMCS) in benzene following the procedure employed by Laskowski and Kitchener (1969).

The mica plates used for H_c measurements were prepared from large plates of muscovite mica from South Dakota, as obtained from the Ward's mineral specimens collection. A molecularly smooth mica surface was obtained in a perfectly clean state by splitting mica sheets along the planes of cleavage. Two different set of experiments were conducted. Pure mica was used in one series of tests, and in another, its surface was modified by adsorbing various amounts of DAH.

c) Reagents

Research grade dodecylamine hydrochloride and sodium dodecyl sulfate supplied by Eastman Kodak Company were the surfactants used in the present work. These reagents were used as received without

further purification. Reagent grade hydrochloric acid and sodium hydroxide solutions were used for pH control. Double distilled water, prepared in an all glass still, was used in all of the experiments. Research grade KCl was the electrolyte used. Research grade benzene and trimethylchlorosilane, $(CH_3)_3SiCl$, supplied by Kodak were used in the methylation of the fused silica plates. Chromic acid and a mixture of potassium hydroxide, water and ethanol were used to clean all the glassware. Ultra-pure nitrogen (99.999%) from AIRCO Industrial Gas Company was used to dry the samples.

2.3.2 Procedure

The mineral plate under investigation was placed at the bottom of the all-glass optical cell containing 25 ml of $5x10^{-4}$ M KCl solution. After pH adjustment, the plate was allowed to equilibrate for 15-30 minutes. The cell was then placed on the stage of the microscope for measurement.

Inside the cell, an air bubble approximately 4 mm in diameter was formed at the tip of a glass capillary tube using a microliter syringe, and left to stand for one minute to reach equilibrium. The bubble which was held in place by the inverted cup was lowered slowly and pressed lightly against the solid plate using a precision micrometer. The film formed between the plate and bubble was observed from beneath with the Zeiss microscope. The passing of monochromatic light (wavelength (λ) 600 or 533 nm) through the film resulted in the formation of an interference pattern (Newton's rings). The appearance

of a typical interference pattern is illustrated in Fig 2.2.

In a typical test, the bubble was lowered to the solid plate until the first interference pattern was formed. This image was immediately digitized with the image processing system. The film was allowed to equilibrate for a period of one to two minutes. If during that time rupture did not occur, the film was considered stable and the test was therefore continued, reducing the separation distance between the bubble and the plate incrementally. This procedure was continued until rupture, and the last digitized image was used to determine H_c. A typical sequence of the images digitized during a test is presented in figure 2.3.

The thickness (H) of the film was obtained from the reflectance (R) of the interference pattern. The relationship between R and H is given by the Raleigh equation:

$$R = \frac{A^2 + B^2 + 2AB\cos\theta}{1 + A^2B^2 + 2AB\cos\theta} \qquad [2.1]$$

where

$$A = (n_1 - n_0)/(n_1 + n_0) \qquad [2.2]$$

$$B = (n_0 - n_2)/(n_0 + n_2) \qquad [2.3]$$

$$\theta = (4\pi n_0 H)/\lambda \qquad [2.4]$$

in which λ is the wavelength of the incident light and n_0, n_1 and n_2 are the respective refractive indices of the solution, solid and gas

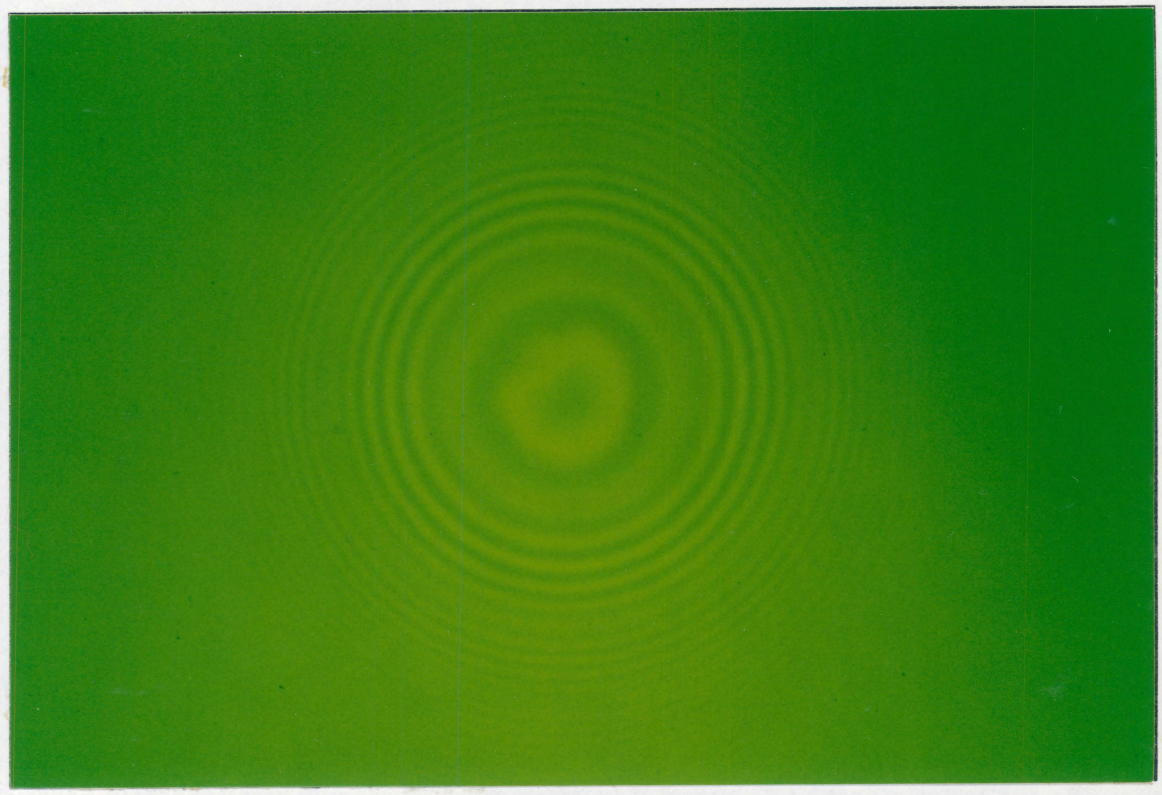

Figure 2.2 Photograph of a typical interference pattern as seen through the microscope viewer

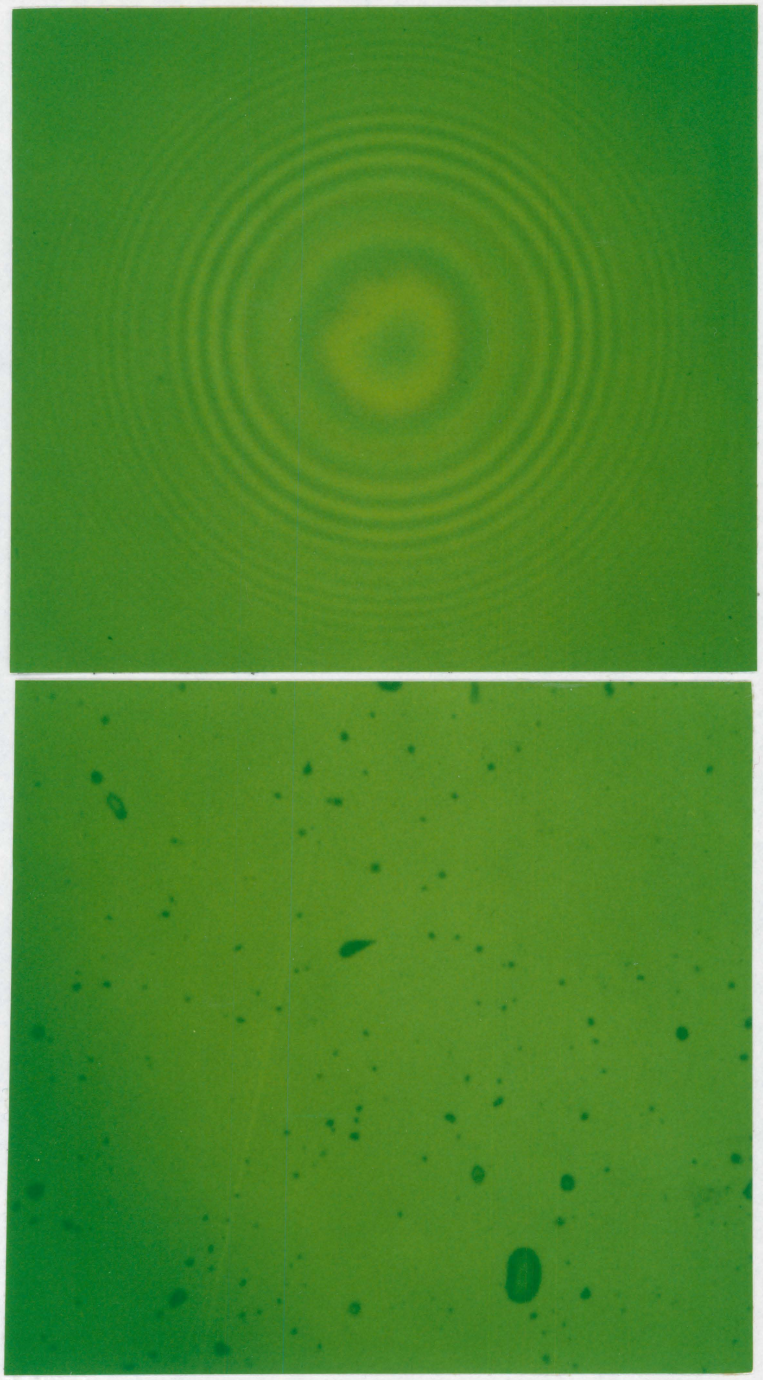

Figure 2.3 Photographs of a typical sequence of digitised interfacence patterns. a) initial pattern. b)after rupture and attachment

phases. Table 2.1 shows the refractive indices of the phases involved in this study. Plots of reflectance versus film thickness for the two systems under investigation, namely, fused silica-water-air and mica-water-air, calculated with the above equations are presented in Figs. 2.4 and 2.5 respectively. Note that two sets of curves were produced for each system using two different wavelengths of monochromatic light, i.e., 600 and 533 nm.

Figure 2.6 shows a typical IPS output. Since the IPS can only measure the grey level intensity of a digitized image, the reflectance (R) of the interference pattern cannot be measured directly. Therefore, a calibration procedure was necessary. This was accomplished by measuring the gray level intensity of calibration standards of known reflectance (R). The calibration curve obtained is shown in Fig. 2.7. It provides a means of obtaining the reflectance of the interference pattern by simply measuring gray level intensity. Reproducibility of the measurements was usually better than ± 2%. All of the tests were conducted at ambient temperature. The H_c values reported in this investigation are the average of at least five independent measurements.

2.4 Results

2.4.1 Thin films on hydrophilic silica and mica plates

Table 2.2 shows the results of tests performed on hydrophilic fused silica and mica plates using various types of aqueous solutions. Note that, in pure water and electrolyte solutions, the film remains

TABLE 2.1

Values of the Refractive Indices of the Interfaces Involved in the Critical Rupture Thickness (H_c) experiments

Interface	n
Fused Silica	1.448 (1)
Mica	1.600 (2)
Water	1.331 (1)
Air	1.000 (1)

(1) Blake and Kitchener (1972)
(2) Pashley and Israelachvili (1981)

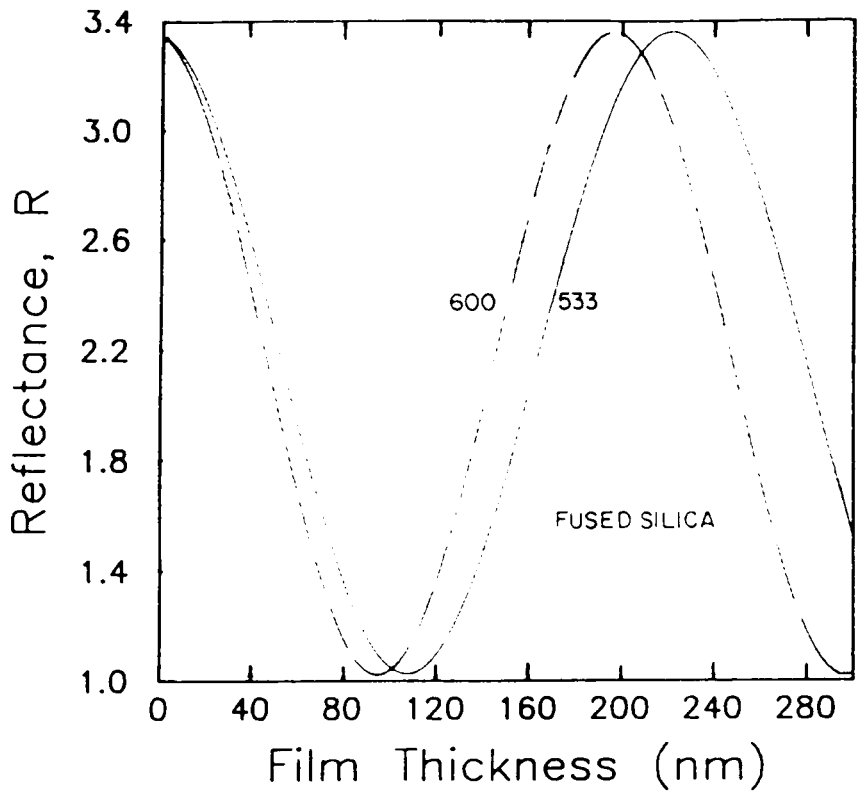

Figure 2.4 Theoretical relationship between reflectance (R) and film thickness (H) for the fused silica-water-air system and monochromatic light with λ = 600 and 533 nm

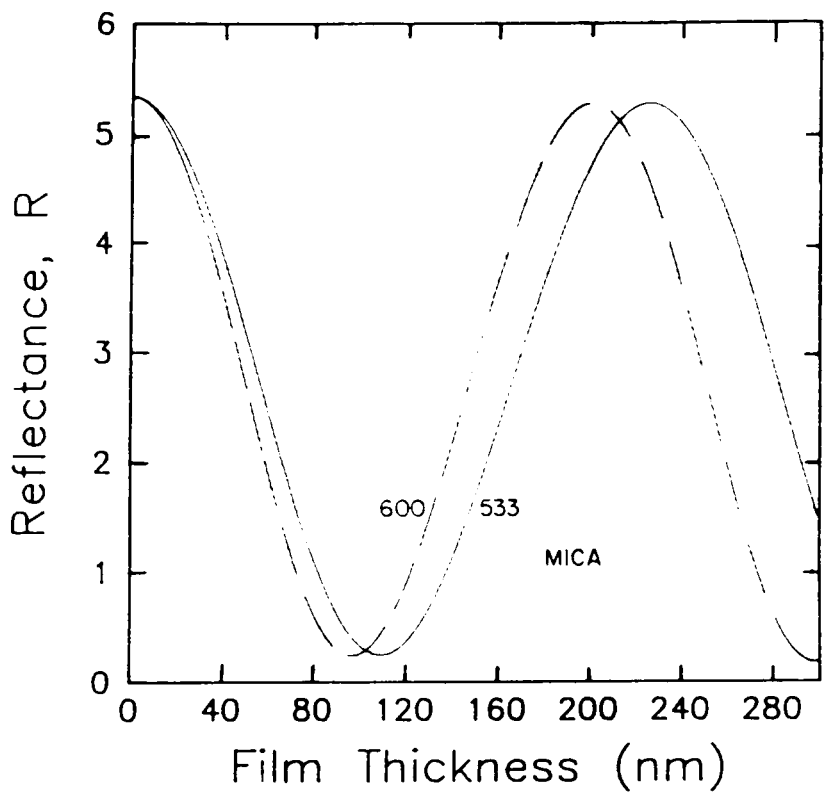

Figure 2.5 Theoretical relationship between reflectance (R) and film thickness (H) for the mica-water-air system and monochromatic light with λ = 600 and 533 nm

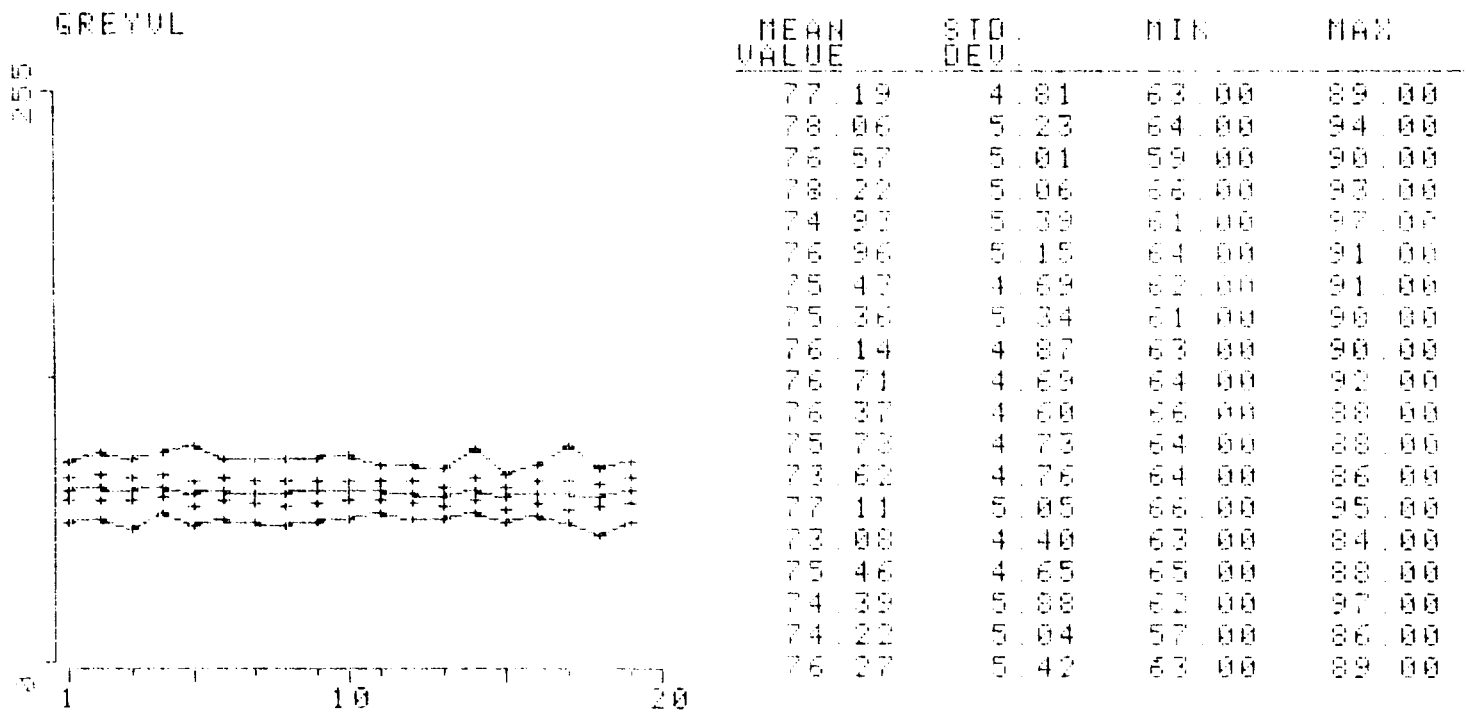

Figure 2.6 Typical output of the Image Processing System (IPS)

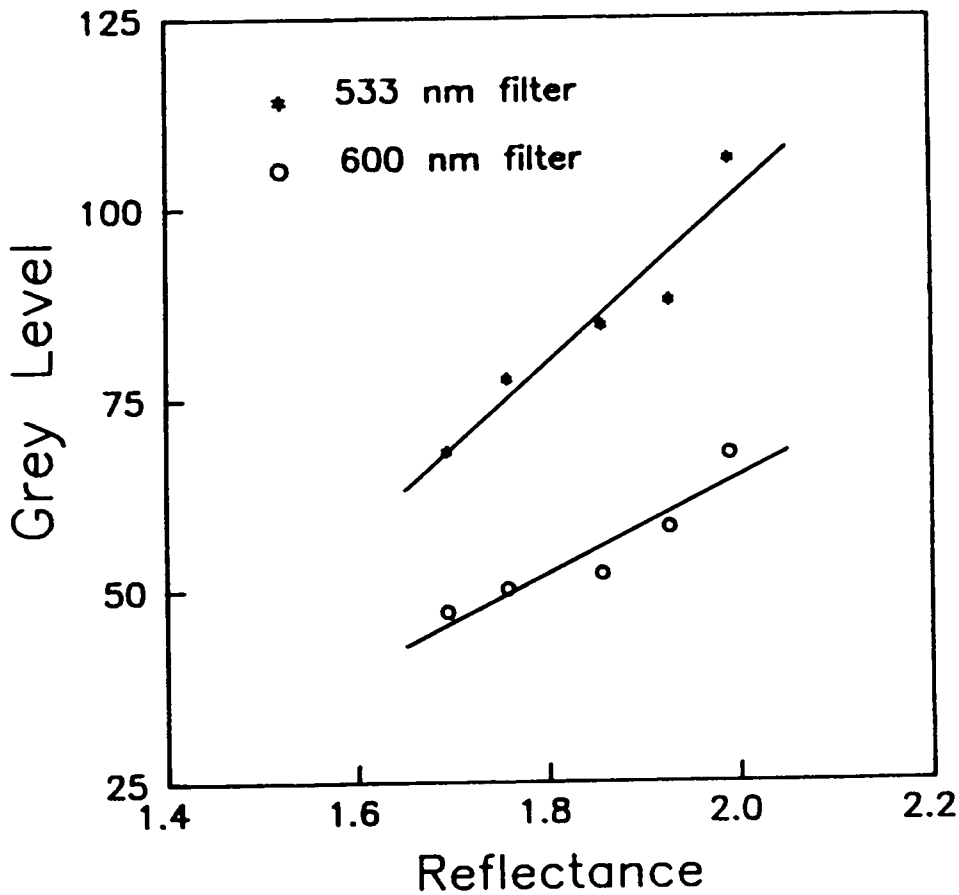

Figure 2.7 Reflectance versus grey level for monochromatic light with λ = 600 and 533 nm

TABLE 2.2

H_c measurements on hydrophilic mineral surfaces

MINERAL SURFACE	LIQUID	RESULTS
Fused Silica	Water	No rupture
Fused Silica	$1x10^{-3}$ M KCl	No rupture
Fused Silica	$1x10^{-4}$ M Sodium Dodecyl Sulfate	No rupture
Mica Plate	Water	No rupture

stable and does not rupture. This condition prevents flotation of the mineral by preventing the attachment of air bubbles to the mineral surfaces. Similar findings have been reported by others (Derjaguin and Kussakov, 1939; Read and Kitchener, 1969). These scientists attributed film stability to hydration of the mineral surface and the electrostatic energy barrier between the mineral and bubble. It is interesting to note that the film remains stable not only in pure aqueous solution but also in solutions of sodium dodecyl sulfate (SDS). This indicates that SDS molecules do not adsorb at the solid/liquid interface, and, as a result, the fused silica plate remains hydrophilic.

2.4.2 Thin films on methylated fused silica plates

Many investigators have used methylated silica as a model hydrophobic mineral in flotation research (Laskowski and Kitchener, 1969; Laskowski and Iskra, 1970 ; Blake and Kitchener, 1972; Blake and Ralston, 1985; Crawford and Ralston, 1988; to name a few). It has been shown that the methylation procedure is very convenient. It renders the silica surface hydrophobic in the absence of a water-soluble surfactant. This, of course, reduces the number of variables in the system and makes it simpler for a researcher to elucidate the mechanisms responsible for flotation. Furthermore, it allows the preparation of silica surfaces with different degrees of hydrophobicity by simply controlling the concentration of trimethylchlorosilane (TMCS) solution used. The mechanism of the methylation reaction has been discussed by Laskowski and Kitchener (1969).

a) **Effect of trimethylchlorosilane concentration**

Figure 2.8 shows the results of the H_c measurements performed with methylated fused silica plates. The tests were conducted in pure water of pH 6.5±0.2 as a function of trimethylchlorosilane concentration. As shown, for each of the four plates investigated, the thin film between the plate and bubble ruptures at the critical distance. This is attributed to the presence of hydrocarbon molecules (trimethylsilyl groups) anchored to the silica surface which reduces the cohesive energy of water molecules in the film and makes it easier for the bubble to displace the wetting film from the plate. Note, however, that H_c is not constant. It increases from 75 nm to 145 nm as the concentration of the methylating reagent increases from 1% to 10%. This, of course, indicates that the higher the concentration of hydrophobic species at the silica surface, the more unstable the film becomes. It is interesting to point out that Laskowski and Kitchener (1969) reported that the contact angle of methylated silica specimens increased with increasing organosilane concentration. Since contact angle is a measure of hydrophobicity, perhaps, H_c is too. All of the above results agree favorably with those reported by Blake and Kitchener (1969).

b) **Effect of pH**

The pH is an important variable in flotation. In this work, its effect on H_c has been studied using methylated fused silica plates. The results obtained are presented in Figure 2.9. Two different set of tests were conducted. In the first test, a very hydrophobic plate

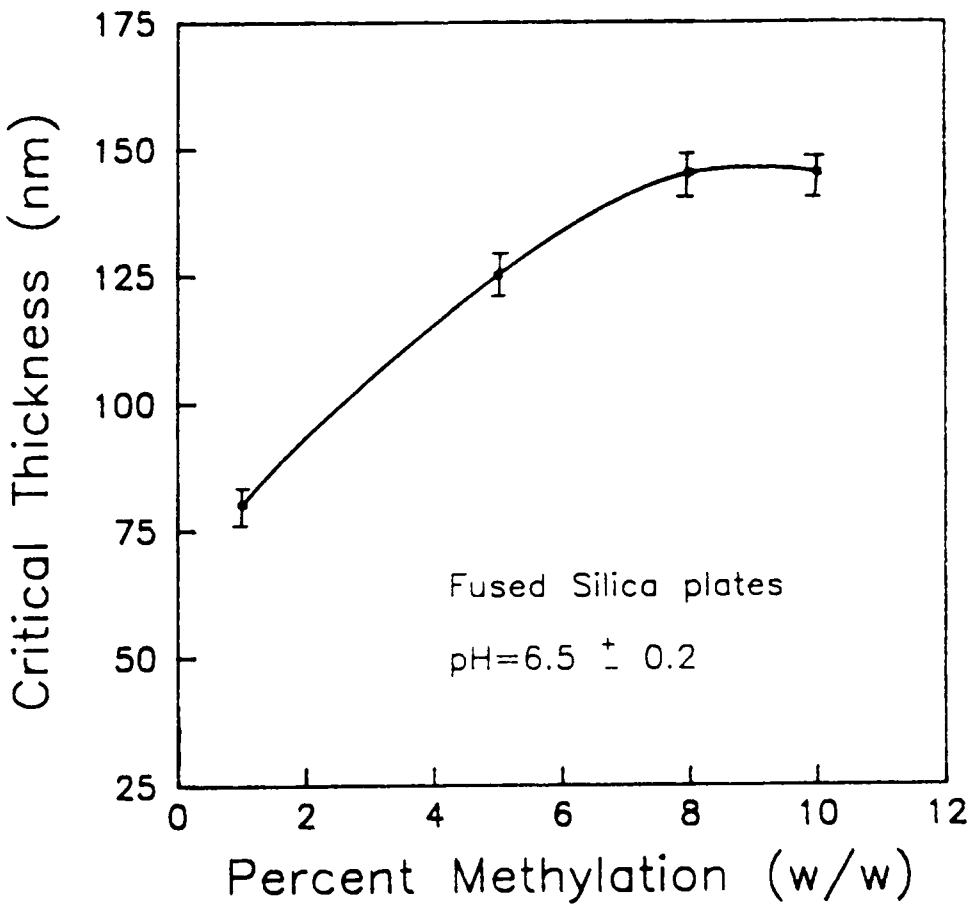

Figure 2.8 Effect of concentration of TCMS on the critical rupture thickness (H_c) of fused silica plates at pH 6.5

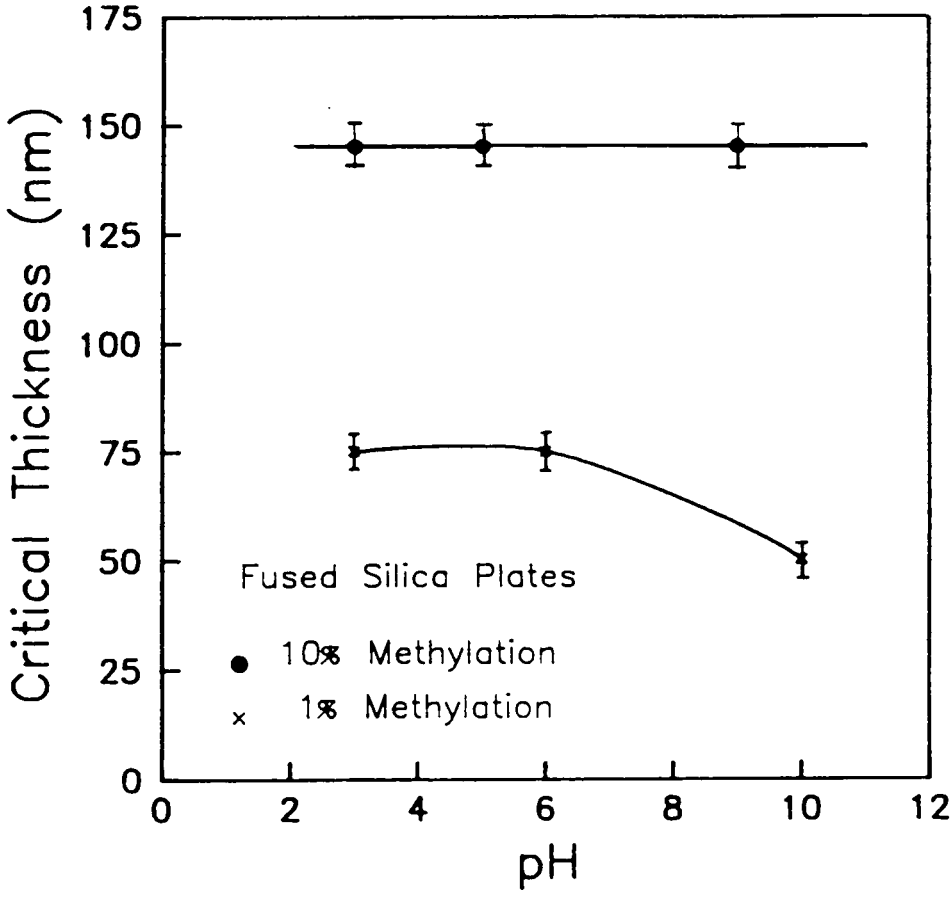

Figure 2.9 Effect of pH on the critical rupture thickness (H_c) of fused silica plates treated with 1 and 10% TMCS.

(10% methylation) was used. As shown, H_c was not affected by pH in this case. It remained constant at about 145 nm for the pH range studied. In contrast, when a less hydrophobic plate (1% methylation) was used, H_c decreased significantly with increasing pH. It is interesting to note that Laskowski and Kitchener (1969) observed a decrease in the contact angle of weakly methylated silica plates at high pH. This seems to corroborate that there seems to exist a relationship between H_c and the contact angle.

2.4.3 Thin films on fused silica-DAH system

Dodecylamine hydrochloride is a commonly used surfactant in the flotation of silica. It is well recognized that, depending on concentration and solution pH, amminium ions adsorb on the silica surface and render it hydrophobic. While numerous studies have been devoted to different aspects of the surface chemistry of the DAH-silica system, the thin film rupture process has not received the attention that it deserves. Only few investigators (Schulze,1974; Aronson and Princen, 1978) have reported H_c measurements. In this work, H_c has been determined as a function of DAH concentration and solution pH.

a) Effect of DAH concentration

Figure 2.10 shows the results of H_c measurements conducted as a function of dodecylamine hydrochloride (DAH) concentration at pH 6.5 ± 0.2. Note that, depending on DAH concentration, the film does or does not rupture. More importantly, however, Figure 2.10 shows that

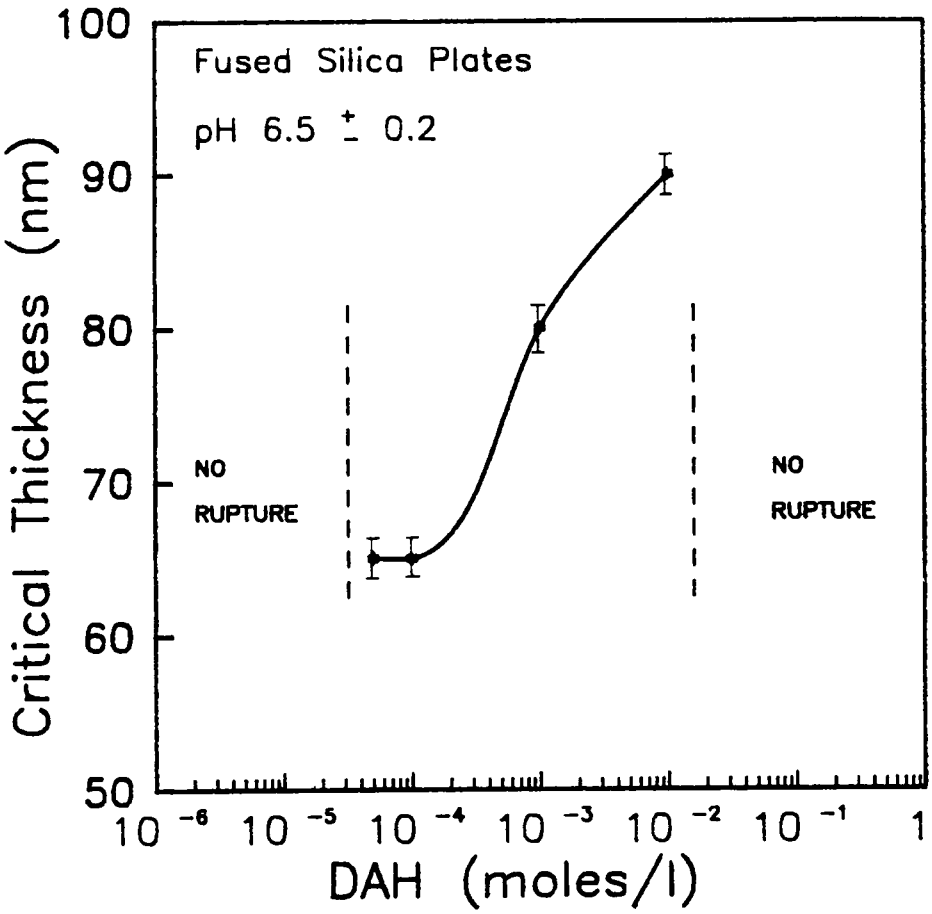

Figure 2.10 Effect of dodecylamine hydrochloride concentration on the critical rupture thickness (H_c) of fused silica plates at pH 6.5

there appears to be two critical concentrations that characterize film stability. These are marked in the figure with dashed lines. In very dilute DAH solutions, i.e., less than $5x10^{-5}$ moles/l, the thin film does not rupture; it remains stable and thus prevents the formation of a finite contact angle. However, this initially stable film becomes unstable when the DAH concentration exceeds 10^{-5} Moles/l. At this critical concentration, rupture begins to occur spontaneously. In the region of film instability, H_c increases with increasing DAH concentration. This finding can be attributed to increasing adsorption density at the silica surface with increasing collector concentration (de Bruyn, 1955; Fuerstenau, 1957), which renders the silica plate increasingly hydrophobic. The film remains unstable until the DAH concentration reaches the upper critical concentration at about 10^{-2} moles/l. Beyond this concentration, the film becomes stable once again and does not rupture. Considering that the CMC of DAH is $1.3x10^{-2}$ moles/l (Phillips, 1955), adsorption of micelles may be considered responsible for the stability of the wetting film. It is possible also that at such a high concentration, the formation of a bimolecular layer of adsorbed collector species could take place. The net effect on the film's stability, however, would be the same.

b) Effect of pH

Table 2.3 shows the results of the H_c measurements performed with the fused silica-DAH system conducted as a function of pH. The experiments were carried out using $5x10^{-4}$ moles/l of DAH. As shown, in the pH region between 4 and 9, the film ruptures spontaneously and

TABLE 2.3

Effect of pH on the Critical Rupture Thickness (H_c) for Fused Silica Plates treated in $5x10^{-4}$ DAH solution

pH	H_c (nm)
4.0	75
6.5	90
8.3	120
11.0	NO RUPTURE

H_c increases rapidly with increasing pH, indicating that the wetting film becomes increasingly more unstable as the pH of the solution increases. This can be attributed to the fact that the adsorption density of the amminium ions at the mineral surface increases with pH. (deBruin, 1955; Fuerstenau, 1957). It is important to mention that H_c reaches a maximum in the pH region where the flotation recovery of quartz particles in DAH is also maximum (Yordan and Yoon, 1985). In contrast, the experiments conducted at pH 11 and above indicate that the initially unstable film becomes stable and does not rupture. Furthermore, the aqueous solution becomes turbid which seems to indicate that the collector ions precipitate out as neutral amine. Recently, Laskowski, et al (1988) have observed a drastic drop in the flotation recovery of different minerals when precipitated amine is present in solution.

2.4.4 Thin films on mica-DAH system

In recent years, mica has become one of the most investigated mineral in surface chemistry. This is because it provides a molecularly-smooth surface which makes it ideal for the direct force measurements using the apparatus developed by Israelachvili. In addition, its intrinsic hydrophilicity can be easily modified by the adsorption of cationic collector. In the present study, the critical rupture thickness has been measured on mica plates that have been exposed to solutions of different concentrations of DAH.

a) Effect of DAH concentration

The results of the H_c measurements conducted with mica plates as

a function of DAH concentration are presented in Figure 2.11. The tests were conducted at constant pH of 6.5±0.2. The results obtained are similar to those obtained with the silica-DAH system, i.e., the thin film on mica can be either stable or unstable depending on DAH concentration. In the concentration range where rupture occurs, H_c increases with increasing DAH addition. It is interesting to note that the H_c values obtained for mica compare very favorably with those of the silica plates. This finding suggests that, in the presence of surfactant, H_c is perhaps independent of the substrate and mainly dependent on the hydrophobicity imparted to the substrate by the adsorbed collector layer. The question of the relationship between H_c and hydrophobicity of mineral surfaces will be addressed in the following chapter.

2.5 Discussion

The results presented in the foregoing section clearly indicate that the film on a mineral surface can be, depending on the nature of the surface and the chemical environment, either stable or unstable. Stable wetting films such as those on fresh hydrophilic minerals do not rupture upon thinning. In contrast, unstable films on hydrophobic surfaces rupture when the distance of separation between the mineral plate and the approaching bubble reaches a critical value. The bubble-against-the-plate technique used in this work have proven to be useful in the measurement of the critical distance of rupture (H_c).

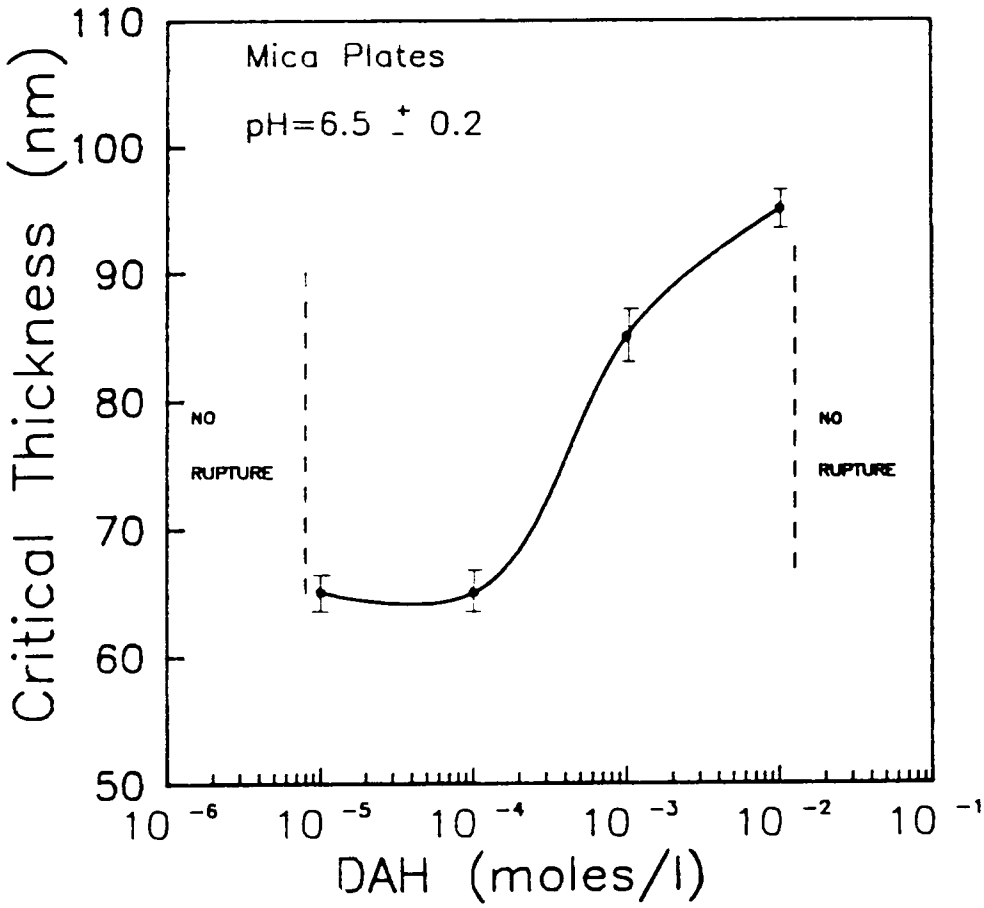

Figure 2.11 Effect of dodecylamine hydrochloride concentration on the critical rupture thickness (H_c) of mica plates at pH 6.5

It has been shown that H_c varies with flotation variables such as pH and collector concentration. In general, H_c increases as the mineral specimen becomes more hydrophobic.

It is generally recognized that interfacial surface forces govern the stability of wetting films. Three kind of surface forces are important, i.e., dispersion, electrostatic and structural forces. They can be attractive or repulsive and depending on their relative magnitudes, the thin film can rupture spontaneously at the critical thickness or remain stable indefinitely. In flotation systems, the molecular force appears to be almost always repulsive as discussed in the previous Chapter. The other two components, which are of much higher magnitude, can be either attractive or repulsive depending on the charge of the interfaces involved, the polarity of the liquid and mineral substrate, their composition and adsorbed species.

The results presented in Table 2.2 indicate that the wetting film on pure mineral surfaces is stable and does not rupture. In this case, all three interfacial forces are repulsive (Laskowski and Kitchener, 1969). However, the magnitude and radius of action vary from one force to another. Typically, molecular forces are of much smaller magnitude than the other two and, therefore, do not contribute as much to film stability. Of the two remaining, the electrostatic force has the longest range (30-300nm) and is partly responsible for the stability of thick films on silica and mica (Read and Kitchener, 1969). Its magnitude depends primarily on the electrical charges on the air bubble and mineral substrate. Notably, according to Derjaguin

and Kussakov (1939) wetting films on hydrophilic surfaces do not rupture even when the repulsive electrostatic force is small or nonexistent. They proposed that, under these circumstances, the forces of structural repulsion (hydration) come into play. Typically, they are of shorter range (1-10 nm) with the radius of action depending on the hydrophilic properties of the substrate. The major component of the repulsive structural forces is the cohesive energy of water molecules in the film. More recently, others (Pashley and Kitchener, 1974; Pashley, 1981; Pashley and Israelvilich, 1984) have also concluded that hydration contributes significantly to stability of wetting films.

It has been shown in Fig 2.8 that the film on methylated silica surfaces is unstable throughout the concentration range studied. This, of course, indicates that the attractive interfacial surface forces predominate over the repulsive ones. It has been shown that at a fixed pH the surface trimethylsilyl groups which are anchored to the silica surface do not significantly alter either the electrostatic force's (Laskowski and Kitchener, 1969; Blake and Ralston, 1984; Xu and Yoon, 1989) or the molecular forces (Mahanty and Ninham, 1976; Xu and Yoon, 1989) between the plate and air bubble. Therefore, the attractive force must arise from the conversion of the repulsive structural hydration force into an attractive one. This is accomplished by the adsorbed hydrophobic molecules which help break the hydrogen bonds and thereby reduce the cohesive energy of water in the film. In this regard, Derjaguin (1987) has pointed out that only

traces of adsorbed hydrophobic substance are required to make repulsive hydration forces attractive. The importance of attractive structural force better known as hydrophobic force in flotation has been recently discussed by Kitchener (1984) and Laskowski (1986).

Thin films behave differently in the presence of adsorbed amminium ions. Depending on DAH concentration and pH, they can either rupture or remain stable. Rupture at H_c occurs when attractive interfacial forces induced by collector adsorption predominate over the repulsive ones. The collector coating generally reduces the zeta-potential of the minerals, which may contribute to reducing the electrostatic energy barrier against film thinning. Moreover, the hydrocarbon tails of the adsorbed collector molecules can make the repulsive hydration force become attractive in the same way as the methylation reaction does.

2.6 Conclusions

1. The optical interferometric method used in conjunction with the bubble-against-plate apparatus has been found useful in measuring the critical rupture thickness (H_c) of wetting films on hydrophobic fused silica and mica plates.

2. Thin aqueous liquid films on untreated fused silica and mica do not rupture at any thickness. The stability of such films appears to be due to repulsive interfacial surface forces.

3. Wetting films on hydrophobic methylated fused silica rupture upon attaining the critical thickness. It has been found, that the magnitudes of H_c increases with increasing degree of surface methylation.

4. The stability of thin liquid films on collector (DAH) coated fused silica and mica plates is found to depend on the concentration of collector employed. The film does not rupture at either a very low DAH concentration or above the CMC. When rupture occurs, H_c increases with increasing collector addition.

CHAPTER 3

CRITICAL THICKNESS OF RUPTURE AND HYDROPHOBICITY

3.1 Introduction

The experimental results presented in the foregoing chapter have clearly shown the critical rupture thickness (H_c) of a film to be a function of the degree of hydrophobicity of the solid plates. The objective of this chapter is to obtain a quantitative relationship between H_c and hydrophobicity. To accomplish this goal, contact angles have been measured on fused silica and mica plates having various degrees of hydrophobicity. Water and methylene iodide have been the liquids used. From the contact angle data obtained, the work of adhesion (W_A) of water on the solids and its individual components, i.e., the dispersion (W_A^d) and the non-dispersion (W_A^{nd}), components have been calculated. A useful empirical correlation between the work of adhesion and the critical thickness of rupture has been established. This allows, from simple contact angle measurements, the estimation of the critical thickness of film rupture of other minerals such as coal, for which direct H_c measurement is not possible.

In addition, estimates of the solids surface free energy components, i.e. the dispersion, γ_s^d, and the non-dispersion, γ_s^{nd}, components have been obtained from the contact angle measurements.

3.2 Theoretical Framework

Prior to the presentation of the results obtained in this investigation a brief discussion of the contact angle theory may be appropriate. Figure 3.1 shows that a finite contact angle is formed when a drop of liquid is brought into contact with a flat solid surface, the final shape taken up by the drop depending on the relative magnitudes of the molecular forces that exist within the liquid (cohesive) and between liquid and solid (adhesive). Thus, the contact angle which the liquid subtends with the solid is a measure of the competing tendencies of the drop to spread so as to cover the solid surface and to round up so as to minimize its own area. For example, when a low surface energy (tension) liquid wets a solid surface, giving a zero contact angle, simply indicates that the molecular adhesion between solid and liquid is greater than the cohesion between the molecules of the liquid. On the contrary, liquids with high surface tension (high cohesive force) mostly give a finite contact angle indicating that here the cohesive forces become dominant. This concept of equilibrium of surface forces is expressed mathematically by the Young's equation (Young, 1805):

$$\gamma_{sv} = \gamma_{sl} + \gamma_{lv}\cos\theta \qquad [3.1]$$

where γ_{sv}, γ_{sl} and γ_{lv} are the surface energy (tension) of the solid/vapor, solid/liquid and liquid/vapor interfaces, respectively, and θ the equilibrium contact angle. The Young's equation can be written in terms of the surface free energy of a solid (γ_s) as

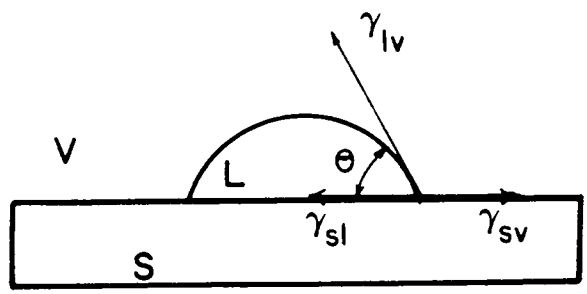

Figure 3.1 Contact angle formed between a liquid droplet and a solid surface

follows:

$$\gamma_s = \gamma_{lv}\cos\theta + \gamma_{sl} + \pi \qquad [3.2]$$

where π is the surface pressure given by:

$$\pi = \gamma_s - \gamma_{sv} \qquad [3.3]$$

Thus, π measures the reduction in the value of the ideal surface free energy of a solid (γ_s) due to adsorption of liquid vapor on the surface. Since the mineral surfaces used in the present study are very smooth and calculations of surface free energies are only conducted when surfaces are hydrophobic, e.g., contact angle above 70 degrees, the surface pressure term (π) is assumed to be zero. Thus, $\gamma_s = \gamma_s^v$ and Equation 3.2 becomes:

$$\gamma_s = \gamma_{lv}\cos\theta + \gamma_{sl} \qquad [3.4]$$

The classical boundary condition for the hydrophilic-hydrophobic transition is equality of the work of adhesion (W_A) of liquid to solid and the the work of cohesion (W_C) of the liquid (Laskowski, 1986). W_A is given by

$$W_A = \gamma_{lv}(\cos\theta+1). \qquad [3.5]$$

and represents the work done per unit area in separating the liquid from the solid. In the case of water, γ_{lv} = 72.6 mJ/m^2; therefore, W_A is determined from water contact angle measurements as follows:

$$W_A = 72.6(\cos\theta+1). \qquad [3.6]$$

The work of cohesion is given by

$$W_C = 2\gamma_{lv} \qquad [3.7]$$

and corresponds to the work required to pull apart a unit area of single phase. For flotation to occur, the work of adhesion of the water to the solid must be less than the work of cohesion of water (which is 145.2 mJ/m^2 at 25°C), so that water can be displaced from the solid surface by the air bubble.

Dispersion, hydrogen bonding and ionization energies are the main components of the work of adhesion. Following Fowkes (1967), these are additive and may be expressed as a sum of work of adhesion terms for the different kinds of interaction energies. Thus, the total work of adhesion for the solid-liquid interface may be given as follows:

$$W_A = W_A^d + W_A^{nd} \qquad [3.8]$$

where W_A^d refers to the work of adhesion due to dispersion interactions and W_A^{nd} that due to non-dispersion interactions. The latter includes interactions due to chemical bonding, hydrogen bonding, and coulombic interactions due to charge separation at the interface. The dispersion forces are always present, and are the dominant term in the case of saturated hydrocarbons and hydrophobic surfaces such as graphite and teflon. In the case of oxide and aluminosilicate minerals such as quartz and mica, the spreading of

water is enhanced by hydrogen bonds and ionic forces. Furthermore, when minerals are crushed or ground, ionic or covalent bonds are broken giving rise to highly reactive, charged sites which readily hydrate, so that the resulting surface has substantial W_A^{nd} components.

Fowkes (1964) has shown that if only dispersion forces are interacting between contacting phases, e.g. a solid and a liquid, W_A^{nd} becomes negligible and Equation [3.8] becomes:

$$W_A = W_A^d \qquad [3.9]$$

where W_A^d is given by:

$$W_A^d = 2(\gamma_{sv}^d \gamma_{lv}^d)^{1/2} \qquad [3.10]$$

where γ_{sv}^d and γ_{lv}^d represent the dispersion components of solid and liquid surface free energy, respectively. Substituting Equations [3.5] and [3.10] into Equation [3.9], one obtains:

$$\gamma_{lv}(\cos\theta+1) = 2(\gamma_{sv}^d \gamma_{lv}^d)^{1/2} \qquad [3.11]$$

Rearranging Equation [3.11] and assuming that $\gamma_{sv}^d = \gamma_s^d$, one can obtain an expression for γ_s^d:

$$\gamma_s^d = \left[\frac{\gamma_{lv}(1+\cos\theta)}{2(\gamma_{lv}^d)^{1/2}} \right]^2 , \qquad [3.12]$$

which has been used in the present work to determine γ_s^d for hydrophobic quartz and mica. When using methylene iodide, whose γ_{lv}

and γ_{lv}^{d} values are 50.8 mJ/m^2 and 48.5 mJ/m^2, respectively, as a reference liquid, Equation [3.12] becomes:

$$\gamma_s^{d} = [3.66(1+\cos\theta)]^2 \quad . \qquad [3.13]$$

The value of γ_s^{d} can, then, be used to determine W_A^{d} for water using Equation [3.10] since γ_l^{d} of water is known (21.8 mJ/m^2). Hence, Equation [3.10] becomes for water:

$$W_A^{d} = 9.34(\gamma_s^{d})^{1/2} \qquad [3.14]$$

In addition, W_A^{nd} can be readily determine by rearranging Equation [3.8] in the following manner:

$$W_A^{nd} = W_A - W_A^{d} \qquad [3.14]$$

Bagnall and Green (1979) proposed that W_A^{nd} can be approximated by:

$$W_A^{nd} = 2(\gamma_s^{nd}\gamma_{lv}^{nd})^{1/2} \qquad [3.15]$$

where γ_s^{nd} and γ_{lv}^{nd} are the non-dispersion components of the surface free energies of the solid and the liquid. For water, γ_{lv}^{nd} has the value of 58 mJ/m^2. Solving Equation [3.15] for γ_s^{nd}, one obtains:

$$\gamma_s^{nd} = \frac{(W_A^{nd})^2}{232.0} \qquad [3.16]$$

Thus, knowing the value of W_A^{nd} from Equation [3.14], γ_s^{nd} can be

readily obtained.

3.3 Experimental

3.3.1 Samples

The solid samples were the same as those used in the critical rupture thickness experiments described in Chapter 2. The fused silica plates were treated either by methylation in the manner described previously, or by adsorbing dodecylamine hydrochloride (DAH) from aqueous solution. Mica plates, on the other hand, were treated in DAH solutions only.

3.3.2 Reagents

Double distilled water prepared in an all glass still was used in all the experiments. The natural pH of the water was 5.8. Research Grade Methylene Iodide obtained from Kodak Co. was used as the reference liquid in the contact angle measurements.

3.3.3 Procedure

The sessile drop method was employed to measure equilibrium contact angles. Measurements were conducted using a Rame-Hart goniometer Model NRC at 22 ± 2°C inside an enclosed stainless steel cell. The size of the drop diameters ranged from 2 to 4 mm. The equilibrium contact angles of the liquid were measured through the liquid phase with a precision of ± 2°. Each angle reported is an average of at least 10 separate measurements taken on different spots

on a plate.

3.4 Results and Discussion

The results of the contact angle measurements are presented in Table 3.1. As shown, the clean solid plates exhibit zero contact angles. In all three cases, the water contact angles increase in magnitude with increasing concentration of adsorbed hydrophobic species. The methylene iodide contact angles, on the other hand, increase initially with increasing surfactant concentration and then level off. Using the contact angle data of Table 3.1 and the equations presented in section 3.2, the work of adhesion of water (W_A) on the solids including its dispersion (W_A) and non-dispersion (W_A^{nd}) have been calculated. The results obtained are presented in Table 3.2. Also included in this Table are the values of the dispersion (γ_s^d) and non-dispersion (γ_s^{nd}) components of the surface free energies of the solids under investigation and the data of critical rupture thicknesses (H_c) obtained in the previous chapter. To better visualize the correlation existing between the critical rupture thickness and the various energy terms, the results given in Table 3.2 are illustrated graphically. Figure 3.2 shows that H_c varies inversely as W_A in the range of variables studied. Since W_A is a measure of the strength of the interaction between water molecules in the thin film and the solid surface, a decrease in its magnitude is indicative of a weakened bonding between water molecules and the solid surface. This makes it easier for an air bubble to displace the thin

TABLE OF RESULTS 3.1

Values of the Water and Methylene Iodide Contact Angles Measured on Silica and Mica Plates Treated in DAH and TCMS Solutions

Mineral	Reagent Concentration	Water θ	Methylene Iodide, θ
Silica	DAH (moles/l)		
	0	0	-
	$5x10^{-7}$	0	0
	$1x10^{-6}$	12 ± 2	0
	$5x10^{-6}$	38 ± 3	16 ± 4
	$5x10^{-5}$	75 ± 3	52 ± 4
	$1x10^{-4}$	72 ± 3	57 ± 5
	$1x10^{-3}$	80 ± 2	56 ± 4
	$5x10^{-3}$	80 ± 2	53 ± 3
Silica	TMCS (% wt)		
	1	80 ± 4	50 ± 4
	5	101 ± 3	58 ± 5
	10	110 ± 4	61 ± 4
Mica	DAH (moles/l)		
	0	0	-
	$5x10^{-7}$	11 ± 3	0
	$1x10^{-6}$	30 ± 3	19 ± 3
	$1x10^{-5}$	78 ± 2	57 ± 6
	$1x10^{-4}$	81 ± 3	54 ± 5
	$1x10^{-3}$	84 ± 2	58 ± 4
	$1x10^{-2}$	84 ± 3	55 ± 5

TABLE OF RESULTS 3.2

Values of H_c, W_A, W_A^d, W_A^{nd}, γ_s^d, γ_s^{nd} for hydrophobic silica and mica plates

Material	H_c (nm)	W_A (mJ/m^2)	W_A^d (mJ/m^2)	W_A^{nd} (mJ/m^2)	γ_s^d (mJ/m^2)	γ_s^{nd} (mJ/m^2)
Silica-DAH [DAH]						
$5x10^{-5}$	65 ± 5	91.4	55.2	36.2	35.00	5.64
$1x10^{-4}$	65 ± 5	95.0	52.8	42.2	32.00	7.68
$1x10^{-3}$	80 ± 5	85.2	53.3	31.9	32.60	4.39
$5x10^{-3}$	95 ± 5	85.0	54.8	30.4	34.40	4.00
Mica-DAH [DAH]						
$1x10^{-5}$	65 ± 5	87.7	52.8	34.9	32.00	5.25
$1x10^{-4}$	65 ± 5	84.0	54.3	29.7	33.80	3.80
$1x10^{-3}$	85 ± 5	80.2	52.3	27.9	31.40	3.36
$1x10^{-2}$	105 ± 5	80.2	53.8	26.4	33.20	3.01
Methylated Silica %TCMS						
1	80 ± 5	85.2	56.2	29.0	36.20	3.64
5	125 ± 5	58.8	52.3	6.5	31.40	0.18
10	145 ± 5	48.0	50.8	0.0	29.50	0.00

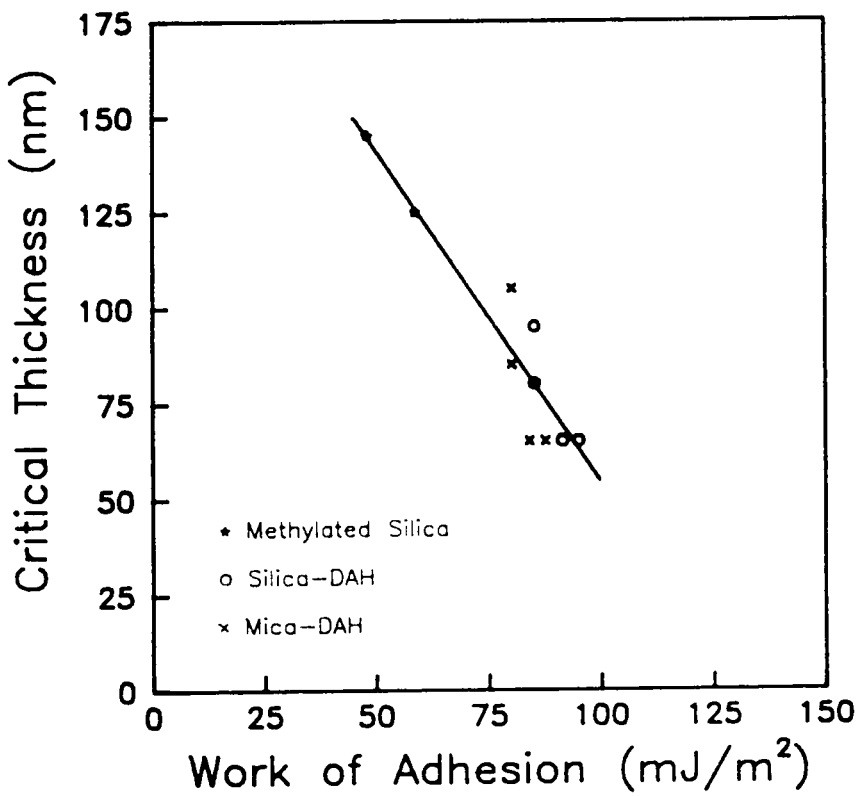

Figure 3.2 Critical rupture thickness (H_c) versus work of adhesion for methylated silica and DAH-treated silica and mica surfaces

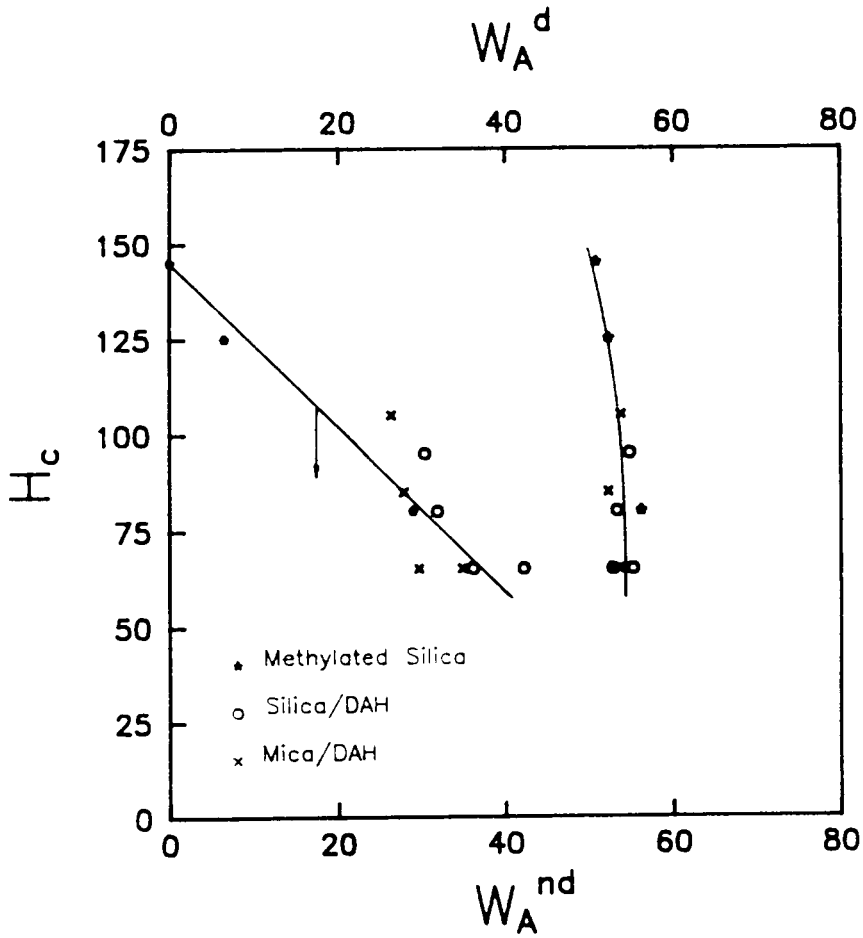

Figure 3.3 Relationships between critical rupture thickness (H_c) and dispersion (W_A^d) and non-dispersion (W_A^{nd}) components of the work of adhesion (W_A) for methylated silica and DAH-treated silica and mica

film. Results obtained by Wakamatsu and Fuerstenau (1973) and more recently by Chibowski and Holysz (1986) showed that the work of adhesion decreases in a linear fashion with increasing adsorption density of collector molecules at the solid-liquid interface.

The relationship existing between W_A and H_c has practical implications. It can be used to estimate the values of critical rupture thickness of water film on other minerals for which direct H_c measurement is not possible. In such a case, only work of adhesion needs to be determined. Estimates of H_c for coal have been made from work of adhesion measurements, the results of which will be presented in chapter 5.

A more fundamental insight into the bubble-particle adhesion process may be obtained by examining the relationships between H_c and the two components of the work of adhesion, i.e. W_A^d and W_A^{nd}. Therefore, H_c values have been plotted against W_A^d and W_A^{nd} as shown in Figure 3.3. It is interesting to see that H_c varies inversely proportional to both W_A^d and W_A^{nd}. Note, however, that W_A^{nd} is more sensitive to changes in H_c and hence to changes in the hydrophobicity of the surface. It, thus, appears that the observed increase in H_c with increasing hydrophobicity of a solid is due to a reduction in the two components of W_A. It is not surprising, then, to see that W_A gives better correlation with H_c (Figure 3.2) than W_A^{nd} or W_A^d. The reduction in the non-dispersion component (W_A^{nd}) with increasing surfactant concentration is achieved by surfactants which by adsorbing at the solid/water interface shield polar sites or

replace them with those that do not ionize or take part in hydrogen bonding. As a consequence, the electrostatic field of a solid surface, which is initially high due to the presence of polar functional groups, i.e. groups having permanent dipole moments, is decreased. Hence, the net result is a reduction in the interaction energy between permanent dipole of water molecules and the electrostatic field of the surface. W_A^{nd} is a measure of such interaction (Fowkes, 1964).

A similar explanation can be furnished for the reduction in W_A^d. It is well recognized that W_A^d has contributions due to London dispersion forces and due to polarization of adsorbed molecules by the field of the solid and is directly proportional to the polarizability of the surface (α_1) and (α_2) of the adsorbed polar molecules. The adsorption of hydrocarbon molecules on the surface of a solid results in the replacement of highly polarizable sites (oxygen in the case of silica) by less polarizable hydrocarbon groups (due to the lower electron density of carbon) which results in a reduction in α_1. The net effect is, therefore, a reduction in W_A^d.

It is well recognized that in flotation the solid/liquid interface is the most important one. A hydrophilic mineral can only be floated after collector molecules adsorb at the surface. As a result, the surface free energy of the solid is reduced. Such a decrease is necessary for the bubble-particle adhesion. In addition, it has been discussed in the above paragraph that the observed reductions in the work of adhesion, and its individual components are

due to changes occuring at the solid surface. It is, thus, of vital importance to examine the changes in surface free energy of the solid occurring upon adsorption of hydrophobic molecules. This has been accomplished in the present work by following the changes in the dispersion (γ_s^d) and non-dispersion (γ_s^{nd}) components of surface free energies. These values have been calculated following the procedure outlined in section 3.2. The results obtained are illustrated graphically in Figure 3.4. It is interesting to see that H_c appears to vary in an inverse fashion with both γ_s^d and γ_s^{nd} in much the same manner as it does with W_A^d and W_A^{nd}. Thus, this result seems to indicate that the changes in the work of adhesion of water are mainly due changes in the surface free energy of the solid surface. Most likely, the polar component of the surface free energy of the solid (γ_s^{nd}) decreases with increasing degree of hydrophobicity due to the substitution of surface polar groups by non-polar groups which carry low or no permanent dipole moment. Similarly, the observed reduction in γ_s^d with hydrophobicity may be due to the replacement of easily polarizable surface groups by non-polarizable ones as explained in the foregoing paragraph. It is important to note that other researchers (Chibowski and Holysz, 1986) have observed a similar trend. These authors found a drastic reduction of the non-dispersion component of quartz surface free energy from 115 mJ/m^2 (bare surface) to 7.2 mJ/m^2 at only 0.25 of a monolayer of DAH. At one monolayer, the flotation recovery was at a maximum and the polar interaction at the quartz-water interface was non-existent. The dispersion component (γ_s^d) was

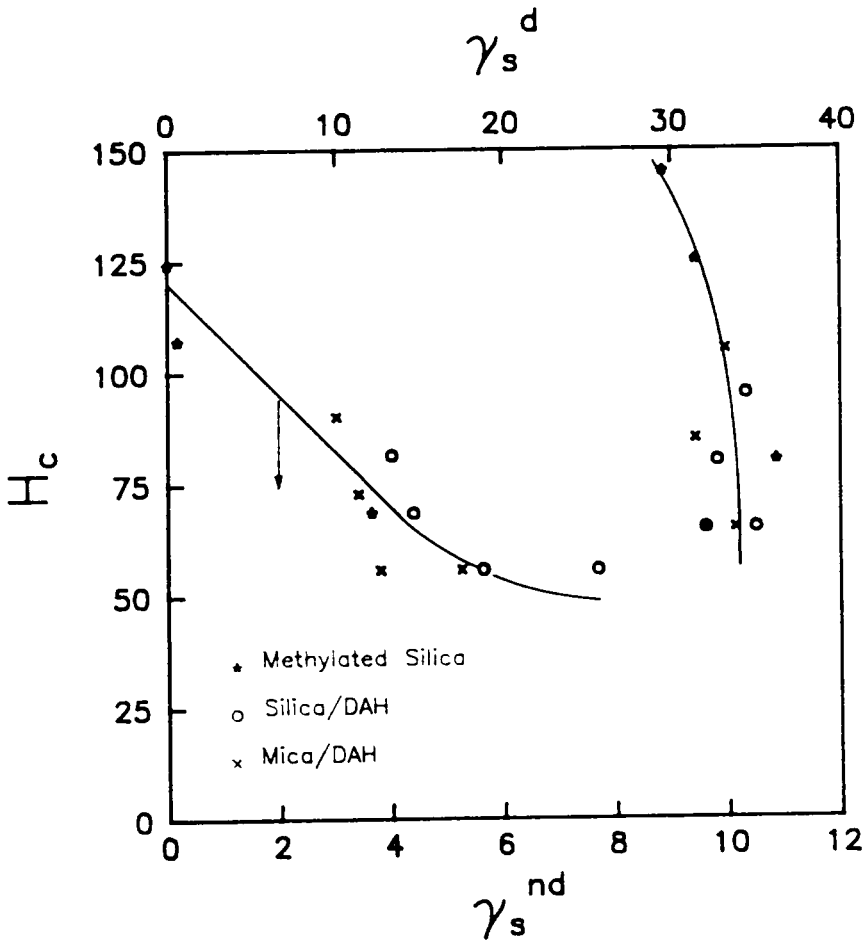

Figure 3.4 Relationships between critical rupture thickness (H_c) and the dispersion (γ_s^d) and non-dispersion (γ_s^{nd}) components of the surface free energies of solids investigated

also measured and it initially changed from 76 mJ/m^2 (bare quartz) to 28.2 mJ/m^2 at 0.25 statistical monolayer of DAH. Successful correlation between the energetic changes induced by collector adsorption with the flotability of barite have been recently reported by Bilinski and Wojcik (1986).

3.5 Conclusions

1.-It has been shown that the critical rupture thickness (H_c) of water film on solids varies inversely with the work of adhesion (W_A). This relationship allows estimation of H_c of various minerals from simple contact angle measurments.

2.-The inverse linear relationship also exist between H_c and the dispersion component of the work of adhesion (W_A^d) and its non-dispersion component (W_A^{nd}). However, W_A^{nd} plays a more important role than W_A^d in the bubble-particle adhesion process.

3.-It has been shown that the adsorption of hydrocarbon molecules at the solid/liquid interface reduces both the dispersion (γ_s^d) and non-dispersion (γ_s^{nd}) components of the surface free energy (γ_s) of the solids investigated. However, as was the case with the work of adhesion, the non-dispersion component (γ_s^{nd}) is more sensitive to the changes occuring at the solid/liquid interface, and gives better correlation with H_c than γ_s^d.

CHAPTER 4

DISJOINING PRESSURE CALCULATIONS FOR THE BUBBLE-PARTICLE ADHESION PROCESS

4.1 Introduction

It is clear from the results presented in the foregoing sections that the bubble-particle attachment process can be divided into various sub-processes which involve different interfaces and forces. It has not been discussed, however, as to which of the individual surface forces is mainly responsible for film rupture and why the film ruptures at the critical thickness. In this chapter, the concept of disjoining pressure is used to quantify the effects of the various forces operating during the process of bubble-particle attachment. Such calculations will be useful in delineating the role of the different surface forces in determining the stability of thin films.

4.2 Theoretical Framework

4.2.1 Introduction

The thermodynamic calculations to be presented in this work attempt to explain quantitatively the behavior of wetting films in terms of the different types of interaction forces between the bubble and the particle. In order to accomplish this the adhesion process is treated as a heterocoagulation process and analysed by means of the classical DLVO theory modified to include the hydrophobic interaction force. It is only recently that the inadequacy of the DLVO theory has

been recognized when it applies to hydrophobic solids (Xu and Yoon, 1989; Churaev and Derjaguin, 1985).

4.2.2 Modified DLVO theory

It is now generally recognized that there are three major physical forces operating between surfaces suspended in liquids. These are (i) electrostatic force (V_E), (ii) dispersion forces (V_D) and (iii) structural force (V_S). Thus, the total interaction energy (V_T) between a bubble and a particle is given by:

$$V_T(h) = V_E(h) + V_D(h) + V_S(h) \qquad [4.1]$$

V_T and its three components V_E, V_D and V_S are functions of the separation distance (h) between the interacting bodies. The magnitude, sign and radius of action of each of the three components vary from one another and the relative contribution of each component determines the shape of the isotherm of $V_T(h)$.

Three basic types of isotherms may be distinguished in the case of bubble-particle interaction. These are schematically represented in Figure 4.1. Curve A denotes a stable thin film which exists between a hydrophilic surface and an air bubble. Note that $dV_T/dh < 0$. This curve also represents the disjoining pressure isotherm of any liquid between two highly charged interfaces (such as those existing in stabilized well-drained froths, dispersed sols, or stabilized emulsions). Curve B, on the other hand, represents the opposite extreme such as a liquid film between a highly hydrophobic

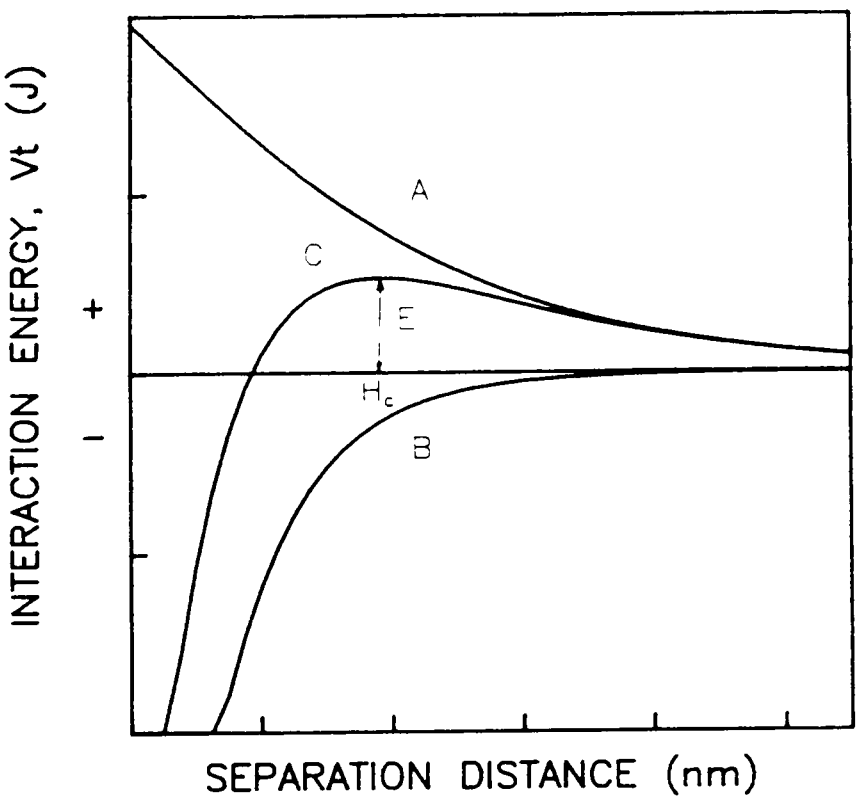

Figure 4.1 Theoretical isotherms of total interaction energy (V_T) for bubble-particle adhesion

solid and an air bubble, the film is completely unstable and will rupture spontaneously. Note that in this case $dV_T/dh > 0$. Curve C represents an intermediate type of thin film. It represents the case of a solid with intermediate degree of hydrophobicity with an activation energy barrier (E). This curve is typical of most flotation systems. In this case, the film ruptures at the critical thickness (H_c). Note that rupture takes place when $dV_T/dh \leq 0$.

The electrical component (V_E) arises from the interaction between two double layers, one at the solid/liquid interface of the film and the other at the liquid/gas interface of the film. If they are of the same sign, V_E is positive. If the bubble and particle surfaces are oppositely charged, V_E is negative and, hence, helps in rupturing the film. Typically, the electrical properties of the particle differ from those of the bubble and it has been shown by Hoggs, et at (1966) that for unequally charged spherical particle (radius r) and a flat plate interacting at constant surface potential V_E is given by:

$$V_E(h) = P\left[Q\ln\frac{(1+e^{-\kappa h})}{(1-e^{-\kappa h})} + \ln(1-e^{-2\kappa h}) \right] \qquad [4.2]$$

where h is the separation distance between the interacting bodies, and κ is the Debye reciprocal length given by the expression:

$$\kappa = (2z^2F^2c/\varepsilon_o\varepsilon RT)^{1/2} \qquad [4.3]$$

in which F is the Faraday constant, R the gas constant, T the absolute

temperature, ε_o the permittivity of vacuum, z the valency of the counterions and C the concentration of the indifferent electrolyte.

In Equation [4.2], P and Q are constants given by:

$$P = \frac{\varepsilon r(\psi_1^2+\psi_2^2)}{4} \qquad [4.4]$$

$$Q = \frac{2(\psi_1\psi_2)}{(\psi_1^2+\psi_2^2)} \qquad [4.5]$$

where ε is the dielectric constant of the medium (78.54 for water at 25°C) and ψ_1 and ψ_2 are the surface potentials of the particle and the bubble, respectively, which in this work are approximated by their respective zeta potentials (ζ_1 and ζ_2).

The dispersion component (V_D) arises from the van der Walls forces between atoms and molecules. The calculation of V_D between interacting bodies has been attempted by two different approaches, one based on a molecular model attributed to Hamaker and the other based on a model of condensed media, attributed to Lifshitz. The former approach also known as the microscopic approach is used in this work. Hamaker (1937) made use of the well known London's expression for the dispersion attraction between two isolated molecules and integrated it for all the molecules in two separate particles to obtain the dispersion energy of interaction between two macroscopic bodies. The work done, at constant temperature, by the interaction forces in bringing the two bodies (1 and 2) from the infinity to a given separation distance (h_{12}) is the Gibbs free energy due to dispersion

interactions ΔG_{12}^{d} and is given by

$$\Delta G_{12}^{d} = -\int_{V_1} dV_1 \int_{V_2} \frac{A_{12}\rho_1\rho_2}{h_{12}^{6}} dV_2 \qquad [4.6]$$

where dV_1 and dV_2 are differential volume elements of V_1 and V_2, and ρ_1 and ρ_2 are the molecular number densities (molecules per unit volume) and A_{12} is the Hamaker constant. These geometric integrals have been numerically evaluated for simple geometries (Mahanty and Ninham, 1976) for which the free energy of interaction has been obtained. For a spherical bubble (3) of radius r interacting with a flat solid plate (1) in liquid (2), as in the bubble-against-plate apparatus, V_D is given by:

$$V_D(h) = \frac{-A_{123}r}{6h} \qquad [4.7]$$

where A_{123} is the complex Hamaker constant for the interaction of two bodies of composition 1 and 3 occuring in a medium of composition 2. In the case of flotation, bodies 1 and 3 refer to particle and gas bubble respectively, and 2 refers to the aqueous solution. A_{123} is evaluated using a combining law in the following manner

$$A_{123} = A_{13} + A_{22} - A_{12} - A_{23} \qquad [4.8]$$

where A_{ij} refers to the Hamaker constant for the interaction between bodies i and j in vacuum and A_{ii} for the interaction of two bodies of i in vacuum. If the root-mean-square approximation is used for

Hamaker constants in Equation [4.8],

$$A_{12} = (A_{11}A_{22})^{1/2}, \qquad [4.9]$$

$$A_{13} = (A_{11}A_{33})^{1/2}, \quad \text{and} \qquad [4.10]$$

$$A_{23} = (A_{22}A_{33})^{1/2}. \qquad [4.11]$$

Substitution of Equations [4.9], [4.10] and [4.11] into Equation [4.8] yields:

$$A_{123} = (A_{11}^{1/2} - A_{22}^{1/2})(A_{33}^{1/2} - A_{22}^{1/2}) \qquad [4.12]$$

where in the case of mineral 1 and gas bubble 3 interacting in medium 2, A_{11} is the Hamaker constant for the solid mineral, A_{33} the Hamaker constant for the air bubble and A_{33} the Hamaker constant for the medium. The typical assumption is to neglect A_{33} on the grounds that an air bubble is not a condensed phase. Hence, Equation [4.12] becomes:

$$A_{123} = A_{22}^{1/2}(A_{22}^{1/2} - A_{11}^{1/2}) \qquad [4.13]$$

When the bubble-particle interaction takes place in water, A_{22} is 4.38×10^{-20} J. A_{11} for common materials can be obtained from the literature or can be estimated in the following manner: Fowkes (1964)

$$A_{11} = 6\pi r_{11}^{2} y_s^d \qquad [4.14]$$

where y_s^d is the dispersion component of the surface free energy of the solid which in this work has been obtained from methylene iodide

contact angle measurements (Table 3.2) and $6\pi r_{11}^2$ is in most cases a constant = 1.44×10^{-21}, Equation [4.14] then becomes:

$$A_{11} = 1.44 \times 10^{-21} \gamma_s^d \qquad [4.15]$$

Substituting of Equation [4.15] into [4.13] yields:

$$A_{123} = 4.38 \times 10^{-20} - 7.93 \times 10^{-21} (\gamma_s^d)^{1/2}, \qquad [4.16]$$

which is used to evaluate A_{123} for the methylated and DAH-treated solid mineral surfaces used in the present work.

Note that if the value of A_{22} in Equation [4.12] is intermediate between the values of A_{11} and A_{33} as is typically the case in flotation, then the Hamaker constant is negative, In this case, V_D is positive and its contribution to bubble-particle adhesion is repulsive. The concept of negative complex Hamaker constant has been discussed in detail by Visser (1972). Israelachvili (1985) explains this concept by means of an analogy:

> "It is known to everyone that both wood and iron are attracted to the earth by gravitational force; however, in water iron sinks while wood rises. Thus, wood is effectively experiencing a repulsion from the earth when in water. This is because it is lighter than water, and if it were to descend, it would have to displace an equal volume of water and drive it upwards to replace the space previously occupied by the wood. Since water is denser and so more attracted to the earth than wood the net effect would be unfavorable, i.e., the energy lost in water

going up is not recovered by the energy gained in wood coming down. This displacement principle applies to all interactions including intermolecular interaction"

It is important to point out that the assumption of zero Hamaker constant for the air bubble may not be valid in the case of air bubbles being stabilized with surfactants. In such a case, the gas bubbles will be armoured with long hydrocarbon molecules which perhaps makes it behave as a condensed phase. Under these circumstances, V_D may be attractive.

The structural component of the disjoining pressure (V_S) arises from the interaction of structurally modified liquid layers which exist in the boundaries of the approaching particle and gas bubble. V_S for a sphere of radius r near a flat surface is given by: (Israelachvili and Pashley (1982)

$$V_S(h) = -CrD_o e^{(-h/Do)} \qquad [4.17]$$

where h is the thickness of a liquid interlayer between interacting bodies, D_o the decay length, and C a constant that has negative values for liquids that wet the substrate, and positive on hydrophobic substrate. When C is negative, V_S becomes positive and therefore repulsive. In this case, V_S is more commonly known as hydration energy. On the other hand, when C is positive, V_S becomes attractive and is named hydrophobic interaction energy.

A thermodynamic interpretation of V_S can be given in terms of the entropic changes associated with water molecules involved at the

solid/liquid and the liquid/gas interfaces. It is well recognised that hydrophilic solid are strongly hydrated and water molecules have a well ordered structure. The hydrated layer also exists around the gas bubbles. Therefore, upon bubble-particle interaction, a large amount of energy is required to disrupt the ordered water structure and ultimately dehydrate the two surfaces as they approach each other. This situation, of course, corresponds to a positive or repulsive V_S. The opposite situation may exist near a hydrophobic mineral surface. Here, the hydrophobic character of the surface prevents the formation a stable structured water layer and water molecules are readily displaced from the interlayer. This leads to a decrease in the order of the system and, therefore, to an increase in entropy. The end result is an increase in the negative value of the free energy of interaction. This phenomenon gives rise to the hydrophobic interaction or negative V_S which accounts for the rapid coagulation of hydrophobic particles in water (Xu and Yoon, 1989) and for the ease with which wetting films rupture on hydrophobic surfaces.

4.2.3 Objectives of the calculations

The goals of the present thermodynamic calculations are twofold: i) to predict under a given experimental condition whether the thin film will be stable or unstable, and ii) to determine which of the individual components of the interaction energy is more responsible for the behavior of the thin film. The first goal is accomplished by estimating the magnitude of V_T as a function of separation

distance while the second is attained by analyzing separately each one of the individual components of V_T. The calculations should be applicable to any mineral systems provided that the appropriate parameters are experimentally determined. It is hoped that the calculations will shed additional light toward understanding the process of bubble to particle attachment in flotation.

4.2.4 Thermodynamic calculations

The total interaction energy $V_T(h)$ can be calculated using Equation [4.1], which may be rewritten as follows

$$V_T(h) = V_E(h,\zeta_1,\zeta_2) + V_D(h,A_{123}) + V_S(h,C,D_o), \qquad [4.18]$$

to identify the parameters, i.e. ζ_1, ζ_2, A_{123}, C and D_o, that determine each term. However, for hydrophobic minerals the values of C, D_o are not available in the literature and are difficult to determine experimentally without using an apparatus that can measure the force directly. Therefore, a new methodology is proposed in this work which allows the estimation of C and D_o from H_c measurements.

Typically, a thin film becomes unstable and ruptures at a critical distance, H_c, as shown in Figure 4.1 (curve C). At H_c, the following conditions must be met:

$$\begin{aligned} V_T &= V_E + V_D + V_S \\ &= E \end{aligned} \qquad [4.19]$$

where E is the activation energy for bubble-particle adhesion. It is also clear that at H_c,

$$\frac{dV_T}{dH} = 0 \ , \qquad [4.20]$$

and

$$\frac{d^2V_T}{dH^2} < 0 \ . \qquad [4.21]$$

Equation [4.21] must be satisfied if V_T is to reach a maximum value at H_c and follow the behaviour of curve C in Figure 4.1.

Subtituting Equations [4.2], [4.7] and [4.17] into Equation [4.18] yields:

$$V_T = P\,Q\ln\frac{(1+e^{-\kappa h})}{(1-e^{-\kappa h})} + \ln(1-e^{-2\kappa h}) - \frac{A_{123}r}{6h} - CrD_o e^{-h/Do} \qquad [4.22]$$

One can, then, substitute Equation [4.22] into [4.20] and [4.21] to obtain:

$$\frac{2P\kappa[e^{-2\kappa h} - Qe^{-\kappa h}]}{(1-e^{-2\kappa h})} + \frac{A_{123}r}{6h^2} + Cre^{-h/Do} = 0 \ , \qquad [4.23]$$

and

$$\frac{2P\kappa^2 e^{-\kappa h}(Q - 2e^{-\kappa h} + Qe^{-2\kappa h})}{(1-e^{-2\kappa h})^2} - \frac{A_{123}r}{3h^3} - \frac{Cr}{D_o}(e^{-h/Do}) < 0 \ , \qquad [4.24]$$

respectively.

Substituting h with H_c in Equations [4.22] to [4.24], one can obtain the following equations,

$$P\left[Q\ln\frac{(1+e^{-\kappa H_c})}{(1-e^{-\kappa H_c})}+\ln(1-e^{-2\kappa H_c})\right]-\frac{A_{123}r}{6H_c}-CrD_o e^{-H_c/D_o}=E, \quad [4.25]$$

$$\frac{2P\kappa[e^{-2\kappa H_c}-Qe^{-\kappa H_c}]}{(1-e^{-2\kappa H_c})}+\frac{A_{123}}{6H_c^{\,2}}+Cre^{-H_c/D_o}=0, \quad [4.26]$$

and

$$\frac{2P\kappa^2 e^{-\kappa H_c}(Q-2e^{-\kappa H_c}+Qe^{-2\kappa H_c})}{(1-e^{-2\kappa H_c})^2}-\frac{A_{123}}{3H_c^{\,3}}-\frac{Cr}{D_o}e^{-H_c/D_o}<0. \quad [4.27]$$

in which all the parameters except C, D_o and E are known. Note, however, that there are only two equations [4.25 and 4.26] and one inequality [4.27]. Thus, the values of C, D_o and E cannot be obtained directly and an assumption has to be made. From the work of other investigators (Pashley and Israelachvili, 1982; Churaev and Derjaguin, 1985) it has been clearly shown that neither C nor D_o are constants and that the values of these two parameters indeed vary from one surface to another as well as with any kind of surface treatment. Therefore, the assumption of a constant C or D_o is not a reasonable one. The only other possible alternative is to use a constant value for the activation energy E. In this regard, the results of Eigeles and Volova (1960) and more recently of Yordan and Yoon (1985) have shown that E is not a constant. It is large for hydrophilic solids and becomes smaller with increasing degree of surface hydrophobicity. E has been shown to become negligible for very hydrophobic surfaces.

Thus, since in the present study the surfaces investigated are very hydrophobic, one can perhaps assume E=0 and solve Equations [4.25] and and [4.26] for C and D_o. This approach was implemented in the present work and although the values of C and D_o obtained were in the same range as those reported in the literature, one problem was found. The inequality [4.27] was not satisfied. Therefore, the solution was not considered to be a feasible one. However, it was also found that by increasing the value of E incrementally, at a certain value of E the inequality [4.27] changes sign and becomes negative. At this minimum value of E all three criteria are satisfied and the solution obtained is a feasible one. Nevertheless, the solution was not unique since any value of E larger than the minimum would produce a feasible solution. In the present study, the minimum value of E was used to solve for C and D_o. The selection of the minimum E was based on the following facts: i) the activation energy for the systems investigated should be very small and ii) it is well known that any thermodynamic system will tend to accomodate itself at a point of minimum energy. A series of computer programs have been written to obtain the values of E, C and D_o. The codes and the instruction manuals are presented in appendix 1.

The values of C, D_o and E determined as such can be used to obtain the isotherms of $V_T(h)$ and its individual components, i.e., $V_E(h)$, $V_D(h)$ and $V_S(h)$ for different experimental situations.

4.3 Experimental

4.3.1 Mineral Samples and Materials

High purity silica powder obtained from Fisher Scientific Co. was used in the zeta potential measurements. The powder has an average size of 5 microns in diameter and an average surface area of 3.8-4.0 m^2/g as determined by the B.E.T. method. Research grade potassium chloride obtained from Fisher Scientific Co. was used to stabilize bubbles in aqueous solution. Reagent grade Sodium hydroxide and hydrochloric acid from Fisher Scientific Co. were used for pH control. Research grade dodecylamine hydrochloride (DAH) and trimethylchlorosylane (TMCS) were the reagents used to modify the silica surface in the zeta potential measurements.

Hamaker constants of the fused silica and mica plates used for the H_c measurments were determine using the methylene iodide contact angle technique as described in the previous section.

4.3.2 Apparatus and Procedure

a) Zeta Potential Measurements

The zeta potentials of pure silica and of silica treated by DAH and TMCS were measured using a Laser Zee-Meter manufactured by Pen Kem, Inc. In each experiment, a sample of fine silica powder was conditioned in the DAH or TCMS solution of appropriate concentration and pH in a beaker using a magnetic stirrer for about 15 minutes. After conditioning, a small amount of sample was removed for measurement. For methylated silica, the powder was dispersed in

stock solution of pH 11 and the solution pH was manipulated to obtain other pH values. For the DAH-treated silica, the stock solution was prepared at pH 3.7 and manipulated to the alkaline range. All the experiments were performed at ambient temperature, and at least ten particles were counted and averaged for each experimental point.

The zeta potentials of air bubbles in pure electrolyte and in DAH solutions were obtained using a vertical flat-type electrophoretic cell described in detail by Yoon and Yordan (1986). A Rank Brothers Mark II microelectrophoretic apparatus was used to determine the electrophoretic mobility of the microbubbles. The mobility was then converted to zeta potential using Smoluchowski's equation. The zeta potentials of bubbles stabilized in DAH solutions were obtained from previous publications (Yoon and Yordan, 1985; Laskowski, et al, 1988).

4.4 Results and Discussion

4.4.1 Zeta Potentials of methylated and DAH-silica systems

Figure 4.2 shows the results of the zeta potentials measurements conducted on pure and methylated silica samples in the presence of $1x10^{-3}$ moles/l of KCl as a function of pH. Silica samples treated with TMCS concentrations of 5% and 10% were investigated. It is shown that in the alkaline and neutral pH range, the zeta potentials of pure silica are negative and the magnitude increase with increasing pH. The zeta potential changes rapidly as the pH is decreased from 6 to 3, becoming positive below the isoelectric point (i.e.p.) of pH 2.0. This result is similar to those reported by other researchers

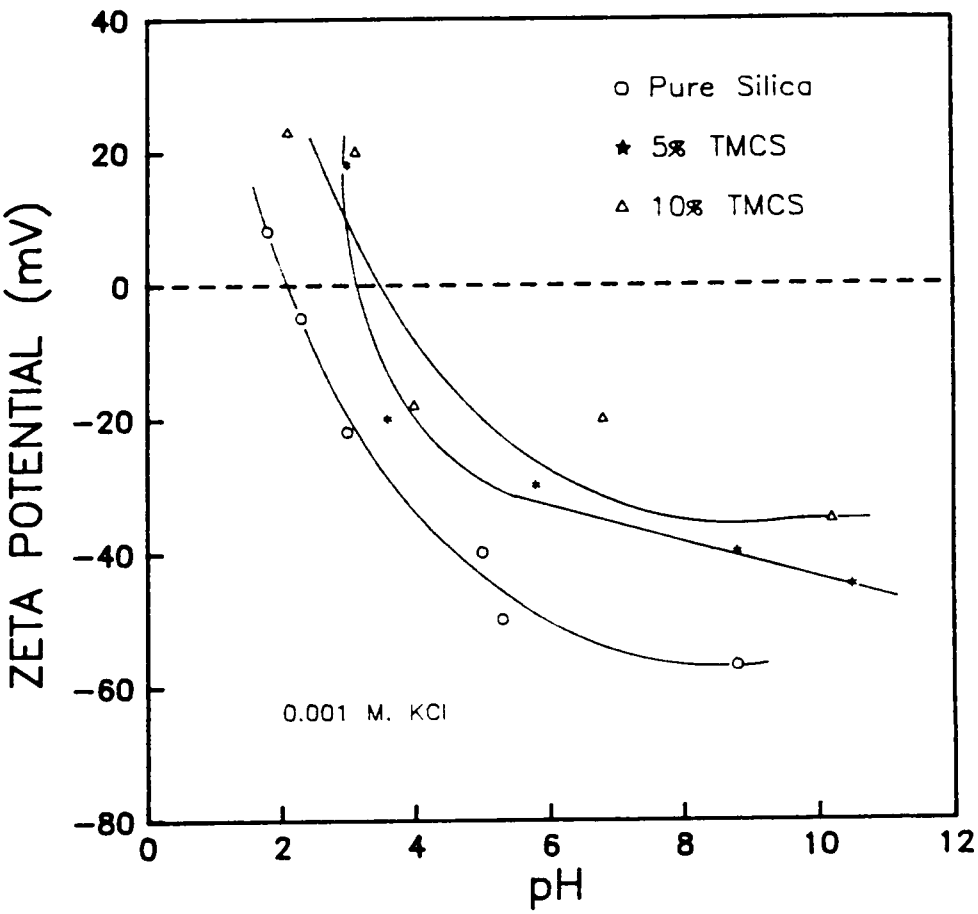

Figure 4.2 Effect of pH on the zeta potential of pure and methylated silica in 0.001 M. KCl solution

(De Bruyn, 1955; Gaudin and Fuerstenau, 1955).

Also shown in Figure 4.2 are the results of the methylated silica samples methylated at 5 and 10% TMCS solutions. As is the case of pure silica, the zeta potentials are negatives in the alkaline and neutral pH. Nevertheless, the magnitude decreases with increasing methylation. The i.e.p also shifts to the higher pH with increasing methylation. These results contradict those results reported by Laskowski and Kitchener (1969) and more recently by Blake and Ralston (1985). These investigators showed that the zeta potential vs. pH curve for silica remained the same before and after methylation. The reason for this apparent discrepancy is the fact that the concentration of methylating reagent used in the present investigation was higher than those used by other workers by one or two orders of magnitude.

Figure 4.3 illustrates the results of the zeta potential measurements conducted on the silica powder in solutions of different concentrations of DAH as a function of pH. It is shown that at $1x10^{-5}$ M DAH the zeta potentials remain essentially the same as those of the pure mineral (Figure 4.2), indicating that the electrical properties of the silica surface is not affected in the presence of dilute DAH solutions. This is not the case, however, at higher DAH concentrations. Note that at $1x10^{-4}$ M DAH, the initially negative zeta potential in the acidic range becomes more negative with increasing pH, and then reaches its maximum negative value at about pH 6 before decreasing in the alkaline range. It appears as if the

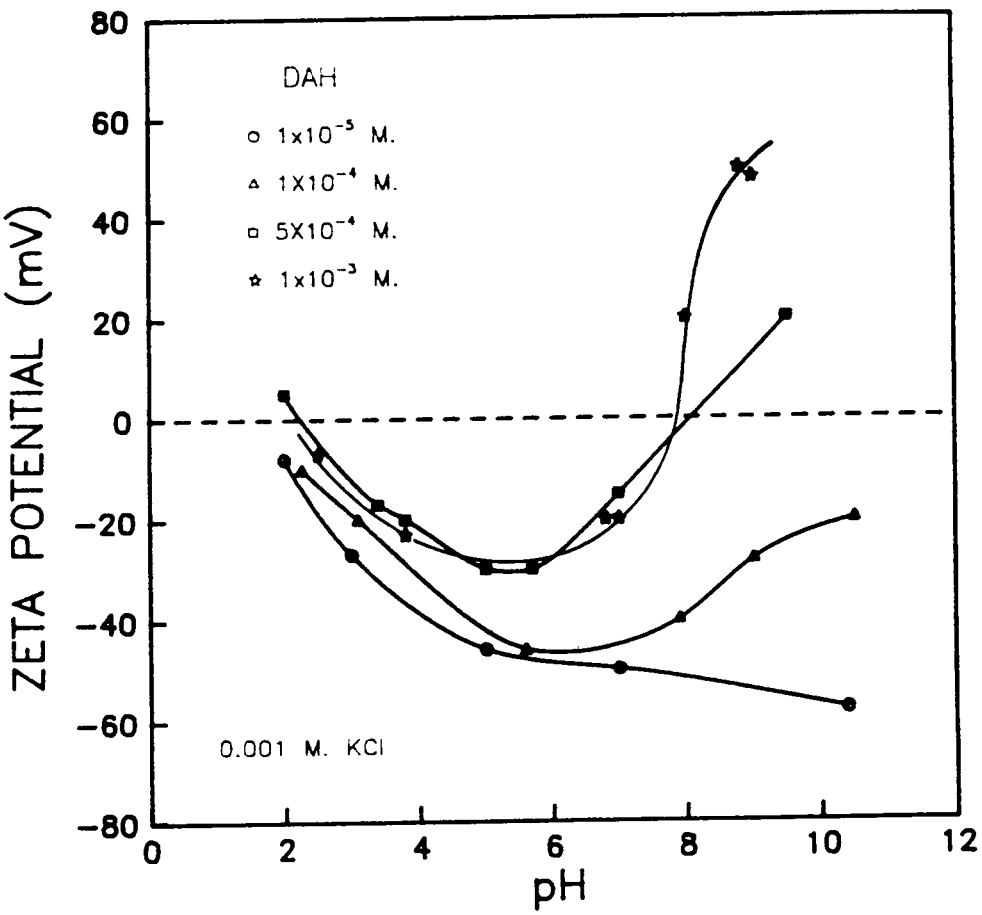

Figure 4.3 Effect of pH on the zeta potential of silica treated with different concentrations of dodecylamine hydrochloride in 0.001 M. KCl solution

negative charges on the silica are neutralized by the adsorption of the cationic surfactant. When the concentration of DAH is further increased to $5x10^{-4}$ moles/l, the zeta potential is reversed to become positive. The points zeta potential reversal (p.z.r) have been observed at $5x10^{-4}$ and $1x10^{-3}$ M and range between pH 7.5-8. The reason that DAH can adsorb at pH higher than these p.z.r's has been attributed to the hemi-micelle formation, which is driven by the free energy change due to hydrocarbon association. Other investigators (DeBruyn, 1955; Gaudin and Fuerstenau, 1955) have also reported p.z.r's in the quartz-DAH system.

4.4.2 Zeta Potential of Air Bubbles in Pure Aqueous Solution

As shown in Figure 4.4 air bubbles generated in 0.5 moles/l KCl solution are negatively charged above pH 4 and its magnitude increases with increasing pH. The zeta potentials are zero in the range of pH 3.7-4.2. These results are in general agreement with those reported by Alty (1924) and Mctaggart (1914), who showed that bubbles have negative charge in distilled water. More recently, McShea and Callagham (1983) confirmed that bubbles are negatively charged in slightly acidic KCl solutions. The charging mechanism of air bubbles in pure electrolytic water is, nevertheless, still not fully understood. Recently, Yoon and Yordan (1985) suggested that the difference in the hydration energy of OH^- and that of H^+ is responsible for the preferential adsorption of OH^- ions at the air/water interface.

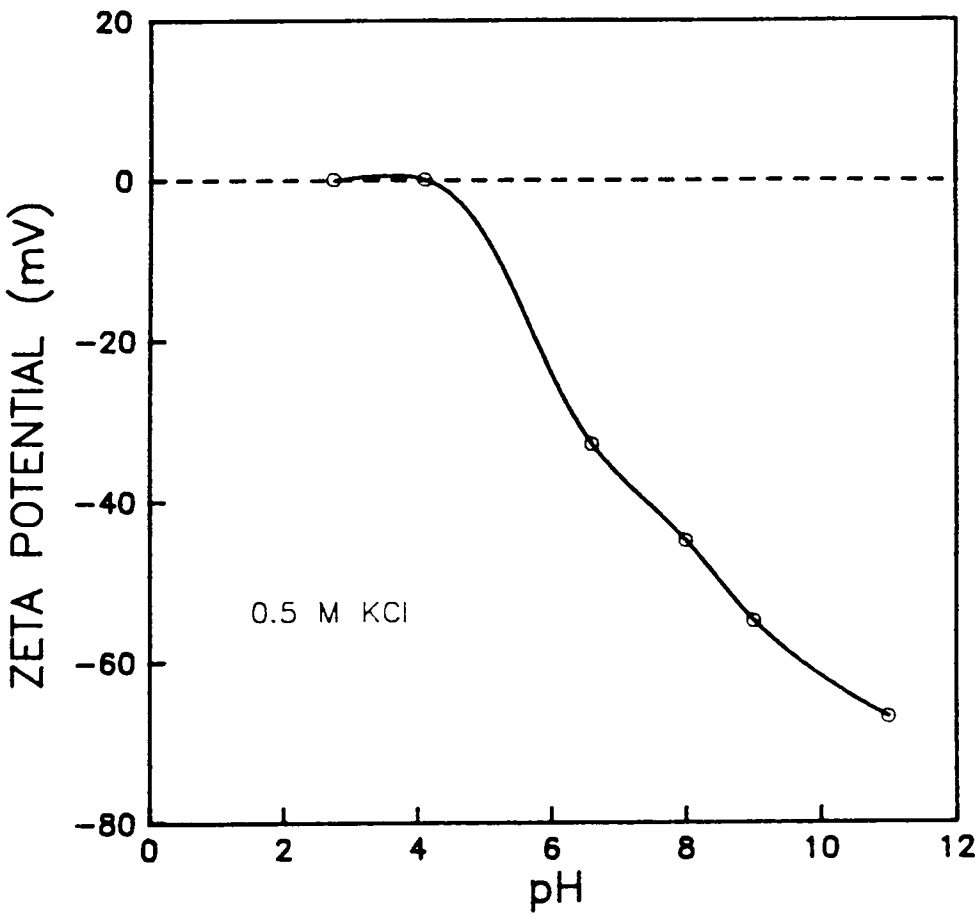

Figure 4.4 Effect of pH on the zeta potential of air bubbles generated in 0.5 M. KCl solution

It is necessary at this point to make clear that the technique for measuring zeta potentials of air bubbles in aqueous solution employed in the present investigation requires small and stable bubbles. Unfortunately, this can only be achieved at a high electrolyte concentration. It was found that a concentration of 0.5 moles/l of KCl was adequate to meet the above requirements. Note, however, that this concentration is much higher than 0.001 moles/l used in the calculation of V_E as presented in section 4.5. This discrepancy, of course, introduces an error in the calculation of V_E because the measured values of ζ for air bubbles are most likely of smaller magnitude than what they should be due to double layer compression. Nevertheless, the value of -40 mv obtained in this work for air bubbles in the neutral pH region, compares well with the value of -50 mv recently used by Churaev and Derjaguin (1985).

The zeta potentials of air bubbles stabilized in solution of DAH have been obtained from previous publications (Yoon and Yordan, 1986; Laskowski, et at, 1988) and the results are presented in Figure 4.5.

4.4.3 Hamaker Constants

Table 4.1 shows the values of the Hamaker constants (A_{123}) for the silica and mica flotation systems investigated. The values for clean surfaces have been obtained from the literature. The complex Hamaker constants have been determined following the procedure described in section 4.2.2. Note that in all cases the complex Hamaker constants are negative. This, of course, will make the

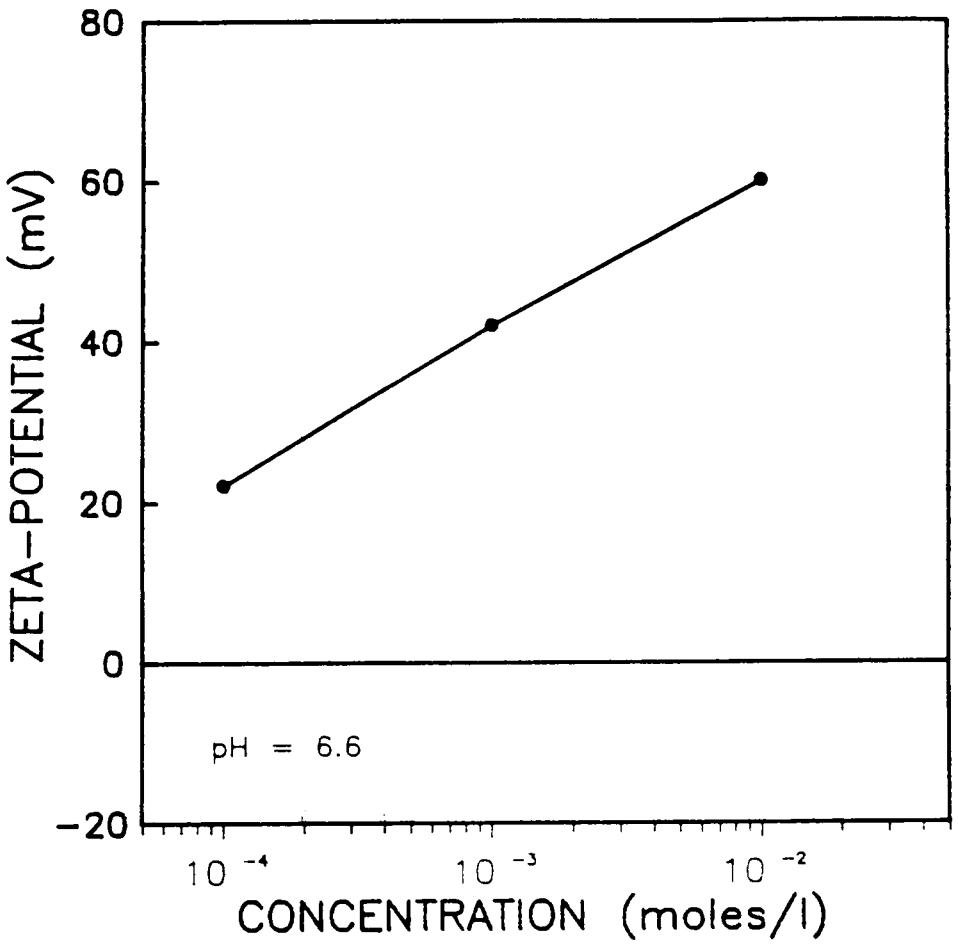

Figure 4.5 Effect of concentration on the zeta potential of air bubbles generated using different concentrations of dodecylamine hydrochloride (Yoon and Yordan, 1986; Laskowski, et al, 1988

TABLE OF RESULTS 4.1

Calculation of A_{131} values for silica and mica samples treated[1,2,3] in DAH and TMCS solutions

System	γ_s^d (mJ/m^2) (2)	A_{131} (J) (3)
Silica-DAH		
[DAH]		
$5x10^{-5}$	35.0	$-3.12x10^{-21}$
$1x10^{-4}$	32.0	$-1.06x10^{-21}$
$1x10^{-3}$	32.6	$-1.48x10^{-21}$
$5x10^{-3}$	34.4	$-2.71x10^{-21}$
Mica-DAH		
[DAH]		
$1x10^{-5}$	32.0	$-1.06x10^{-21}$
$1x10^{-4}$	33.8	$-2.30x10^{-21}$
$1x10^{-3}$	31.4	$-6.36x10^{-22}$
$1x10^{-2}$	33.2	$-1.89x10^{-21}$
Methylated silica		
%TMCS		
1	36.2	$-3.90x10^{-21}$
5	31.4	$-6.36x10^{-22}$
10	29.5	$-1.75x10^{-22}$
Pure Fused Silica		$-8.70x10^{-21}$ (1)
Pure Mica		$-5.20x10^{-21}$ (1)

(1) Israelachvili (1985)
(2) From Table 3.2
(3) Using Equation [3.14]

molecular component of the disjoining pressure always repulsive.

4.5 Results of the Thermodynamic Calculations

4.5.1 Thin films on Methylated Fused Silica Plates

The results of the critical rupture thickness (H_c) measurements presented in Chapter 3 established that the thin films of water on clean hydrophilic fused silica and mica plates are stable. The fact that the film is stable means that the total interaction energy is highly positive. However, contrary to wetting films on clean solids, those on methylated silica are very unstable. Depending on the hydrophobicity of the solid, it has been shown in this investigation that films rupture at thicknesses in the range of 80-145 nm. Nevertheless, the nature of the interfacial force (or forces) responsible for this phenomenon has not yet been identified. It is hoped that the thermodynamic calculations made in the present work can identify the force(s) responsible for the labilization of the disjoining film.

Table 4.2 shows the values of H_c, ζ and A_{123} used for the calculation. These values have been obtained from the results presented in previous sections. Calculations have been executed for fused silica plates treated with three different concentrations of TMCS.

Figure 4.6 shows the isotherms of dispersion interaction energy (V_D) as a function of separation distance for 1, 5 and 10% TMCS. The isotherms have been obtained using equation [4.7]. Note that in all three cases the isotherms are always positive indicating that the molecular interaction is repulsive. Note, also, that the magnitudes

TABLE OF RESULTS 4.2

Data Used for the Interaction Energy
Calculations for Silica Plates
Treated in TMCS Solutions

% TMCS	H_c (nm)	Zeta Potentials solid (mv)	bubble (mv)	A_{123} (J)
1	80	-45	-40	-3.9×10^{-21}
5	125	-30	-40	-6.4×10^{-22}
10	145	-22	-40	-1.8×10^{-22}

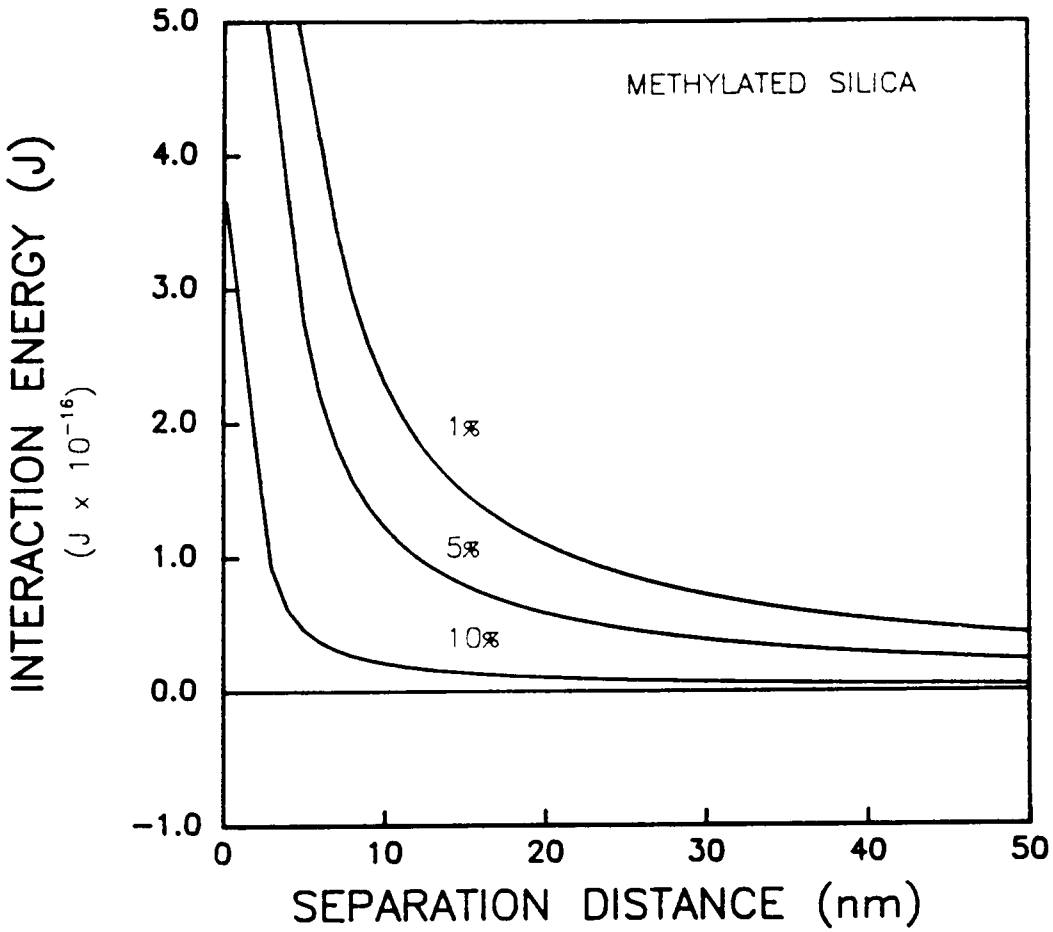

Figure 4.6 Isotherms of the dispersion component (V_D) of the interaction energy for methylated silica plates treated with 1, 5 and 10% TMCS

of the positive (repulsive) interaction energy increases drastically at short distances (1-30 nm). The most interesting observation is that the positive interaction energy decreases with increasing degree of methylation but it never becomes negative or attractive. It can be concluded, therefore, that the molecular component cannot be responsible for rupture of thin liquid films. This finding is in agreement with the suggestion by Laskowski (1986) and Kitchener (1984) on hydrophobicity of a solid but, evidently contradicts the view of Derjaguin and Dukhin (1961).

Figure 4.7 shows the isotherms of the electrostatic component (V_E) of the disjoining pressure obtained via equation [4.2]. The results show that V_E is also repulsive in all three cases studied. This outcome is not at all surprising since both the silica particles and the air bubble bear negative charges at neutral pH. It is well known that interaction between equally charged bodies results in repulsion. Note that the magnitude of the isotherm decreases with increasing methylation. This is obviously due to the reduction in the zeta potentials with increasing degree of methylation.

It is clear now that for the film to become unstable, the structural (V_S) component of the interaction energy must be attractive. Evaluation of V_S using Equation [4.17] requires the values of the parameters C and D_o for methylated silica. However, these values cannot be determined without direct force measurement. Therefore, in the present work, C and D_o have been estimated using the method described in section 4.2. The results of the C and D_o values

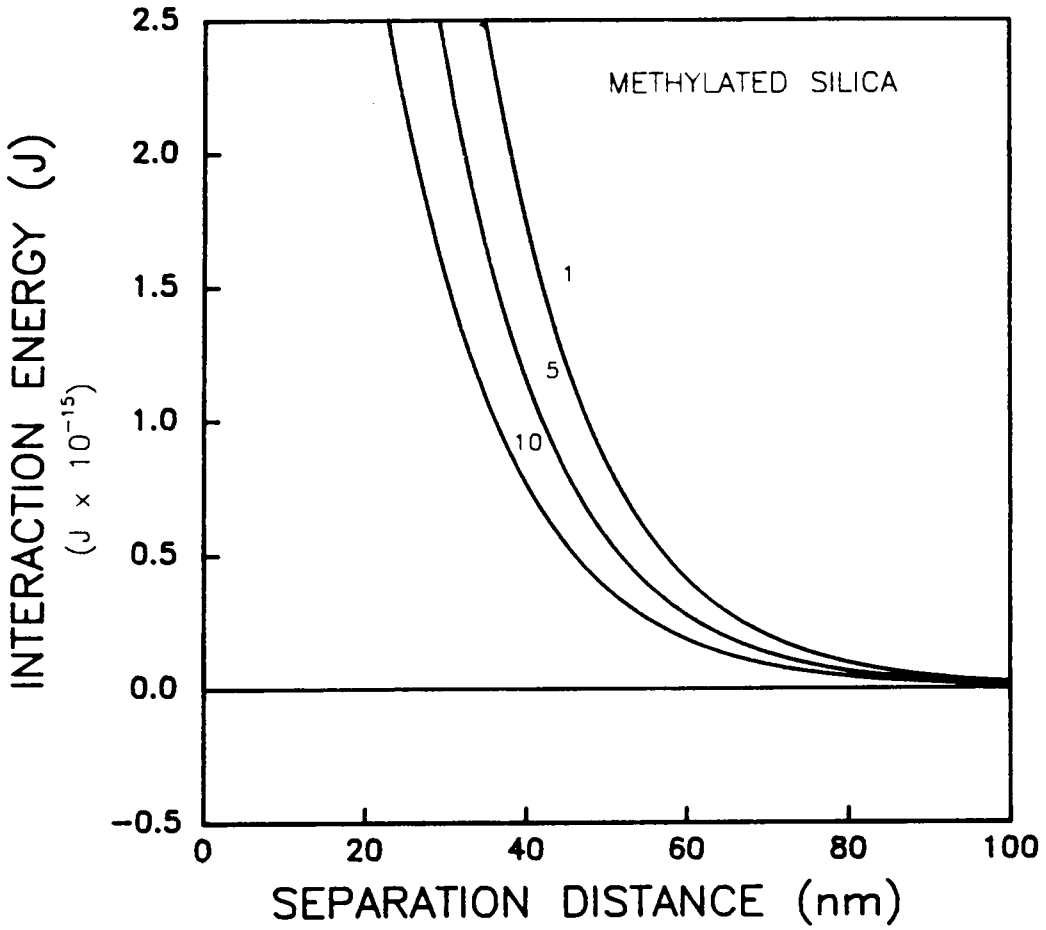

Figure 4.7 Isotherms of the electrostatic component (V_E) of the interaction energy for methylated silica plates treated with 1, 5 and 10% TMCS

are presented in Table 4.3. Note that C increases with increasing methylation suggesting that perhaps C is a good measure of hydrophobicity. As the silica becomes more hydrophobic C becomes increasingly positive because the trimethylsilane groups adsorbed on the surface change the structure of the water film on the surface. The structure changes in such a way that the repulsive structural force due to hydration becomes attractive. Also included in Table 4.3 are the results of D_o which compare very favourably with the value of 12.2 nm reported recently by Rabinovich and Derjaguin (1988).

Introducing the estimated values of C and D_o given in Table 4.3 into equation [4.15], one can calculate the isotherms of structural interaction energy (V_S). The results obtained are illustrated in Figure 4.8. Note that they are always negative (or attractive) and that the structural force increases with increasing methylation.

The combined effect of all three components of the interaction energy is shown in Figure 4.9 for the 1% TMCS fused silica plate. One can see that the shape of the V_T isotherm follows the shape of curve C in Figure 4.1 which is due to the competition between the repulsive components (V_E and V_D) and the attractive hydrophobic one (V_S). Note that in the long range, i.e. h >100 nm, the repulsive forces dominate. Under these circumstances, the total interaction energy is repulsive. However, at a separation distance of about 90 nm, the attractive structural force comes into play and the V_T isotherm reaches its maximum value at 80 nm before beginning to decrease in magnitude and follow the isotherm of V_S. At this critical

TABLE OF RESULTS 4.3

Calculated Values of C and D_o
for Silica Plates Treated
in TCMS solutions

% TMCS	C (J/m^2)	D_o (nm)
1	1.3×10^{-3}	13.44
5	2.5×10^{-3}	12.16
10	3.7×10^{-3}	12.03

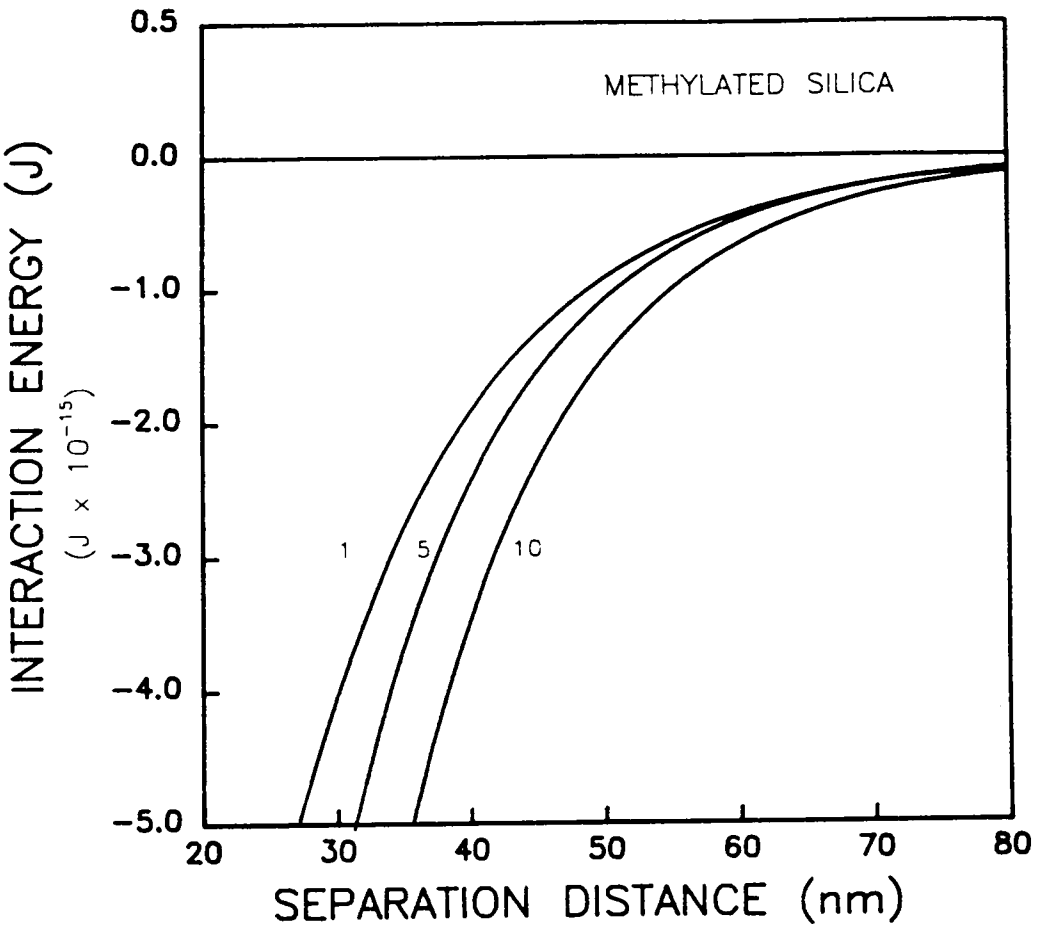

Figure 4.8 Isotherms of the structural component (V_S) of the interaction energy for methylated silica plates treated with 1, 5 and 10% TMCS

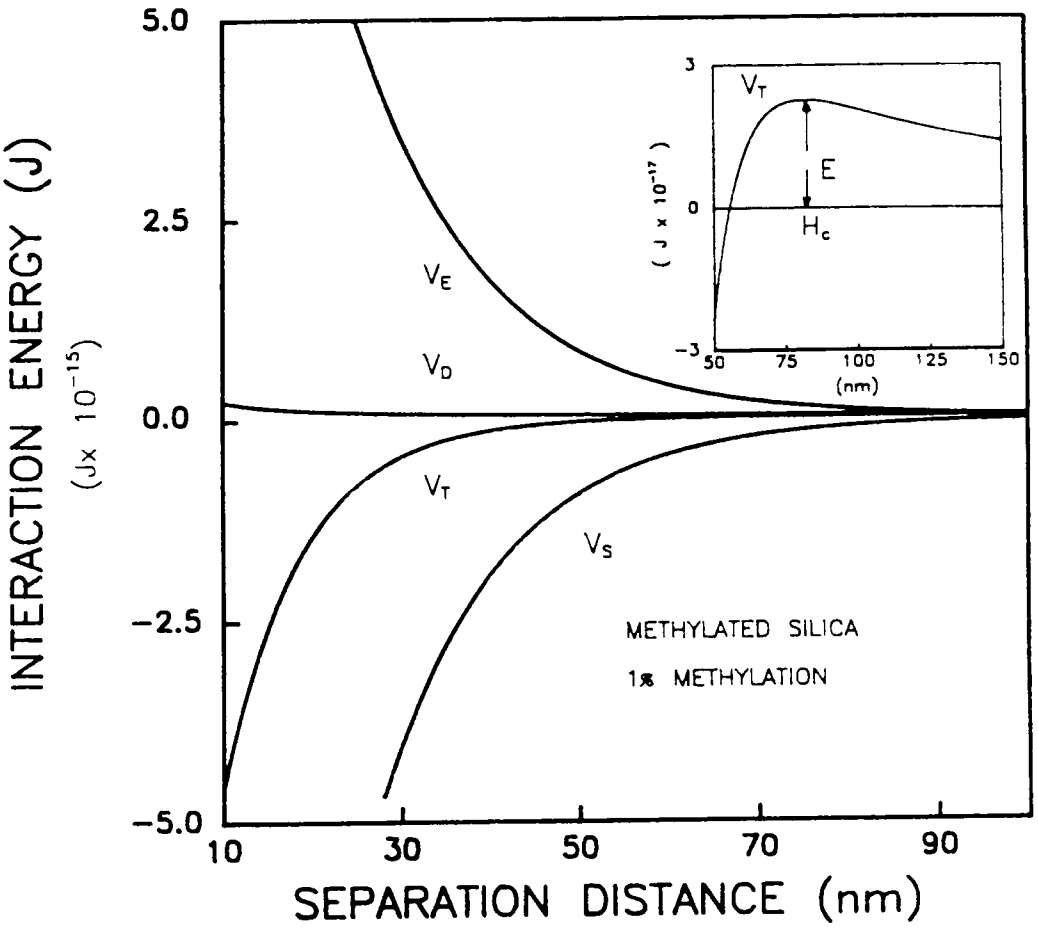

Figure 4.9 Isotherms of the dispersion (V_D), electrostatic (V_E), structural (V_S) and total (V_T) interaction energies for methylated silica plates treated with 1% TMCS. Insert: V_T isotherm around H_c . . . . . .

thickness, the film becomes unstable and ruptures catastrophically.

Figure 4.10 shows the isotherms of total interaction energy (V_T) for the three solid plates investigated. Note that, while all three of them behave as described above, the activation energy (E) decreases with increasing degree of methylation. This makes it easier for the air bubble to displace the thin film and form the three phase contact angle. The values of E calculated in the present work are presented in Table 4.4.

4.5.2 Thin films on Fused Silica-DAH Flotation system

It has been shown in Chapter 2 that wetting films on fused silica plates conditioned in solutions of dodecylamine hydrochloride (DAH) behave differently than those on methylated silica. In the former, the thin film could remain stable or rupture, depending on DAH concentration which in turn affect not only the hydrophobicity of the solid but also the bubble charge. This particular behavior makes the disjoining pressure analysis more complex. As a plausible starting point, let us consider the flotation behavior of quartz in DAH solution in relation to the contact angle, and bubble and particle charge and the contact angle. Figure 4.11 shows that as the concentration of DAH increases the flotation recovery increases concomitanly. Note that the sharp increase in recovery occurring between $1x10^{-5}$ and $1x10^{-4}$ moles/l correlates very well with a drastic increase in the contact angle. This indicates that the solid surface becomes increasingly more hydrophobic which

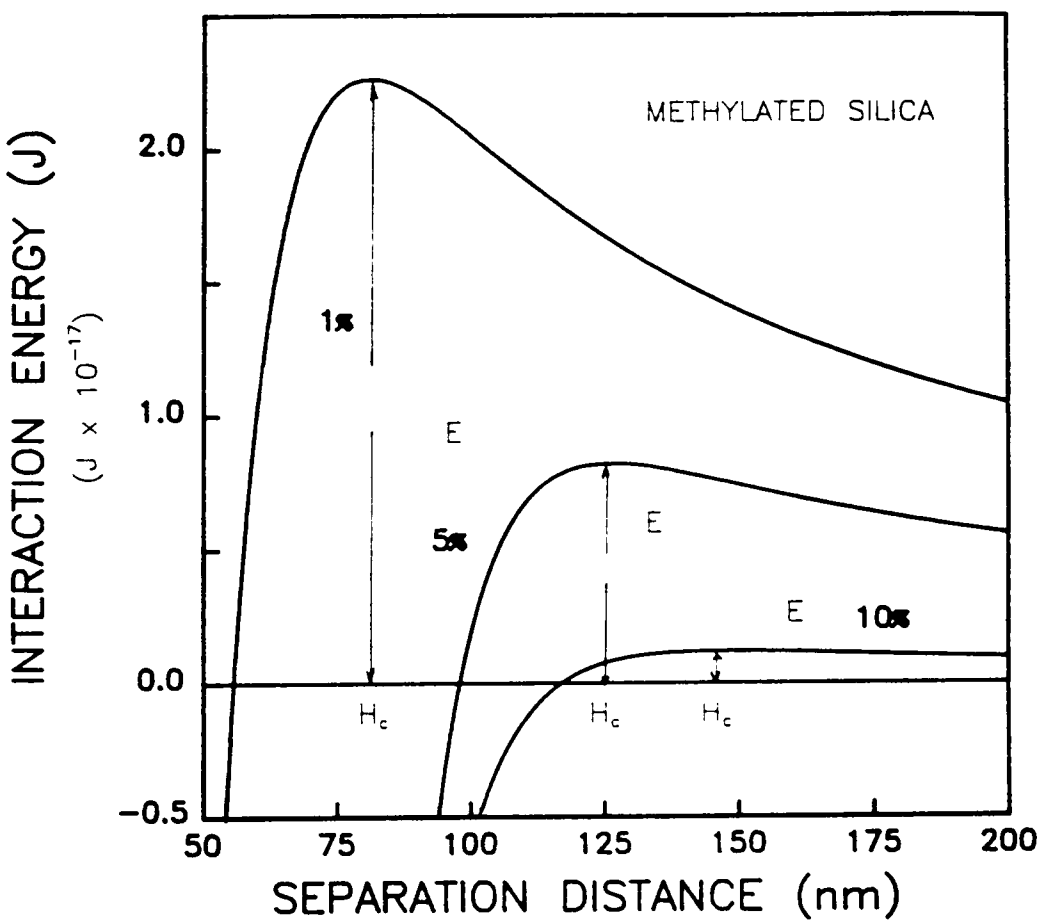

Figure 4.10 Isotherms of total interaction energy (V_T) for methylated silica plates treated with 1, 5 and 10% TMCS

TABLE OF RESULTS 4.4

Calculated Values of Activation Energy (E) for Silica Plates Treated in TCMS solutions

%TMCS	E (J)
1	2.26×10^{-17}
5	8.20×10^{-18}
10	1.19×10^{-18}

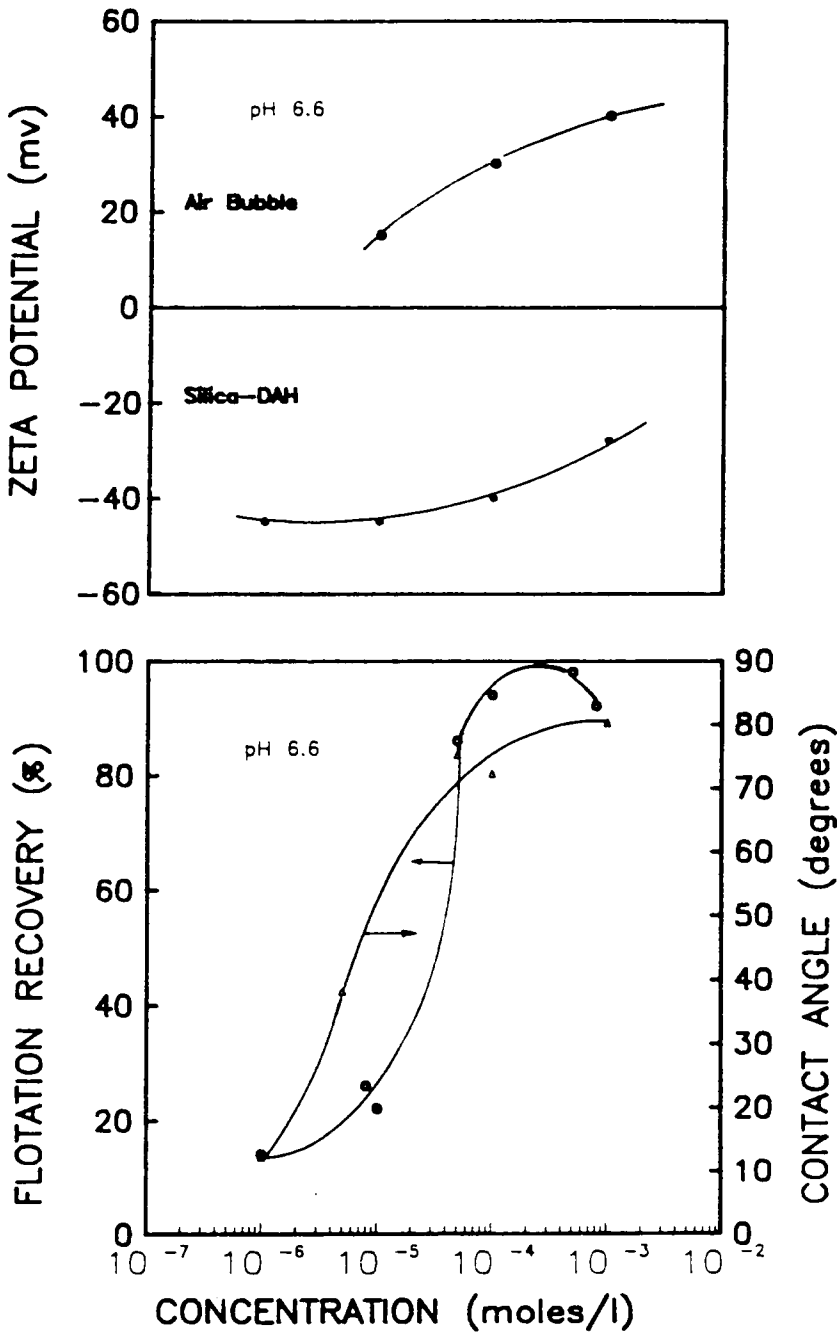

Figure 4.11 Top: Effect of DAH concentration on the Zeta Potentials of air bubbles and silica particles at pH 6.6.
Bottom: Effect of DAH concentration on the contact angles and flotation recovery of quartz at pH 6.6

renders the wetting film unstable and prone to rupture. This relationship has been previously reported by others (deBruyn, 1955; Fuerstenau, 1957). What has not been reported previously is the fact that the air bubbles and silica particles seem to carry opposite electrical charge throughout the concentration range investigated. It seems that in this case the electrostatic force is attractive rather than repulsive as was the case with methylated silica. In this regard, Claesson (1987) has recently measured, using the Israelachvili's surface forces apparatus, the attractive forces between a negatively charged hydrophilic mica surface and a positively charged hydrophobic one. These findings show that electrostatic forces can be attractive in flotation systems.

To explain the stability of the thin film at low DAH concentration (less than $5x10^{-6}$ Moles/l), one can make use of the interesting findings of Churaev and Derjaguin (1985) who showed that the value of C of Equation 4.17 remain positive on glass and quartz surfaces showing contact angles up to 20 degrees and V_s remains repulsive. Figure 4.12 shows the isotherms of V_s obtained using Churaev and Derjaguin data. It is, thus, possible to say that at low concentration of DAH the stability of thin films is controlled by hydration forces. However, C is still negative and, hence, V_S is positive at low DAH concentration. Only at a certain critical DAH concentration the constant C will change its sign and V_S becomes negative. Thus, one can say that the role of the collector is to displace hydration force with hydrophobic force.

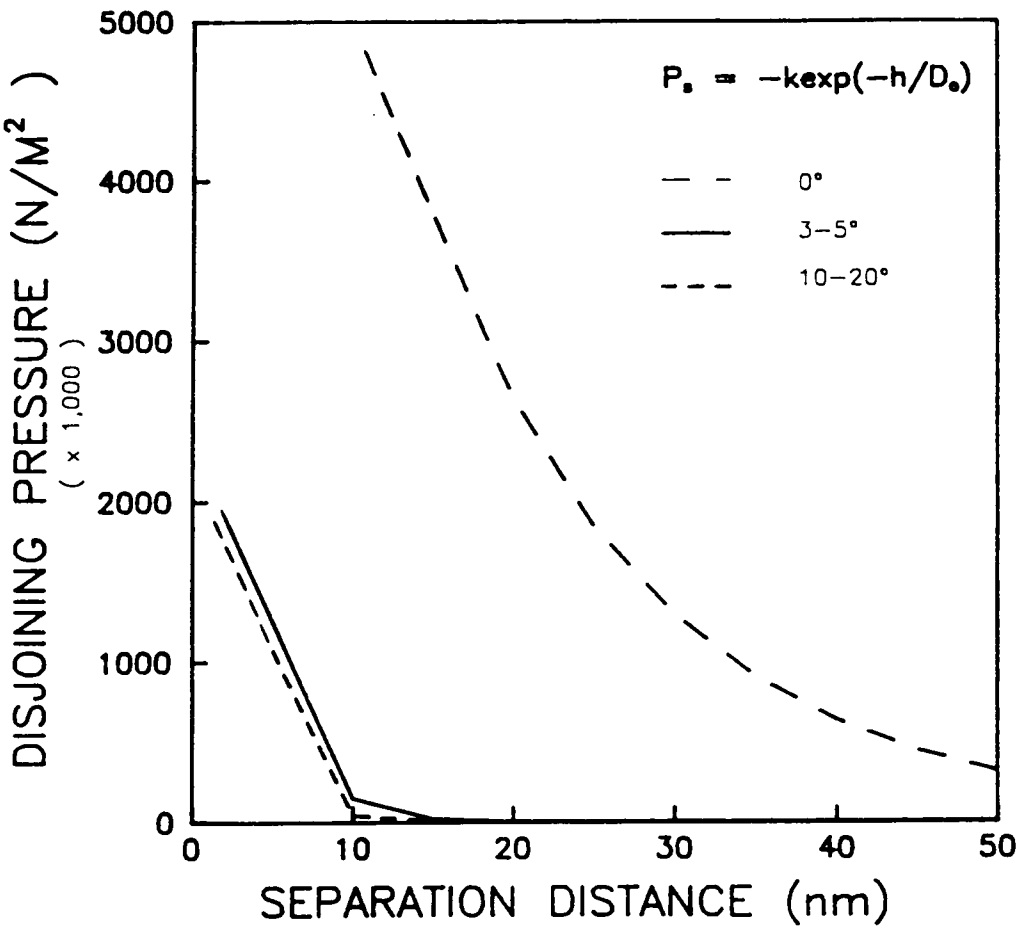

Figure 4.12 Isotherms of the structural component (V_S) of the disjoining pressure for silica plates forming different water contact angles. (calculated using Churaev and Derjaguin (1985) data)

Using the concept of reduction in the repulsive V_S and the thermodynamic calculations for bubble-particle adhesion, one can explain the rupture process of thin films at relatively low DAH concentration ($1x10^{5}$ moles/l) and also at a higher concentration ($5x10^{-4}$ moles/l). The values of the zeta potentials of air bubble and silica and complex Hamaker constant used in the calculations are given in Table 4.5.

Table 4.6 presents the values of C and D_o calculated following the procedure described in section 4.2. Note that C is negative indicating that V_S is repulsive at the DAH concentrations and pH range studied. However, the magnitude of C decreases with increasing DAH concentration. Figure 4.13 shows the results of the calculated V_S isotherms for the silica-DAH system. One can see that although in both cases V_S is repulsive, its magnitude decreases with increasing DAH concentration. This indicates that the adsorption of surfactant molecules at the solid/liquid interface reduces the hydration force by -preventing the water molecules to hydrogen bond with the silica surface. Note that the values of D_o calculated are similar to those obtained for methylated quartz and those of Rabinovich and Derjaguin (1988).

Figure 4.14 shows all four isotherms of interaction energy, i.e. V_E, V_D, V_S and V_T, for the silica-DAH system at a concentration of $1x10^{-5}$ moles/l. Note that the repulsive V_S isotherm dominate only in the long range of separation distances, while at shorter ranges (<70 nm), the attractive V_E predominates. Note also that the

TABLE OF RESULTS 4.5

Data Used for the Interaction Energy Calculations for Silica Plates Treated in DAH solutions

[DAH] (moles/l)	H_c (nm)	Zeta Potentials (mV) mineral	bubble	A_{123} (J)
$1x10^{-5}$	65	-50	20	$-3.12x10^{-21}$
$5x10^{-4}$	75	-22	30	$-2.00x10^{-21}$

TABLE OF RESULTS 4.6

Calculated Values of C and D_o
for Silica Plates Treated
in DAH solutions

[DAH] (moles/l)	C (J/m^2)	D_o (nm)
$1x10^{-5}$	$-6.13x10^{-4}$	13.66
$5x10^{-4}$	$-3.96x10^{-4}$	13.63

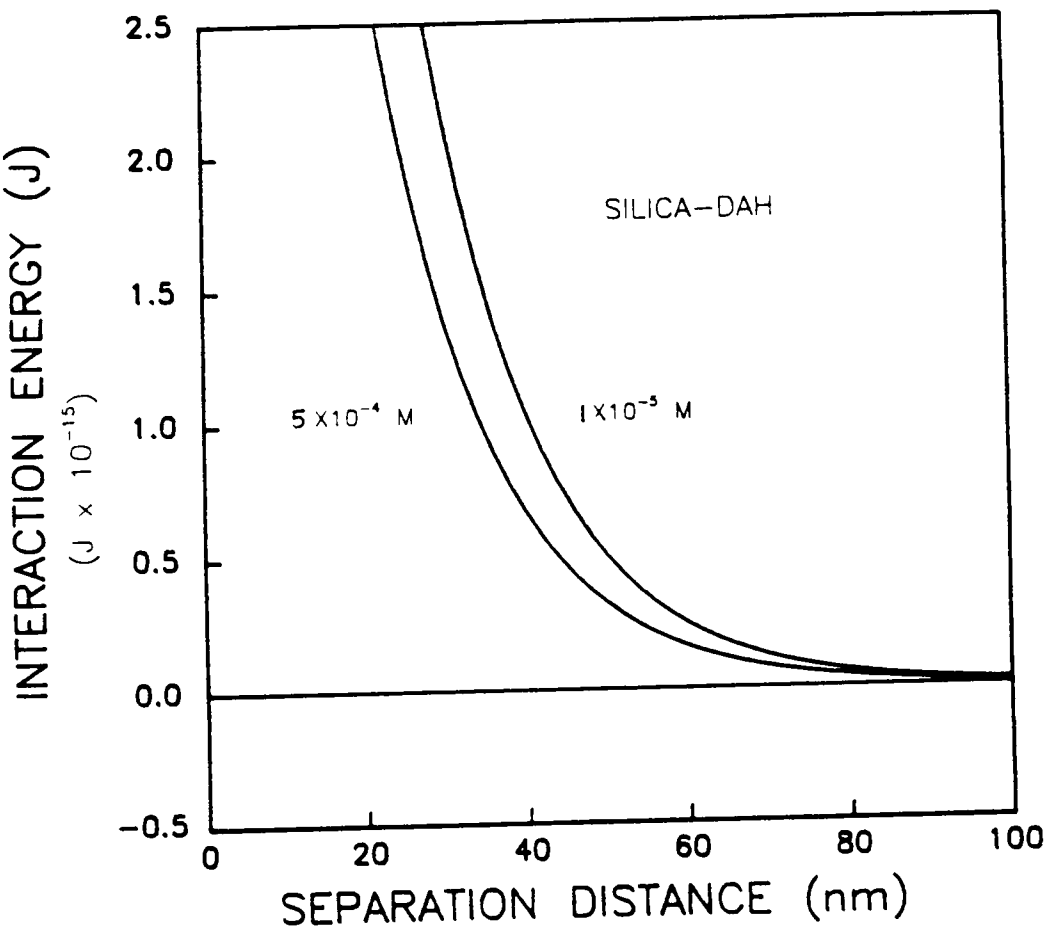

Figure 4.13 Isotherms of the structural component (V_S) of the interaction energy for silica plates treated with $1x10^{-5}$ and $5x10^{-4}$ M. DAH

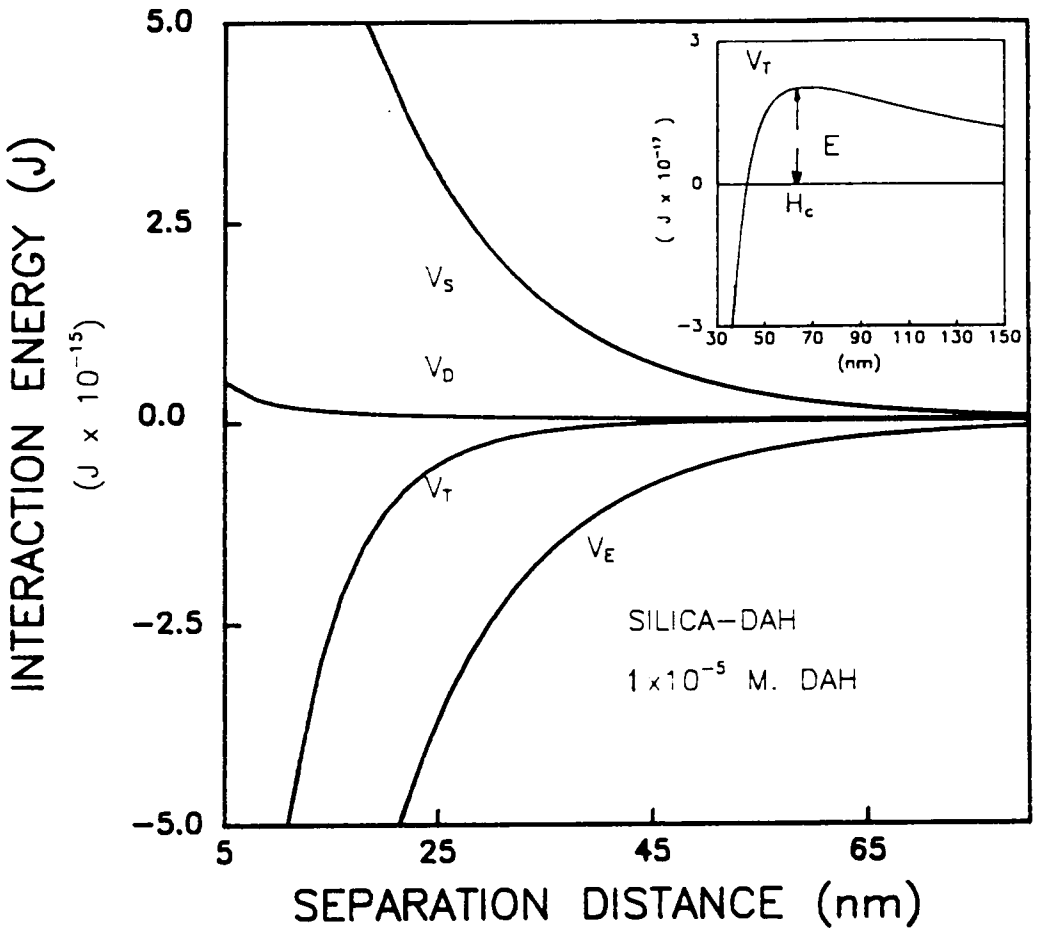

Figure 4.14 Isotherms of the dispersion (V_D), electrostatic (V_E), structural (V_S) and total (V_T) interaction energies for silica plates treated with $1x10^{-5}$ M. DAH.
Insert: V_T isotherm around H_c

contributions from V_D are smaller than those of the other two components. However, the behavior of the V_T isotherm resembles those obtained for methylated silica.

In figure 4.15 the isotherms of V_T for the silica-DAH system are illustrated. Note that the activation energy (E) decreases with increasing surfactant concentration which makes it easier for the particle to stick to the air bubble. The calculated values of E are presented in Table 4.7. Perhaps the more important conclusions to be drawn from this calculation is that the role of the surfactant in the adhesion process is threefold: i) to reduce the hydration force at the solid/liquid interface, ii) to provide the air bubble with an electrical charge opposite to that of the mineral surface and iii) to reduce the activation energy barrier (E).

One of the most interesting finding concerning the flotation of minerals with ionizable surfactants such as DAH is that the flotation behavior is almost always a function of the solution pH. Maximum recovery occurs in general in the pH region where the surfactant undergoes molecular association. The quartz-DAH flotation system is without a doubt the most studied of those flotation systems. It is well known that in this system the flotation maximum occurs in the pH region of 9-10 which correponds to the region where dissociation and hydrolisis of the surfactant molecules takes place. This characteristic behavior has been conveniently explained by Somasundaran (1976) by the hydrolysis of surfactant molecules into pre-micellar aggregates so-called iono-molecular complexes. In the

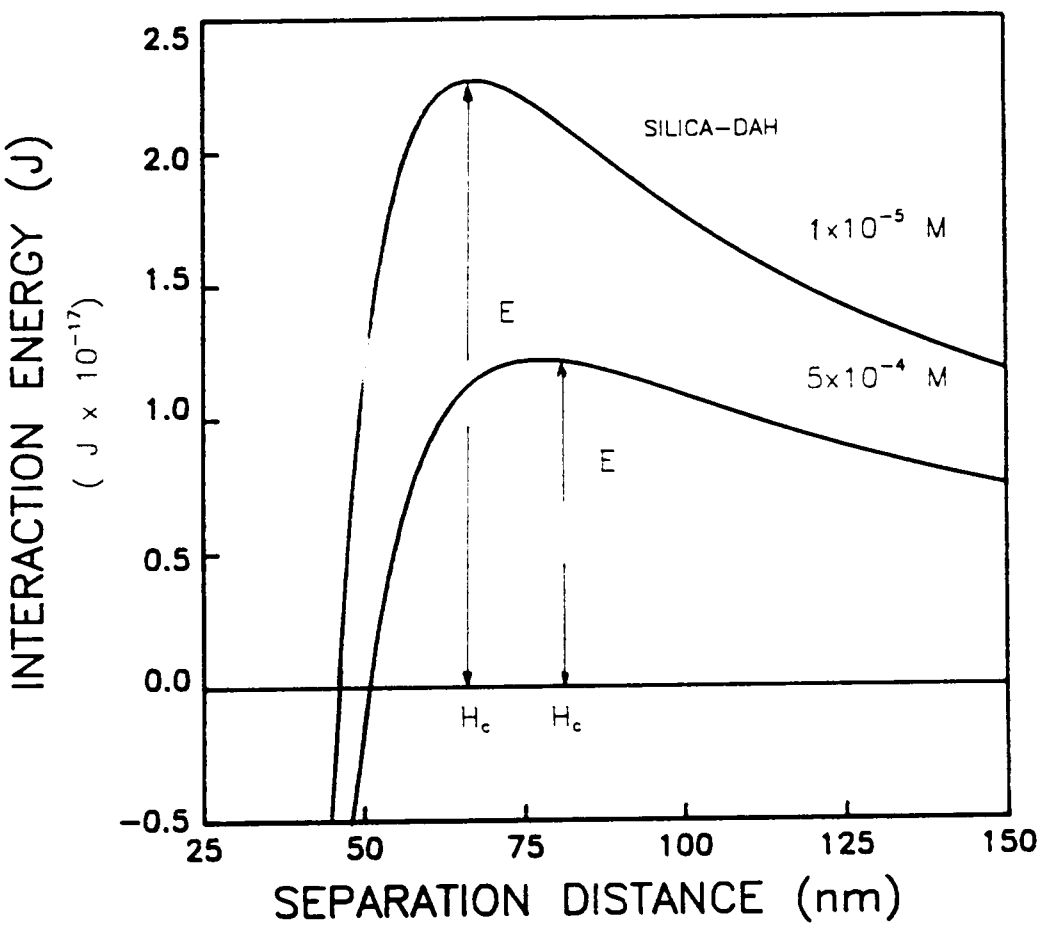

Figure 4.15 Isotherms of the total interaction energy (V_T) for silica plates treated with $1x10^{-5}$ and $5x10^{-4}$ M. DAH

TABLE OF RESULTS 4.7

Calculated Values of Activation Energy (E) for Silica Plates Treated in DAH solutions

[DAH] (moles/l)	E (J)
$1x10^{-5}$	$2.26x10^{-17}$
$5x10^{-4}$	$1.20x10^{-17}$

case of DAH, the complex (RNH_2-RNH_3^+) produced by amine/amminium ion association reaches its maximum concentration at or near pH 10.0. This complex is thought to be considerably more surface active than the monomer because of the increase in molecular size and low intrinsic solubility.

The results of the critical rupture thickness (H_c) measurements made in the present investigation have indeed indicated significant changes in the surface properties of the fused silica plates with increasing pH. Hence, it is of considerable interest to examine this system in the light of the thermodynamic calculations. The zeta potentials of air bubbles and silica particles obtained at $1x10^{-5}$ moles/l as a function of pH are shown in Figure 4.16. Also included in this figure are the results of flotation tests obtained in a previous work (Yordan and Yoon, 1986).

The results presented in Figure 4.16 provide useful information. Note that in the acidic to neutral pH range, the interacting bubble and particle carry opposite charges which induces an attractive double layer interaction (negative V_E); however, the flotation response is very poor. It appears that the onset of flotation takes place when the charge on the bubble is minimal or non-existent. Perhaps even more noteworthy is the fact that flotation maximum actually occurs at the pH where both of the interacting bodies carry negative charge. This seems to indicate that forces other than electrostatic attraction are maybe more important.

In an attempt to explain this particular flotation behaviour,

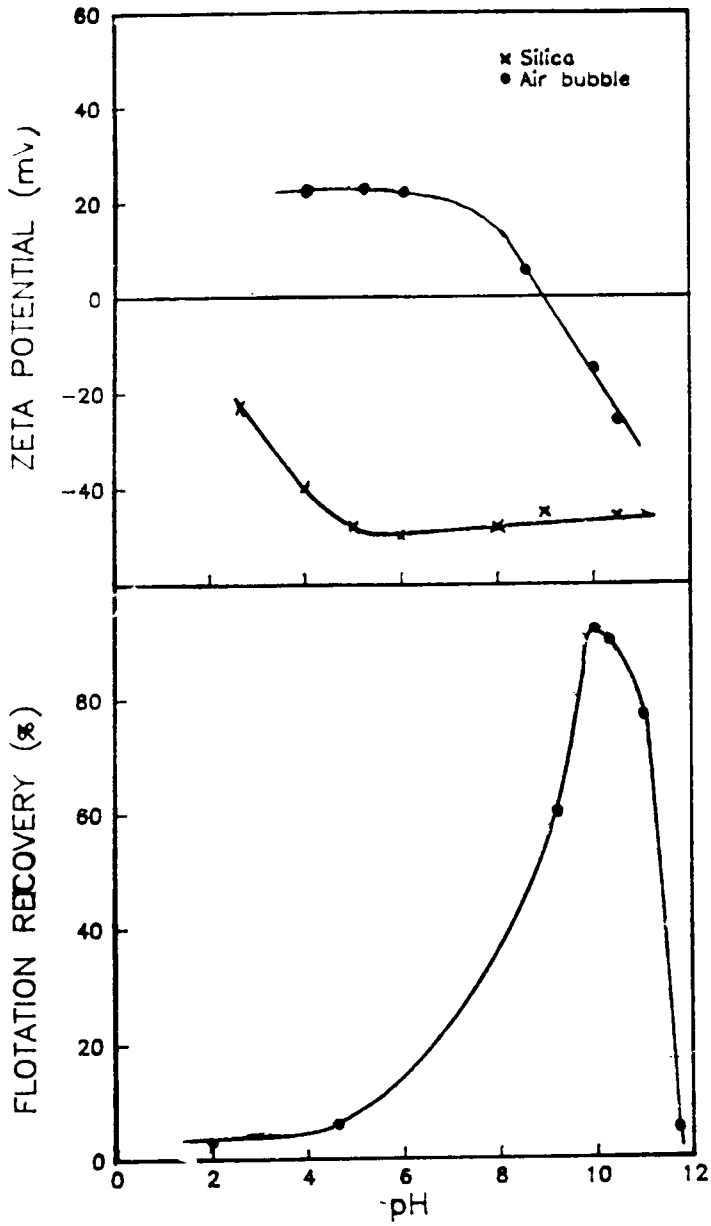

Figure 4.16 Top: Effect of pH on the zeta potentials of air bubbles and silica particles treated with $1x10^{-5}$ M. DAH.
Bottom: Effect of pH on the flotation recovery of quartz using $1x10^{-5}$ M. DAH

thermodynamic calculations similar to the ones carried out in section 4.5 have been conducted at pH 6 and at pH 10 to obtain the isotherms of V_E, V_S and V_T. The values of H_c, ζ and A_{123} used in the calculations are presented in Table 4.8.

Figure 4.17 illustrates the isotherms of V_E which clearly shows that while V_E is attractive at pH 6, it becomes repulsive at pH 10 as a result of the change in the sign of the zeta potential of the air bubble. The values of C, D_o and E obtained from the calculations are presented in Table 4.9. Note that C is negative at pH 6 and becomes positive at pH 10. The isotherms of V_S at pH 6 and 10, respectively, obtained using the corresponding values of C and D_o are illustrated in Figure 4.18. Note that V_S is positive at pH 6.0 indicating repulsion, becomes negative (attractive) at pH 10.0. Thus, it can be be concluded that the flotation maximum observed at pH 10 is the result of the conversion of a repulsive structural force into an attractive hydrophobic force. Figure 4.19 shows the isotherms of the total interaction energy (V_T) at the two pH's investigated. It is interesting to observe that the activation energy barrier (E) is reduced with increasing pH. The calculated values of E_o are given in Table 4.9.

TABLE OF RESULTS 4.8

Data Used for the Interaction Energy Calculations for Silica Plates Treated in $1x10^{-5}$ M. DAH Solutions of pH 6 and 10

pH	H_c (nm)	Zeta Potentials (mV) mineral	bubble	A_{123} (J)
6	65	-50	20	$-3.12x10^{-21}$
10	110	-45	-20	$-3.12x10^{-21}$

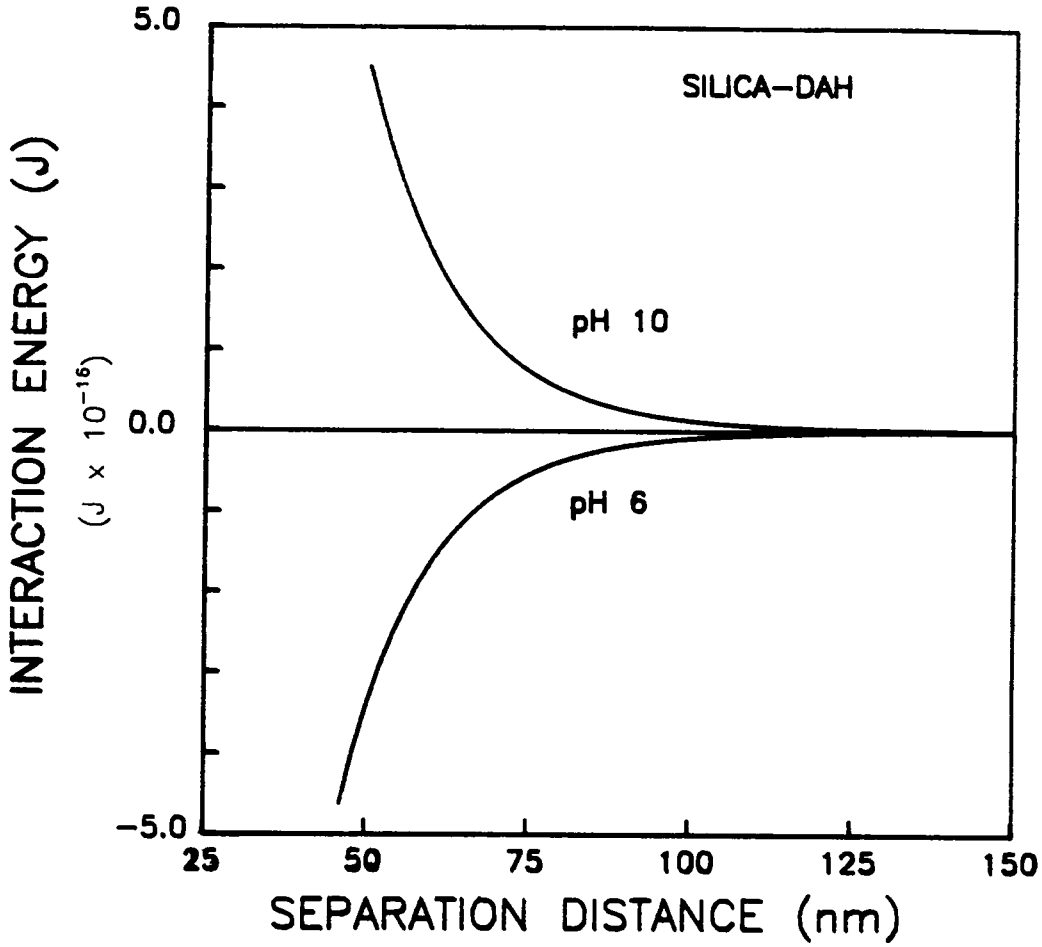

Figure 4.17 Isotherms of the electrostatic component (V_E) of the interaction energy for silica plates treated with $1x10^{-5}$ M. DAH at pH 6 and 10.

TABLE OF RESULTS 4.9

Calculated Values of C, D_o and E for Silica Plates Treated in $1x10^{-5}$ M. DAH Solutions of pH 6 and 10

pH	C (J/m^2)	D_o (nm)	E (J)
6	$-6.13x10^{-4}$	13.66	$2.26x10^{-17}$
10	$4.90x10^{-4}$	14.27	$8.00x10^{-18}$

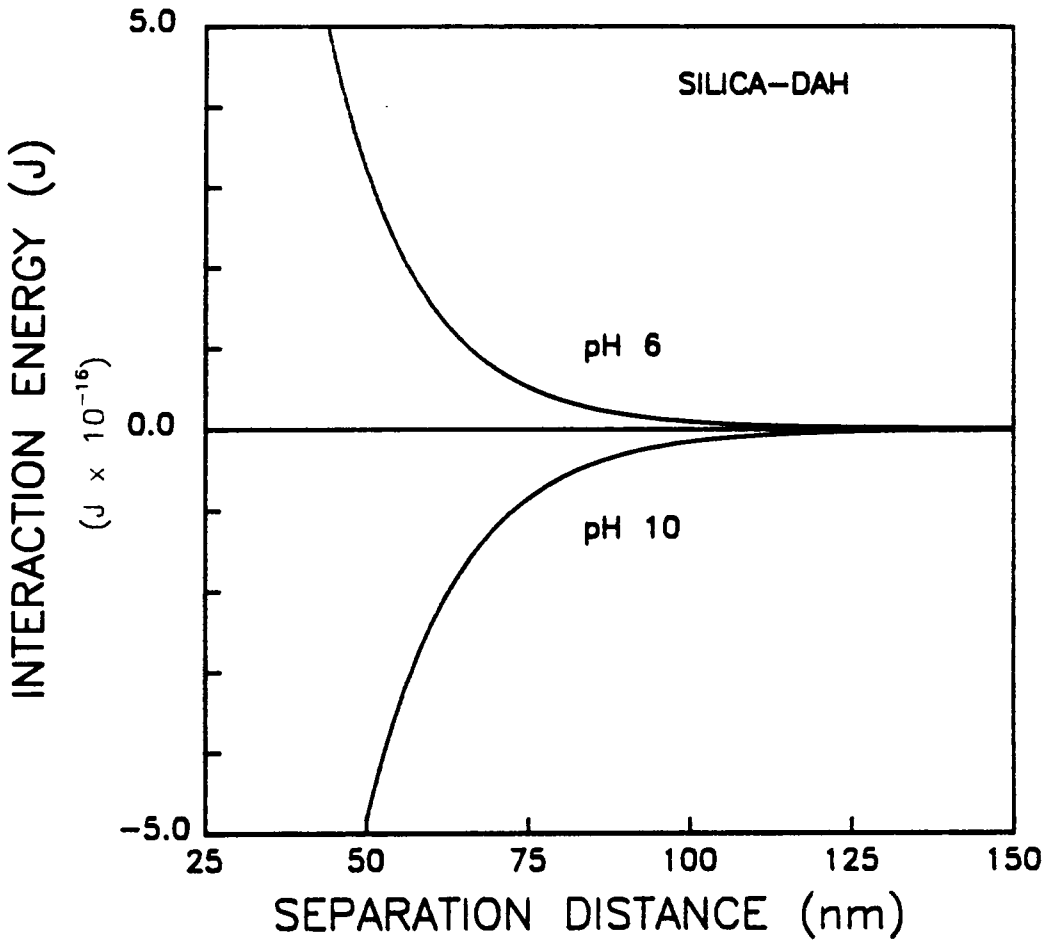

Figure 4.18 Isotherms of the structural component (V_S) of the interaction energy for silica plates treated with $1x10^{-5}$ M. DAH at pH 6 and 10.

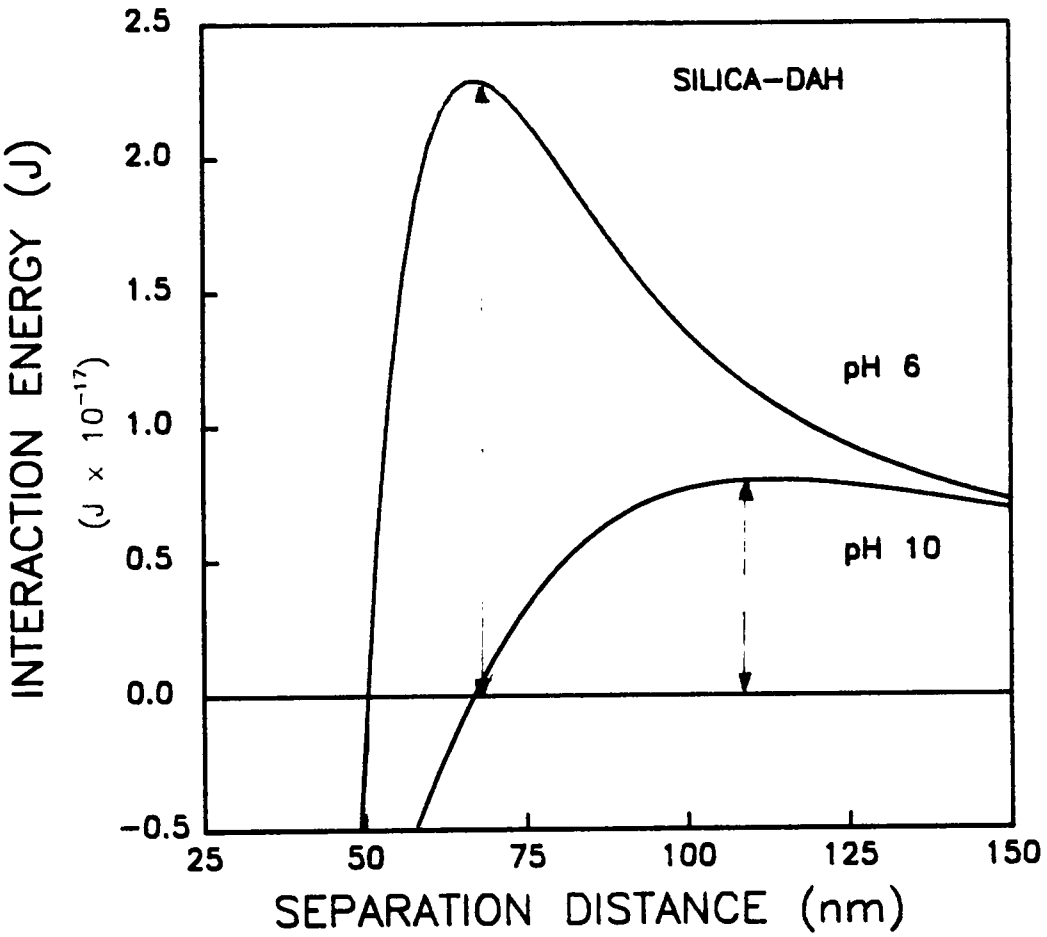

Figure 4.19 Isotherms of the total interaction energy (V_T) for silica plates treated with $1x10^{-5}$ M. DAH at pH 6 and 10 .

4.6 Summary and Conclusions

1.- Thermodynamic calculations of the bubble-particle adhesion process conducted in this work make it possible to estimate the individual interfacial surface forces involved. The calculations are based on the concept of disjoining pressure and make full use of parameters such as zeta potentials, Hamaker constants and critical rupture thickness.

2.- Through these calculations, the force(s) responsible for the behavior of thin film in flotation have been elucidated. It has been shown that repulsive electrostatic, dispersion and hydration forces are responsible for the stable films existing on hydrophilic minerals. It has also been shown that film rupture takes place when the repulsive surface forces are replaced by the attractive ones. In the case of methylated silica plates, it was the conversion of the repulsive hydration force into an attractive hydrophobic force that accounted for film rupture.

3.- In the presence of dodecylamine hydrochloride, the attractive force (forces) responsible for film rupture varies with solution pH. At low pH values the electrostatic force is attractive while the structural force is repulsive. Thus, although the disjoining film ruptures, the flotation recovery is not very significant. At a pH of 10, on the other hand, it has been found that the signs of these surface forces are reversed, i.e., the structural

force becomes attractive or hydrophobic whereas the electrostatic force becomes negative. Under these circumstances, the flotation recovery is at a maximum.

CHAPTER 5

APPLICATION TO COAL FLOTATION

5.1 Introduction

The production of superclean coal has been of considerable interest in recent years. Of all the cleaning-processes, flotation is one of the most versatile and economical processes. Microbubble flotation is a new technology developed at Virginia Tech by Yoon and his co-workers (1987). It involves several steps. First, coal is pulverized into micron-size particles to liberate the mineral matter, and then introduced into the microbubble flotation column to separate the liberated ash and sulfur from the coal. This process has two advantages over conventional froth flotation processes. Firstly, bubble particle collision efficiency is higher than in conventional flotation processes because of the small bubble size which leads to increased recovery; and secondly, entrainment of fine mineral matter in the concentrate is minimized due to quiescent conditions provided by bubbles that carry no wake. The result is the better coal recovery with improved ash rejection. The potential for the production of superclean coal by microbubble flotation has been shown in bench scale and pilot plant flotation experiments (Yoon, et al, 1988).

For the past several years, one of the prime interests of the Mineral Processing group at Virginia Tech has been to closely study the fundamentals of column flotation. One aspect that has deservedly received a great deal of attention is the bubble-particle

attachment process. A remarkable achievement in this area has been the development of a hydrodynamic model by Luttrell (1986). In his model, expressions for the probability of collision (P_c) and that of adhesion (P_a) have been derived for fine particle flotation by calculating the trajectory of particles as they flow past a bubble in streamline flow. This model was validated using a very hydrophobic coal from New Zealand (Buller Coal). Nevertheless, the parameter which characterized the probability of adhesion, i.e. the critical rupture thickness (H_c), was not experimentally accessible and was assumed to be constant. In the present investigation, the value of H_c for Buller coal is estimated from water contact angles using the method developed in Chapter 3. Since H_c has been shown to be a measure of mineral hydrophobicity, the coal samples have been oxidized at different temperatures and the effect of oxidation on H_c investigated.

5.2 Theoretical Background

Coal is a mixture of various organic and inorganic compounds. Its organic matrix is made of a wide spectrum of aromatic and aliphatic building blocks in which several heterogenous functional groups are incorporated. In addition, inorganic components such as clay minerals, pyrite, quartz, etc are present.

In general, coal is a predominantly hydrophobic solid and is relatively floatable; however, its natural hydrophobicity varies

considerably with its rank, origin and degree of surface oxidation. Also, chemical additives or collectors, such as kerosene, can be used to increase the natural hydrophobicity of coal particles and thus to increase their floatability. The main factors controlling the surface properties of coals are the following:

1) its hydrocarbon/aromatic skeleton (related to coal rank)
2) the content and nature of the active oxygen functional groups, and
3) the inorganic impurities in the coal.

Weathering and oxidation alter the surface properties of coals. These processes proceed in-situ for coal deposits that outcrop near the earth's surface. Alternatively, oxidation may occur during mining, stockpiling or processing especially when fine grinding is involved. Oxidation, whether it affects the bulk-coal sample or only a thin outer layer on the coal surface, is known to dramatically influence the wettability of the particle and hence such processes as flotation, filtration, flocculation and dispersion. In recent studies, Fuerstenau, et al (1983,1987) have shown that the products of oxidation which mainly are oxygen containing phenolic and carboxilic functional groups affect both flotation kinetics through film thinning phenomena and flotation thermodynamics through the control of the hydrophilic/hydrophobic distribution of surface sites.

Among the techniques available to study the effect of oxidation on the wetting characteristic of coals are: i) the contact angle,

ii) salt and film flotation, iii) induction time, iv)immersion time, v)critical surface tension and vi)immersion calorimetry.

The selection of a technique to determine wettability varies with sample type. For smooth surfaces, the contact angle provides a useful measure of the wettability of solids. In this classical method the angle formed when the solid, liquid and gas phases are brought together is measured. When the sample is in the form of a powder, the flotation techniques provide a more average measure of a coal's wettability (Fuerstenau, et al 1987). Salt flotation is a process in which a high concentration of inorganic electrolyte is employed. The first known use of salt flotation stems from the discovery that some coals were readily floated in sea water with no additional reagents. Only naturally hydrophobic materials float under such conditions (Klassen and Mokrousov, 1963; Laskowski, 1966). This process is very sensitive and flotation ceases completely if coal is heavily oxidized, so that it can be used as a standard test indicating the degree of relative surface oxidation. Film flotation is a relatively new technique introduced by D. W. Fuerstenau and his co-workers (1988) in which the separation of coal from its mineral matter is carried out by adjusting the surface tension of the flotation solution. In the present investigation both the contact angle and salt microflotation are employed.

The traditional methods discussed above are excellent indicators of the macroscopic hydrophobicity of coal surfaces. However, to better describe the hydrophobic-hydrophilic balance at a coal surface,

it is important to establish the corresponding chemical characteristics of coals. In this regard, numerous analytical and spectroscopic techniques have been used including: i) potentiometric titration, ii) microcalorimetry, iii) chromatography and iv) spectroscopic tecniques such as XPS and FTIR. In this work, microcalorimertry and FTIR spectroscopy has been used for the study of the coal surface.

5.3 Literature Review

It is well recognized that oxidation deteriorates the hydrophobicity and floatability of coal. According to Gutierrez and Aplan (1984b), oxidation makes a high rank coal behave as if it were one of lower rank. Coal can be oxidized in different ways. Although, dry oxidation has been the method most commonly used, wet-oxidation (Yordan and Yoon, 1988) and chemical oxidation (Celick and Somasundaran, 1980) are not uncommon.

The classical contact angle technique has been used extensively in the study of coal oxidation. Measurements have been conducted with either the captive bubble method developed by Wark and Cox (1934) or the sessile-drop method introduced by Zisman (1964). Recently, Gutierrez and Aplan (1984b) showed that wet-oxidation of a bituminious coal caused significant reductions in contact angle.

Because of the difficulties involved in the preparation of specimens required in the contact angle measurements, other techniques have been preferred. Microflotation and bench-scale flotation experiments have been employed. One of the first investigations of

the effect of oxidation on coal flotation was that of Sun (1954) who found that as oxidation proceeds coal becomes progressively more hydrophilic. Low temperature oxidation (100-150°C for 250 h) lowered the coal floatability only slightly, but more extensive heat treatment (200-350 °C) reduced it seriously. The loss of floatability was attributed to the accumulation of water-insoluble oxidation products at the coal surface. Celik and Somasundaran (1980) have shown that chemical oxidation of coal by as little as 10 mg per liter of potassium permanganate can almost totally depress coal flotation.

Recently, induction time measurements were shown to be useful in the study of coal oxidation (Yordan and Yoon, 1988). These investigators showed that the induction time increased with wet oxidation while the flotation recovery decreased concomitanly.

Infrared and XPS spectroscopy are two quite different surface sensitive techniques which have been shown to yield complementary chemical information applicable to the characterization of coal sufaces. Both techniques have in recent years become important tools in the study of the mechanism of coal oxidation. Infrared studies by Painter, et al (1981) and Mielzarski, et al (1986, 1988) have conclusively shown that incorporation of oxygen as carbonyl and carboxyl groups on the coal surface is the dominant effect of oxidation. The work of Phillips, et al (1986) using XPS indicated a drastic increase in the oxygen/carbon ratio when coal was dry-heated above 150°C.

Microcalorimetry has also proven to be a powerful tool for the

investigation of coal surfaces. Studies of heat of immersion of coals subjected to various degress of oxidation have recently been conducted (Phillips, et al, 1986; Melkus, et al, 1987). In general, the heat of wetting increases with oxidation. Adsorption calorimetry has been used to study surface polarity and site energy distribution. Typically, the results obtained by Templer (1987) and Grozeck (1988) indicate that oxidation increases the polarity of the surface.

5.4 Objectives

The aim of this chapter is to study the bubble-particle adhesion process for fresh and oxidized coal. To accomplish this goal, estimates of H_c are obtained from contact angle measurements using the methodology developed in Chapter 3. In addition, the thermodynamic aspects of the adhesion process are studied in light of the disjoining pressure calculations presented in Chapter 4. The necessary model parameters such as zeta potentials and Hamaker constants are experimentally determined. To correlate these finding with actual flotation conditions, salt flotation tests are conducted. Finally, the surface chemical properties of fresh and air-oxidized Buller coal are examined by calorimetry and infrared spectroscopy.

5.5 Experimental

5.5.1 Materials

a) Coal Sample

It is well recognised that the application of surface analysis tools to the understanding of the interfacial properties of coals is complicated by the heterogeneity and variability of the coal surface. To alleviate this problem and to isolate the effect of minerals matter, an extremely low ash coal (0.13-0.25%), Buller coal, from New Zealand has been used in this investigation without further cleaning.

b) Reagents

Double distilled water and research grade methylene iodide were the liquids used in the contact angle measurements. Research grade potassium chloride (KCl) supplied by Fisher Scientific Company, was used in the salt flotation tests, and hydrochloric acid (HCl) and sodium hydroxide (NaOH) were used for pH control. Double-distilled water, prepared in an all-glass still, was used in all the experiments. Ultra-pure nitrogen (99.999%) from AIRCO Industrial Gas Company was used to produce the bubbles for the microflotation tests.

Fuel reference grade n-heptane and research grade n-butanol from Fisher Scientific Co. were the reagents used in the calorimetry experiments. N-heptane was purified by successive passage through a column containing silica gel and activated 4 A molecular sieve. To keep it dry, n-butanol was stored over a molecular sieve. Solutions of n-butanol in n-heptane were prepared by weighing the appropriate

amounts of reagents.

5.5.2 Equipments and Procedures

a) Sample Preparation

The Buller coal from New Zealand was received as a +1/2" fraction and immediately stored in a freezer until needed. Large size chunks were hand-picked and appropriately cut for contact angle measurements. Coal slabs of 10x30 mm in size were cut by means of a diamond saw using water as cooling medium. Each specimen was wet-polished with emery paper (No. 600 and 1200) and washed in water in an ultrasonic bath to dislodge any adhering particle. Only homogeneous specimens were selected, avoiding those with cracks, different macerals, occlusions, etc. For the microflotation and microcalorimetry tests, the +1/2" fraction was passed through roll crushers to obtain a +150 micron fraction. The -150 micron fraction was discarded to avoid any iron contamination. The coarse material was further ground in a coffee grinder equipped with a cooling medium. Grinding for 2 minutes was adequate to produce a wide range of sizes. The Buller coal ground as such was wet-sieved and samples were sealed in plastic zipper bags and stored in a freezer. The +300-210 μm size fraction was used in the salt flotation and microcalorimetry experiments while the -210 μm size was further hand-ground using an agate mortar to obtain a -25 μm size fraction that was required in the infrared and electrophoresis measurements.

The coal samples used for salt flotation, microcalorimetry and

FTIR measurements were oxidized with air by heating them in a furnace for twelve hours at different temperatures. The coal samples were spread thinly in a pyrex dish in order to achieve fairly even oxidation. After oxidation the samples were removed from the oven, immediately covered with aluminium foil, allowed to cool in a dessicator over silica gel and finally stored in a freezer inside a zipper plastic bag until needed.

b) Microflotation

Microflotation tests were made using a Partridge and Smith (Partridge and Smith, 1971) type flotation cell. Bubbles were produced by sparging ultra-pure nitrogen gas through a medium-porosity glass frit at the bottom of the cell. The gas flow rate of 45ml/min STP was monitored using a flowmeter. Gentle agitation was provided by means of a teflon-coated magnetic stirring bar.

The flotation tests were conducted in electrolyte solution containing 0.01 M. KCl. One gram samples were conditioned for 10 minutes in 75 ml salt solution of different pH. After the conditioning the solution and the sample were transfered to the cell.
The recovery after one minute of flotation time was taken as a convenient measure of floatability.

c) Contact Angle Apparatus

The contact angle goniometer and the procedure employed was exactly the same as the one described previouly (Chapter 3). Oxidation of the coal specimens was carried out at 100 and 250°C in

air for a period of twelve hours.

d) Electrophoresis

The zeta potentials of fresh and oxidized Buller coals were determined following the procedure presented in Chapter 4.

e) Calorimetry

A Microscal Mark III flow microcalorimeter manufactured by Microscal, Inc. was used to study the surface and interfacial properties of fresh and oxidized Buller coal via heats of immersion and adsorption measurements.

The schematic representation of the instrument is illustrated in Figure 5.1. The instrument has a central stainless steel block (A) with a long 6-mm diameter cylindrical cavity in which a 6-mm deep adsorption bed (B) is enclosed between inlet and outlet tubes. The two thermistors (C) that project into the bed and the two thermistors in the block are in a Wheatstone bridge circuit that is very sensitive to the changes in bed temperature. Calibration of the heat sensing system is done with a calibration coil of fine wire place in the adsorption chamber. The unit is operated with two syringe pumps (D) for pumping solvent or solution at various flow rates and two VALCO valves (with loops) for switching from carrier fluid (solvent) to solution and back again. The calorimeter is also equipped with a vacuum pump and liquid nitrogen trap to evacuate the sample in-situ.

In a typical experiment, 150-160 mg of -300+250 μm size Buller coal was dry-loaded into the bed and outgassed for 45 minutes to 1

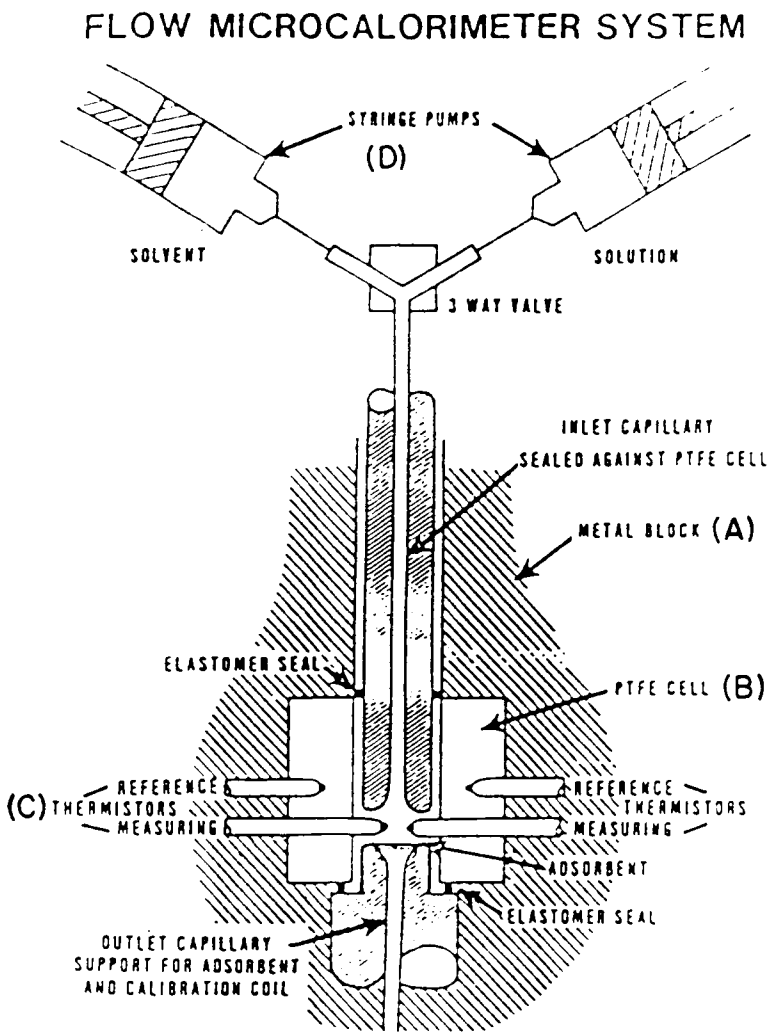

Figure 5.1 Schematic representation of the Microscal Flow microcalorimeter

hour at room temperature. During the pumping stage the decrease in pressure was monitored. The endothermic peak (Peak A in Fig. 5.2) occuring as a result of evaporative cooling of the bed as traces of adsorbed water evaporates was recorded. The pumping continued until the evaporative cooling process was over. Then, the sample was wetted with pure solvent and the resulting heat of immersion recorded (Peak B). The flow of solvent was continued at a rate of 3.3 ml/h until thermal equilibrium was again reached. The flow of solvent was stopped and replaced by the flow of the same solvent containing known amounts of adsorbent. A heat effect (Peak C) was recorded when adsorbent molecules adsorb onto the coal surface. Typically, the entire sequence of heat evolutions was completed in less than two hours. Desorption of the adsorbent was also studied by exchanging the flow of the solution for that of pure solvent. This process usually lasted a little longer than the corresponding adsorption and was accompanied by a heat effect (Peak D) which is opposite in sign to that of adsorption. All of the experiments were carried out at room temperature with the temperature in the block kept at 22±0.5°C

f) FTIR

The infrared spectra were recorded on a Perkin-Elmer Model 1710 FTIR with an MCT detector using an attenuated total reflection attachment (Spectra Tech, Inc) with a KSR-5 crystal with 50 reflections. This crystal was selected following the recomendations of Mielzarski, et al (1986). The spectra were taken at 4 cm^{-1} resolution by co-adding 100 scans in the 4000-500 cm^{-1} region. The

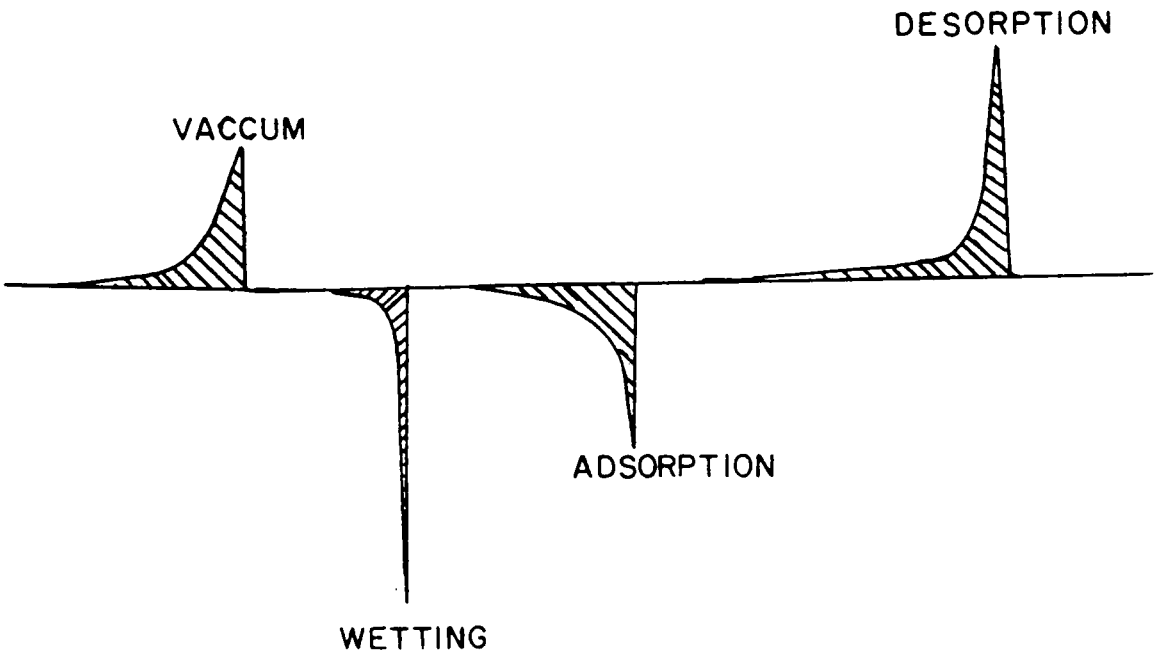

Figure 5.2 Typical output of the microcalorimeter: a:vacuum; b:wetting; c:adsorption and d:desorption

data were manipulated with a Perkin-Elmer Model 7500 computer. The preparation of the sample was reduced to simply contacting of the coal particles with the reflection element.

5.6 Results and Discussion

5.6.1 Contact angle measurements

The results of the water sessile drop contact angles measured as a function of oxidation temperature are presented in Table 5.1. As seen, the contact angle decreases with increasing oxidation temperature. This finding indicates that the surface hydrophobicity of fresh coal is deteriorated by the oxidation process. Other authors have observed similar results (Gutierrez and Aplan, 1984b). Also included in table 5.1 are the calculations of work of adhesion obtained using the results of the contact angle measurements. Note that the W_A increases with oxidation indicating that the surface of oxidized coal interacts more strongly with water molecules than that of fresh coal.

The values of H_c for fresh and oxidised Buller coals have been estimated calculated from the work of adhesion using the H_c vs W_A plot shown in Figure 3.3. The results of the estimation are also included in table 5.1. As expected, H_c is maximum for fresh coal and decreases steadily with increasing oxidation temperature.

5.6.2 Salt flotation experiments

The adhesion characteristics for attachment of air bubbles to fresh and oxidized coals are measured in this investigation by the salt flotation method. It has been shown by Laskowski (1966) that salt flotation is sensitive to the degree of oxidation of coal surfaces.

Figure 5.3 shows the results of the salt flotation tests

TABLE OF RESULTS 5.1

Contact Angle measurements for
Fresh and Oxidized coal

Oxidation Temperature °C	Contact Angle (degree)	Work of Adhesion (mJ/m^2)	Critical Rupture Thickness (nm)
Fresh	82±2	83.0	85±5
100	74±2	92.5	65±5
175	60±3	108.8	45±5
250	52±4	117.2	30±5

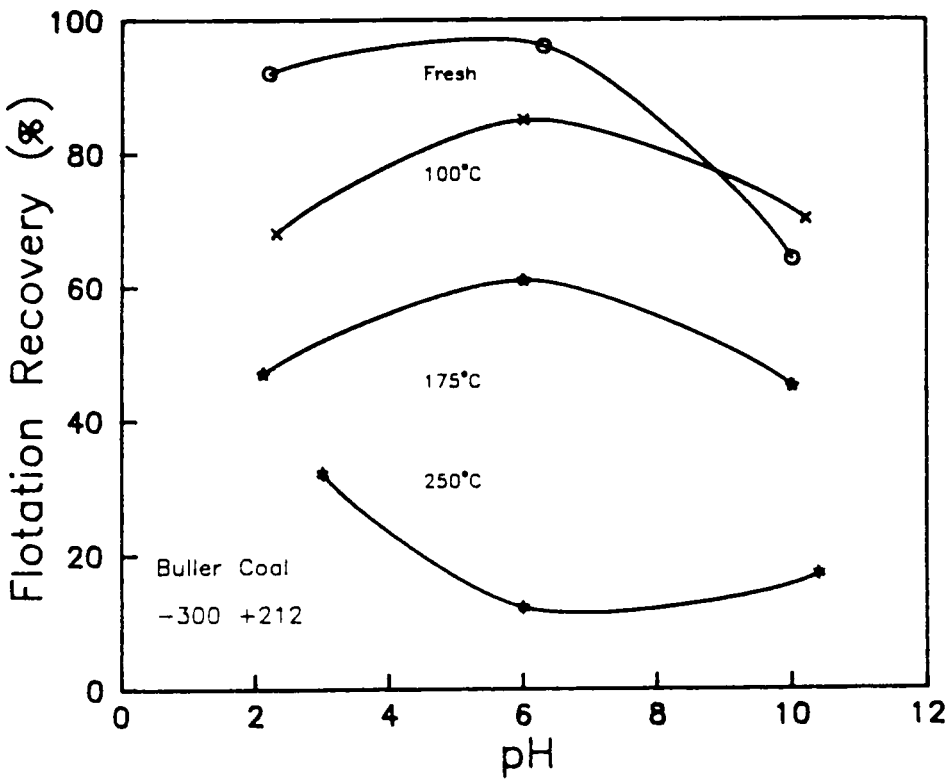

Figure 5.3 Effect of pH on the salt flotation recovery of fresh and oxidized Buller coals

conducted as a function of pH for fresh and oxidized coal. For the sake of clarity, the results of the tests conducted at about pH 6 are replotted as a function of oxidation temperature in figure 5.4. It shows more clearly that the recovery decreases with increasing oxidation temperature. The flotation recovery of fresh coal is at a maximum (98%) in the neutral pH region and then decreases steadily as the oxidation progresses. After 12 hours of oxidation at 250°C, the flotability is substantially reduced to approximately 12%. This indicates that as the oxidation of the coal surface progresses, the displacement of the wetting film by an air bubble from the surface of the coal becomes increasingly difficult. The reason is, of course, that oxidation produces hydrophilic species on the coal surface. The most likely oxidation products are carboxylic and phenolic groups (Fuerstenau, et al,1987). These weak acid functional groups ionize in aqueous solutions and affect the electrical charge of the coal. In addition, water molecules may form hydrogen bonds to these surface oxygen molecules.

The relationship between flotation recovery and critical rupture thickness H_c for Buller coal is illustrated in figure 5.5. As shown the flotation recovery increases with increasing H_c. This result can be explained by examining the results of the hydrodynamic collection model (Figure 1.2) developed by Luttrell (1985) which indicate that the probability of collection increases drastically with increasing H_c. Since the probability of particle flotation is directly proportional to the probability of collection, it is logical

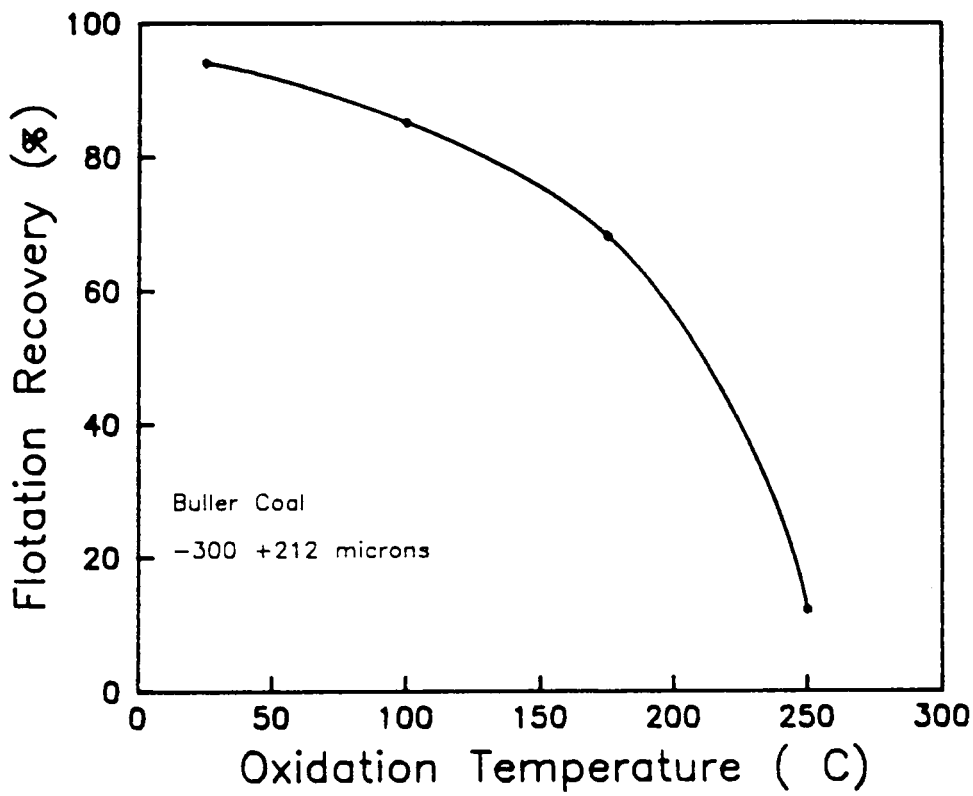

Figure 5.4 Effect of oxidation temperature on the flotation recovery of Buller coal

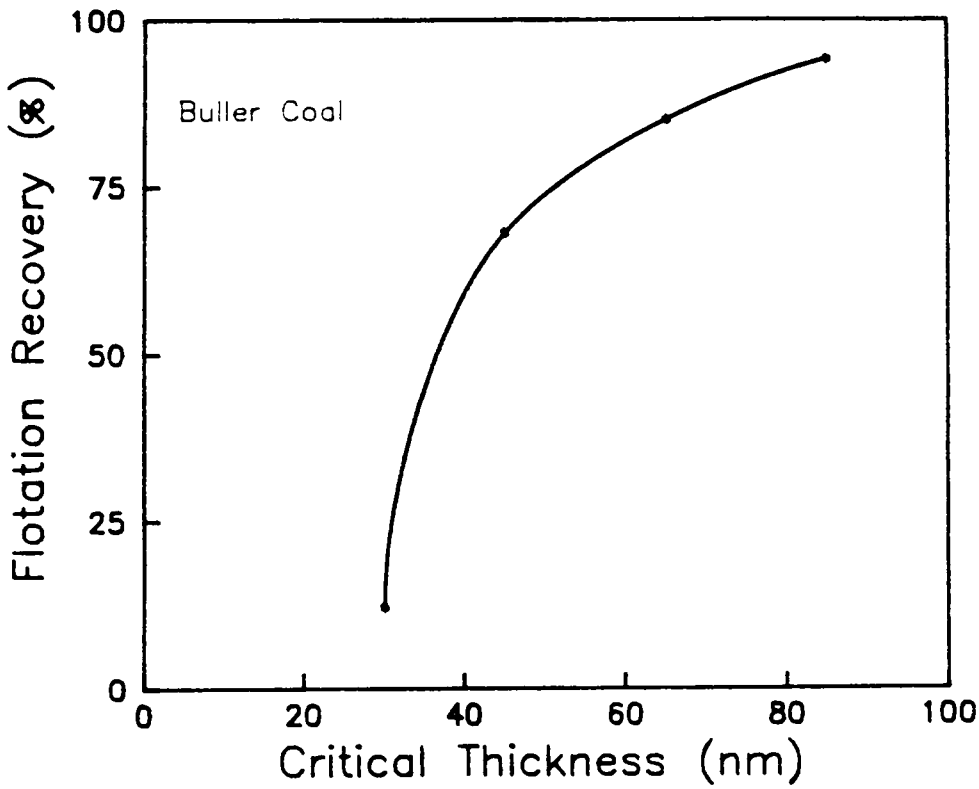

Figure 5.5 Critical rupture thickness (H_c) versus flotation recovery of Buller coal

to expect that a physico-chemical variable such as H_c that affects probability of collection will affect flotation recovery as well.

5.6.3 Thermodynamic calculations

The results presented in the previous sections have indicated that the bubble-to-coal adhesion process is seriously affected by oxidation. It has been speculated that this occur as a result of changes in the surface of the coal and therefore in the nature of the interfacial surface forces involved. In this section, the attachment process is examined in the light of the thermodynamic calculations presented in Chapter 4. It is hoped that through this analysis the forces responsible for the observed changes are identified. Prior to using the model, the necessary parameters i.e. zeta potentials of coal and air bubble, complex Hamaker constants of fresh and oxidized coal and estimates of H_c are determined as described in previous sections.

The electrophoretic behavior of Buller coal in 0.001 M. KCl solution was studied as a function of pH and degree of oxidation. The results obtained are illustrated in Figure 5.6. As shown, fresh Buller coal exhibits an isoelectric point at about 3.9 which is closed to that reported by other authors using different types of coals (Fuerstenau, et al, 1987; Wen and Sun, 1977; Campbell and Sun, 1970). For fresh coal, a charging mechanism similar to that of oxide minerals has been proposed by Campbell and Sun (1970). It has been suggested that OH^- and H^+ are the potential determining ions. The zeta potentials of oxidized coals are also presented in figure 5.6. Note

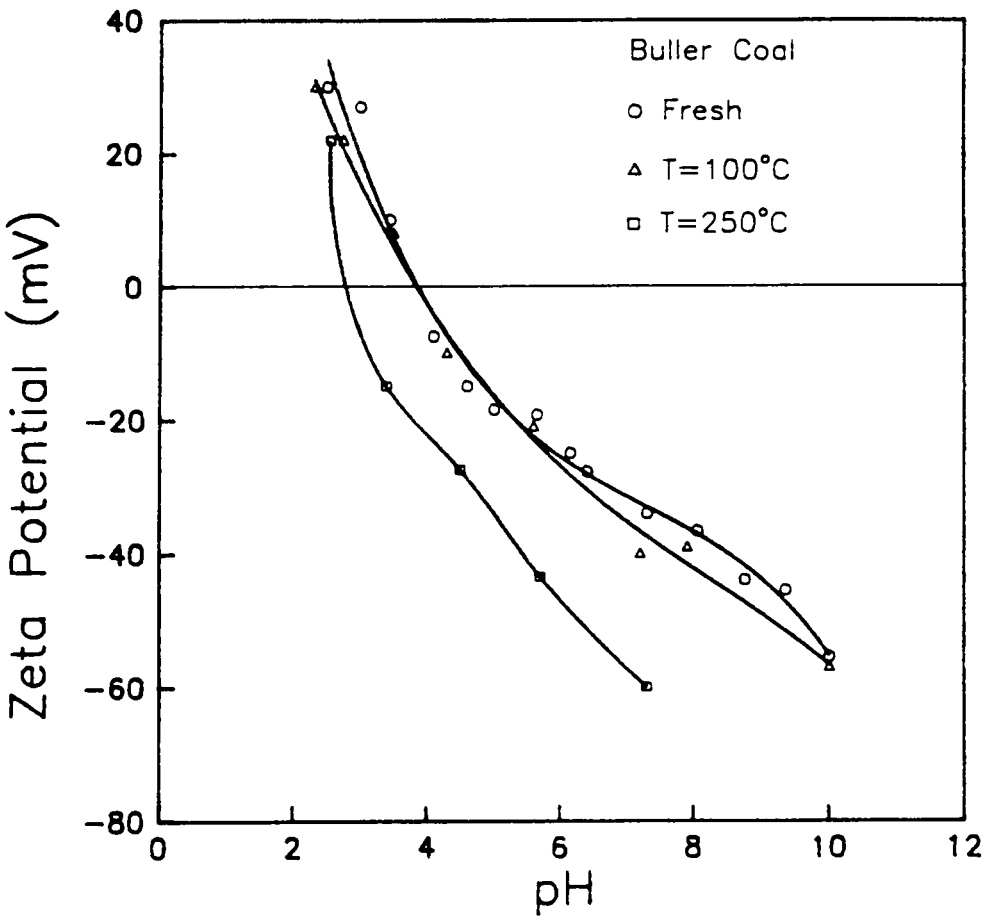

Figure 5.6 Effect of pH on the zeta potentials of fresh and oxidized Buller coal

that the electrokinetic behaviour of the Buller coal treated at 100°C is very similar to that of fresh coal. This suggests that low-temperature oxidation does not produce significant quantities of acidic surface groups on the coal surface at least not enough to affect the zeta potentials. This result seems to follow those of the salt flotation tests in which it was shown that the recovery was not drastically affected by heating at 100°C. On the other hand, coal oxidized at 250°C shows a different electrokinetic behavior. From the results, it is clear that the isoelectric point (iep) shifts towards the acidic pH range. Such a shift has been observed by many other researchers (Campbell and Sun, 1970; Wen and Sun, 1977; Fuerstenau, et al, 1987) and has been attributed to the presence of carboxylic (COOH) and phenolic (OH) functional groups on the coal surface. It appears that the surface charge is determined mainly by the degree of dissociation of such groups. The extent of dissociation varies with pH. At high pH values, the carboxyl groups tend to dissociate and the surface acquires a strong negative charge. In acidic medium the carboxyl group reprotonate, resulting in the reduction of the negative surface charge.

Oxidation can also affect the zeta potentials in a different way. Note that the magnitude of the zeta potential is increased at any given pH. This increases in the charge of the coal as oxidation proceeds increases the repulsive electrostatic forces when coal interacts with negatively charged air bubbles. Repulsive electro-static forces are known to retard the kinetic of the attachment

process.

In order to evaluate the molecular forces of fresh and oxidized coals, the sessile drop contact angle of methylene iodide was measured. The estimates of the Hamaker constants were obtained using Equation [4.16].

The values of the parameters used in the thermodynamic calculations are presented in Table 5.2. Calculations have been made for fresh coal and coal oxidized for 12 hours at 2 different temperatures, i.e., 100°C and 250°C. The methodology followed is essentially the same as that presented in chapter 4. Firstly, the unknown parameters C, D_o and E are determined and secondly the isotherms of the individual and total interaction energy are evaluated.

Figure 5.7 shows the isotherms of the dispersion component (V_D) of the interaction energy for fresh and oxidized coal. These isotherms were evaluated using Equation [4.7] and the data of A_{123} given in table 5.2. As shown, in all three cases the isotherms are always positive indicating that the dispersion forces are repulsive. These results are in accordance with those obtained for the other flotation systems studied in chapter 4. Notably, the magnitudes of the repulsive forces do not seem to be very much affected by the oxidation process.

The isotherms of the electrostatic component (V_E) of the interaction energy for fresh and oxidized coals have also been calculated using Equation [4.2] and the zeta potential data given in

TABLE OF RESULTS 5.2

Data used in the Interaction Energy
Calculations for fresh and oxidized coal

Treatment	H_c (nm)	Zeta Potentials (mV) Bubble	Coal	A_{123} (J)
Fresh	85	-40	-25	-8.5×10^{-21}
100°C	65	-40	-27	-9.3×10^{-21}
250°C	30	-40	-45	-1.1×10^{-20}

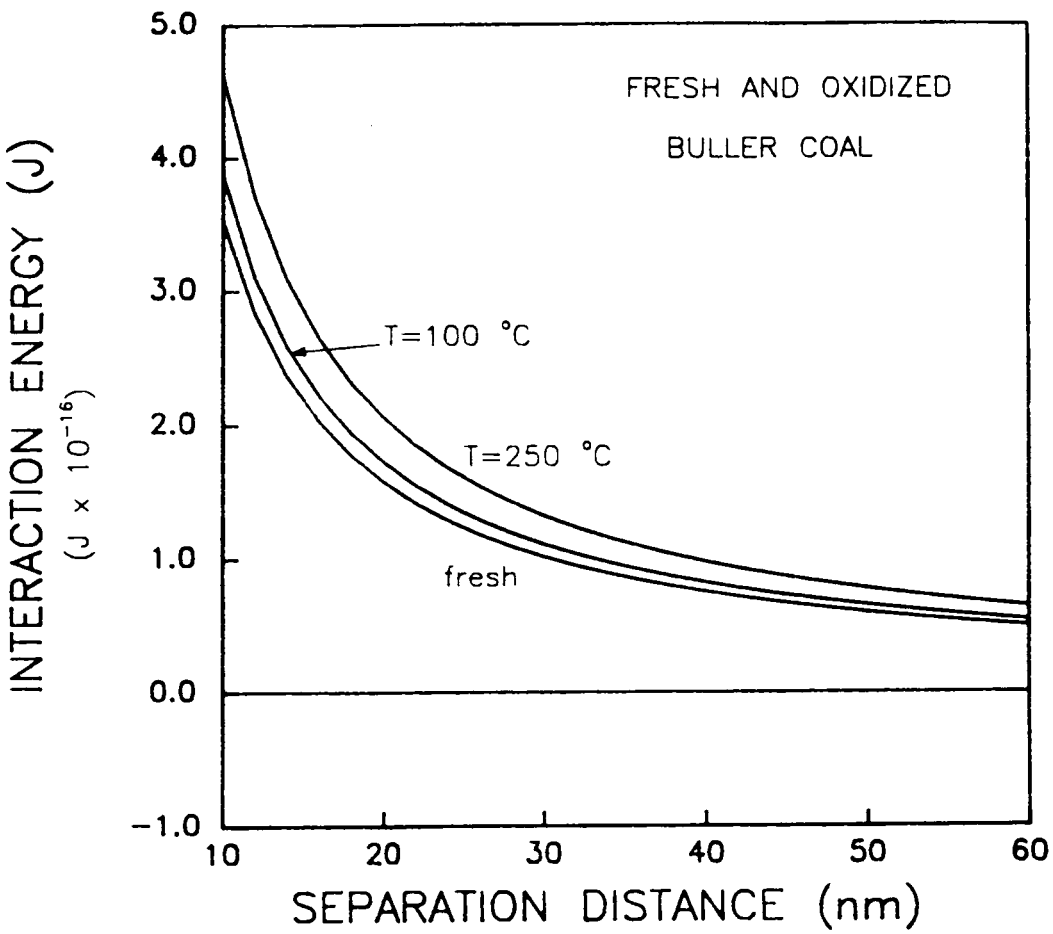

Figure 5.7 Isotherms of dispersion component (V_D) of bubble-particle interaction energy for fresh and oxidized Buller coal

Table 5.2. The results obtained are illustrated in Figure 5.8. As can be seen, the electrostatic component is also repulsive due to the negative zeta potentials carried by the air bubbles and coal particles. The magnitude of the repulsion increases with decreasing separation distance. Note, however, that in this case oxidation plays a significant role. The magnitude of the repulsive electrostatic forces increases with increasing oxidation temperature. This is, of course, the result of the increase that takes place in the zeta potentials of the coal particles with oxidation.

Since the molecular and electrostatic components of the disjoining pressure are both repulsive, film rupture must occur under the influence of attractive structural force or hydrophobic force. Figure 5.9 shows the isotherms of attractive structural (V_S) force as a function of coal oxidation obtained using Equation [4.17] and the calculated values of C and D_o given in Table 5.3. Note that the structural force is always negative and its magnitude increases with decreasing separation distance. However, V_S decreases with increasing oxidation temperature indicating that oxidation reduces the natural hydrophobicity of the coal.

Figure 5.10 shows the isotherms of the individual components of the interaction energy along with the total (V_T) isotherm for the case of Buller coal oxidized at 100°C. One can see that the shape of the isotherm of total disjoining pressure is determined primarily by the competition between the repulsive electrostatic force and the attractive structural force. The dispersion force does not play a

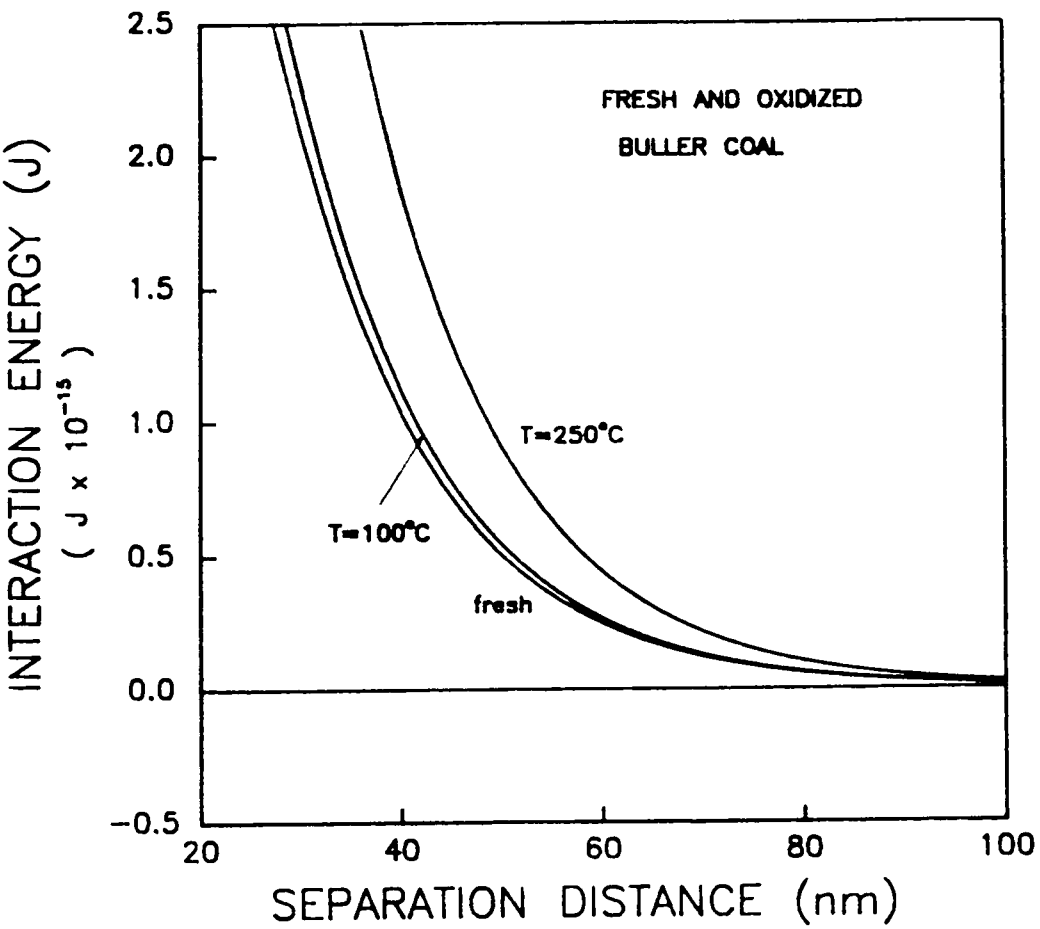

Figure 5.8 Isotherms of the electrostatic component (V_E) of bubble-particle interaction energy for fresh and oxidized Buller coal . . . . .

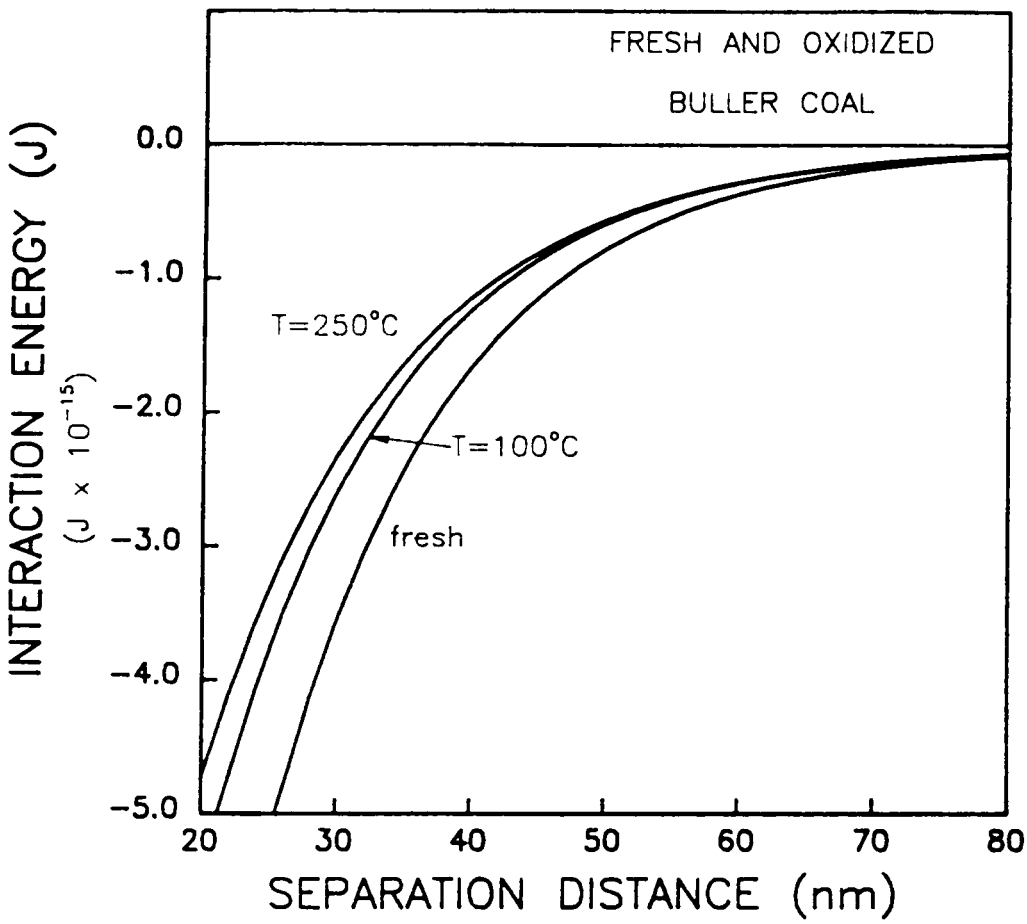

Figure 5.9 Isotherms of the structural component (V_S) of bubble-particle interaction energy for fresh and oxidized Buller coal

TABLE OF RESULTS 5.3

Calculated Values of C and D_o for Buller Coal

Treatment	C (J/m^2)	D_o (nm)
Fresh	7.52×10^{-4}	13.57
100°C	7.83×10^{-4}	13.41
250°C	1.14×10^{-3}	13.14

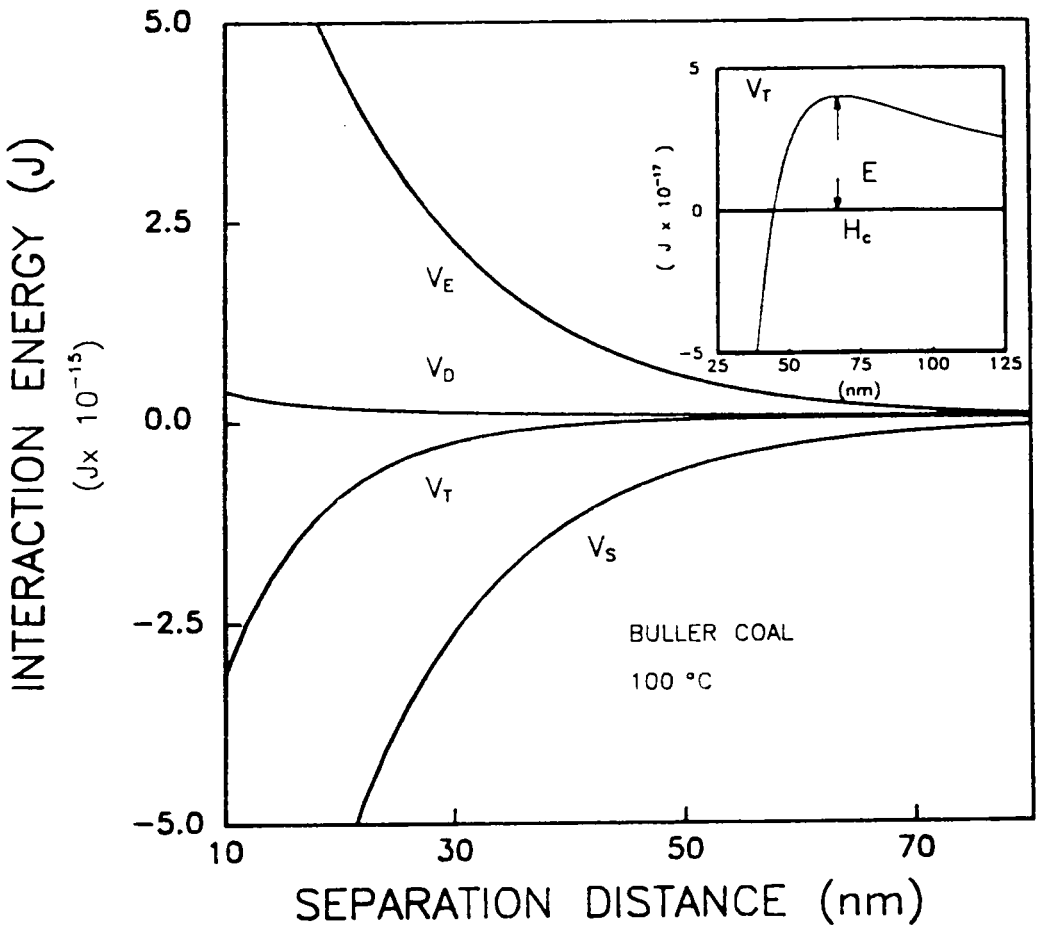

Figure 5.10 Isotherms of the dispersion (V_D), electrostatic (V_E), structural (V_S) and Total (V_T) bubble-particle interaction energies for Buller Coal oxidized at 100°C

significant role. At longer distances, the repulsive electrostatic force dominates the scene while at short ranges the attractive structural force predominates.

Figure 5.11 presents the isotherms of the total interaction energy (V_T) for fresh and the two oxidized coal samples. Note that at longer distances, i.e. h > 100 nm, all three isotherms are repulsive, however, as the separation distance decreases the interaction energy becomes attractive. Note, however, that the transition point between repulsion and attraction which occur at the critical rupture thickness (H_c) varies from one to another. For fresh coal, H_c is observed at about 80-85 nm whereas for coal oxidized at 250 °C, H_c is found at 30-35 nm. The net effect is a decrease in the probability of collection (P) which is the product of P_A and P_C (Equation [1.4]). Luttrell (1985) has shown that as H_c decreases P decreases exponentially. The end result is a reduction in the flotation recovery as previously shown (Figure 5.5). It is interesting to point out that the activation energy (E) barrier also increases with oxidation as shown in Table 5.4.

5.6.4 Microcalorimetry

a) Heat of Adsorption

Heat of adsorption measurements have been conducted in this investigation on fresh and oxidized Buller coals. According to the work of Templer (1987) and Grozsek (1988), coals immersed in non-polar solvent such as n-heptane adsorb polar compounds such as n-butanol dissolved in the solvent. The driving force for the adsorption being

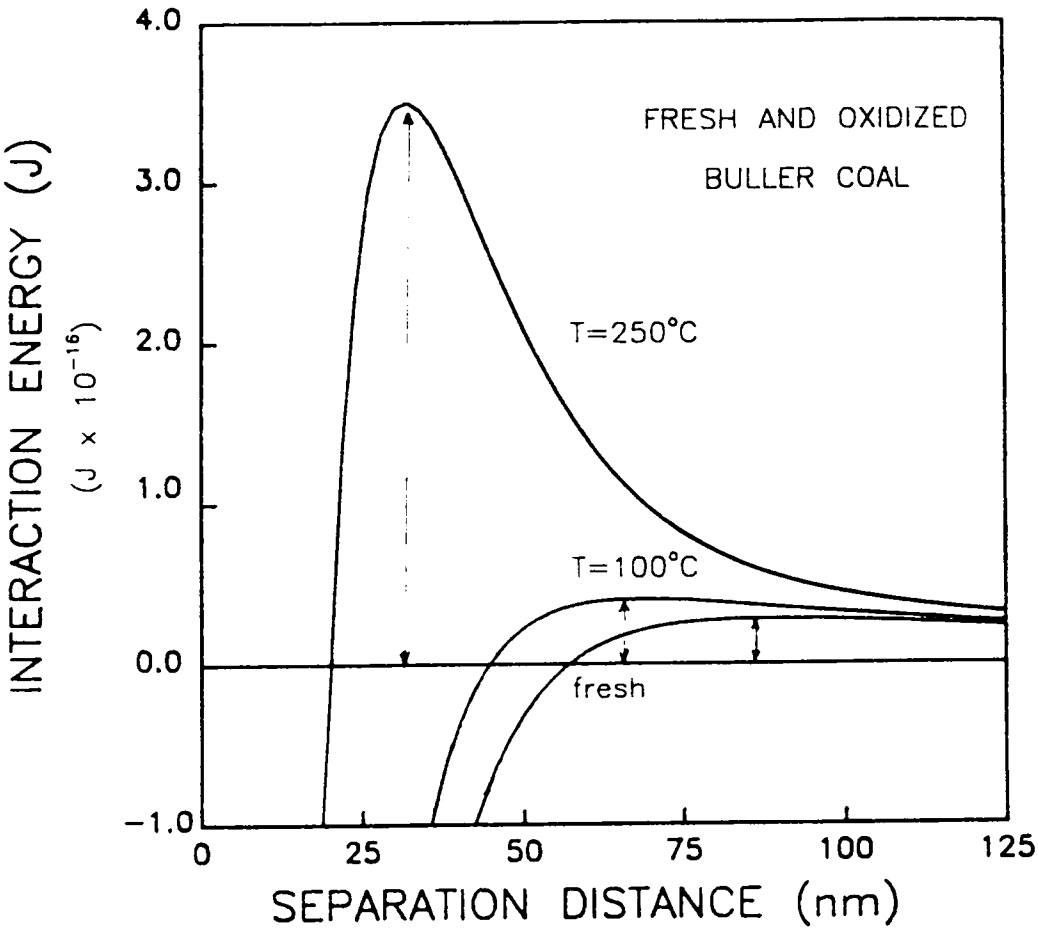

Figure 5.11 Isotherms of the total (V_T) bubble-particle interaction energy for fresh and oxidized Buller coal

TABLE OF RESULTS 5.4

Calculated Values of Activation Energy (E) for Buller Coal

Treatment	E (J)
Fresh	2.81×10^{-17}
100°C	4.11×10^{-17}
250°C	3.40×10^{-16}

the attraction of the hydrophilic OH groups in the alcohol molecules to the polar sites of the coal.

The results of the heat of adsorption measurements are presented Table 5.5. It can be seen that heating the coal powder at a temperature of 100°C does not seem to increase the heat evolution from that of fresh coal. On the contrary, heating at 250°C increases the heat of adsorption significantly indicating that the number of polar sites on the coal surface has increased. Oxidation, thus, makes the coal surface more polar. Also included in Table 5.5 are the results of microflotation experiments. As expected flotation recovery decreases as the coal surface becomes more polar.

b) Heat of Immersion

The effect of oxidation on the wetting charateristics of Buller coal were also investigated. The immersional fluids employed in these tests were water and n-heptane. As given in Table 5.6, the heat of immersion decreases slightly with increasing oxidation temperature when a non-polar wetting agent such as n-heptane is used whereas it increases significantly when the wetting agent is water. Since water is a highly polar liquid, these results indicate that the surface species formed on the surface of oxidized coal are also polar in nature. This, of course, makes the coal surface more hydrophilic. These results correlate very well with those of Phillips, et al (1986) and Melkus, et at (1987). On the other hand, the decrease observed in the heats of wetting of n-heptane with increasing oxidation

TABLE OF RESULTS 5.5

Results of the Heat of Adsorption of n-butanol and Flotation Experiments for Buller coal

Treatment	ΔH_{imm} (mJ/g)	Flotation Recovery (%)
Fresh	41.0	92
100°C	40.6	87
250°C	106.3	12

TABLE OF RESULTS 5.6

Results of the Heat of wetting of water and n-heptane experiments for Buller Coal

Treatment	ΔH_w water (J/g)	ΔH_w n-heptane (mJ/g)
Fresh	2.5	0.108
100°C	2.5	0.103
250°C	7.6	0.080

indicates that the number of hydrocarbon species on the coal surface is reduced by the oxidation process. However, at this point, it can only be speculated that the oxidation process appears to produce on the coal surface, polar species at the expense of hydrocarbon ones.

5.6.5 Infrared spectrocopy

The results of contact angle, salt flotation and microcalorimetry tests presented in the foregoing sections have shown that the hydrophobicity of Buller coal is seriously deteriorated by high temperature heating. The formation of polar groups containing oxygen functional groups may be the cause. In this section , the exact chemical nature of the surfaces of fresh and oxidized coal is determined using FTIR spectroscopy. The ATR-FTIR technique is chosen because it can record the spectra of coal surfaces rather than the bulk composition of the coal specimen.

A prerequisite for the application of FTIR to the identification of surface functional groups on the coal surface is correct band assignments. In the present work, the assignments have been based on the information available in the literature (Painter, et al, 1985; Mielczarski, et al, 1985); Table 5.7 shows the assignments.

The ATR-FTIR spectra of fresh and oxidized Buller coal as well as the difference spectrum obtained by spectral substraction are presented in Figure 5.12. For fresh coal, the broad band at 1600 cm^{-1} is attributed to the stretching vibrations of the aromatic ring. The band at 1440 cm^{-1} is due to CH_2 and CH_3 bending vibration,

TABLE 5.7

Band Assignments for the
FTIR spectra of Buller coal

Aliphatic and Aromatic groups		Oxygen-containing functional groups	
Wavenumber	Assignment	Wavenumber	Assignment
1600	Aromatic ring stretch	1690-1720	C=O, COOH, Ketone, Aldehyde
1450	CH_2 and CH_3 bend	1600	Highly conjugated hydrogen-bonded C=O
900-700	Aromatic C-H out-of-plane bending modes	1230	CO stretch and OH bend in phenols and ethers
		920	O-H deformation in carboxyl group

and indicates the presence of aliphatic groups, while that at 1030 cm^{-1} is most likely due to mineral matter in coal. Lastly, the minor bands observed at 860 and 810 cm^{-1} are designated to C-H out-of-plane bending mode of aromatic C-H.

As shown in Figure 5.12, the FTIR spectrum of oxidized coal is significantly different from that of fresh coal. Note that a group of new bands are created due to the oxidation process. The broad bands observed at 1690-1720 cm^{-1} are usually attributed to carbonyl (C=O) and carboxyl (COOH) functional groups, while that at 1230 cm^{-1} is due to C-O group vibrations in phenols and ethers compounds. The band at 920 cm^{-1} is typical of O-H deformation of the carboxylic group.

Figure 5.12 also includes the difference spectrum obtained by substration of the fresh coal spectrum from that of the oxidized coal. It is interesting to note that both positive and negative adsorption bands are observed, suggesting that while some new bands are created (positive) others (negative) are destroyed by the oxidation process.

The absorption bands created after oxidation are as follows: A broad band at 1700 cm^{-1} can be attributed to formation of carbonyl and carboxyl functional groups; a band at 1230 cm^{-1} is due to phenols and ethers and the 920 cm^{-1} band may be associated with carboxilic acid as previously discussed. On the other hand, the following absorption bands become negative after oxidation: the band at 1440 cm^{-1} which was attributed to CH_2 and CH_3 groups of the fresh coal surface and those at 860 and 800 cm^{-1} due to aromatic C-H groups. These results

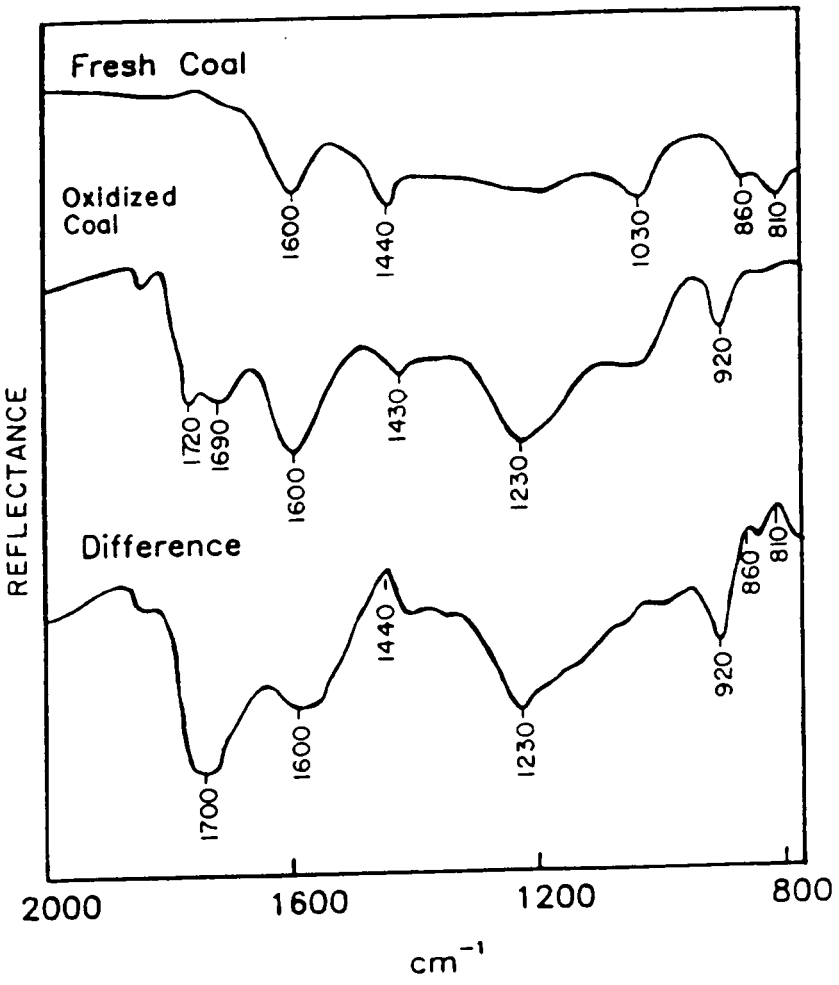

Figure 5.12 ATR-FTIR spectra of fresh and oxidized Buller coal

indicate that due to oxidation the coal surface gains hydrophilic polar groups (carbonyl, carboxylic and phenolic) at the expense of hydrophobic ones (aliphatic and aromatic).

5.7 Summary and Conclusions

1.- Values of the critical rupture thickness (H_c) for fresh and oxidized coal have been estimated from contact angle measurements. It has been shown that H_c is maximum for fresh coal and decreases as the coal surface suffers oxidation. The effect of oxidation on the adhesion process has been investigated by salt flotation experiments. The flotability of Buller coal decreases with decreasing H_c.

2.- Thermodynamic calculations indicate that hydrophobic forces are responsible for the rupture of the disjoining film between coal particles and air bubbles. This attractive force (hydrophobic interaction) is maximum for fresh coal and is reduced by the oxidation process. The decrease in the attractive force results in a reduction in the flotation response of the coal.

3.- Using different analytical tools such as electrophoresis, microcalorimetry and infrared spectroscopy, it has been shown that oxygen functional groups are created on the surface of coal as a result of the oxidation process. These are mainly carbonyl, carboxylic and phenolic groups, and make the coal surface more hydrophilic mainly because of their ability to interact favourably with polar water molecules.

CHAPTER 6

SUMMARY

The major findings of this work and its contribution to the understanding of the bubble-particle adhesion process may be summarized as follows:

1. The critical rupture thickness (H_c) of thin films on hydrophobic silica and mica plates have been measured using an optical interferometry technique. The results obtained show that H_c increases with increasing hydrophobicity of the mineral surface indicating that H_c can be a measure of the hydrophobicity of the particles to be floated. The technique employed in the present work for the H_c measurements is different from that of others investigators in that the optical images are processed in-situ by means of an image processing system rather than by photographic means. This increases the speed of data acquisition and reduces the errors involved in the measurements.

2. It has been clear from the results of the H_c measurements that the behavior of thin films is controlled by interfacial surface forces. Thin films existing on untreated mineral surfaces have been observed to be always stable and do not rupture at any thickness. The stability of such films appears to be due to repulsive surface forces. On the other hand, wetting films on hydrophobic mineral surfaces rupture as the thickness is reduced

to the critical thickness (H_c). In this case, rupture occurs due to attractive surface forces.

3. Using the principles of surface chemistry, it has been found that H_c varies inversely with the work of adhesion (W_A); an empirical relationship between H_c and W_A has been established that can be used to estimate values of H_c of minerals for which direct H_c is not possible.

4. Thermodynamic calculations based on the disjoining pressure concept have been carried out to study the forces involved in the adhesion of methylated silica, silica-DAH and coal to bubbles. The total interaction energy (V_T) and its individual components, i.e. dispersion (V_D), electrostatic (V_E) and structural (V_S) have been obtained. These calculations are more comprehensive than earlier ones of this kind in that the structural component of the interaction energy has been included, whereas only the dispersion and electrostatic components were considered until now. The results obtained show that while thin films on hydrophobic methylated silica and coal rupture under attractive structural force (hydrophobic interaction), those on silica and mica surfaces hydrophobized with DAH rupture under attractive electrostatic force arising from the interaction between bubbles and mineral surfaces bearing opposite charges.

5. The thermodynamic calculations conducted in this work allow one to elucidate the role played by collectors and other surface

treatments in the adhesion process. It has been found that as a result of collector adsorption at the solid/liquid interface the activation energy barrier (E) to be overcome prior to bubble-particle adhesion is significantly reduced. On the contrary, in the case of coal, it has been shown that E increases with increasing degree of surface oxidation. The incorporation of polar groups on the oxidized coal surface which interact favorably with water is responsible for this phenomenon.

6. Microcalorimetry and FT-Infrared spectroscopy techniques, which until now have not been used extensively in coal flotation studies, have been shown to be very valuable tools in the study of the surface chemistry of fresh and oxidized coal. The results of the calorimetry study indicate that coal becomes increasingly more polar with increasing degree of oxidation. The FTIR, on the other hand, showed that these polar groups are mainly carbonyl, carboxilic and phenolic functional groups.

CHAPTER 7

RECOMMENDATIONS FOR FUTURE RESEARCH

On the basis of the research that has been conducted during this investigation, the following areas for future research are suggested:

1. A study should be carried out to delineate the effect of bubble size on H_c. This can be achieved by simply conducting measurements similar to the ones done in this work but using air bubbles of different sizes.

2. Further experiments should be conducted to measure H_c on other mineral systems that due to their optical properties are not suitable for interferometry measurements. Perhaps, ellipsometry can provide an alternative.

3. A study should be carried out using mineral particles to confirm the relationship that has been to found exist between the critical rupture thickness (H_c) and the work of adhesion (W_A). Possible experiments on particles would include:
   i) measuring the contact angle of particles using the technique outlined by Crawford and Ralston (1988)
   ii) estimating H_c from the contact angle measurements using the empirical relationship obtained in this work
   iii) conducting probability of collection experiments using the cell employed by Luttrell (1985)
   iv) comparing the experimental results to the theoretical results

that can be obtained from Luttrell's hydrodynamic model.

4. An effort should be made to incorporate the interfacial surface forces calculated in this work into the hydrodynamic model of Luttrell (1985). This would produce a more realistic hydrochemical model.

5. Experiments should be designed to experimentally determine the parameter C and D_o of the structural force. A modification to the surface forces apparatus is a possible alternative.

6. A series of tests should be conducted to measure the activation energy (E). These experiments should include induction time and microflotation conducted as a function of temperature.

7. Although it was not examined in any detail during this study, how oxidation of coal evolves over time is a very important aspect that needs further research. This can be studied on a polished coal surface by measuring the contact angle as coal is oxidized for varying length of time. In addition, the polished surface can be analyzed for oxidation products using the FTIR-IRAS technique recently employed by Mielczarski, et al (1988). This should provide not only information on the kinetics of oxidation but also on the chemical nature of the oxidation products.

REFERENCES

Al Taweel, A. M., Delory, B., Stefanski, M., Andersen, N., Hamza, H. A. 1986, "Influence of the Surface Characteristics of Coal on its flotability," Colloids and Surfaces, 18:9-18.

Alty, T., 1924. "The cataphoresis of Gas Bubbles in Water," Royal Soc. Proc., A106:315.

Ananthpadmanabhan, K., Somasundaran, P. and Healy, T. W., 1980. "The Chemistry of Oleate and Amine Solutions in Relation to Flotation," Trans. AIME, 266:2003.

Anfruns, J. F. and Kitchener, J. A., 1977. "Rate of Capture of Small Particles in Flotation," Trans. IMM 86, C9-C15.

Aronson, M. P. and Princen, H. M., 1978. "Aqueous Films on Silica in the Presence of Cationic Surfactants," Colloid Polymer Sci. 256, 140:149.

Bagnall, R. D., and Green, G.F., 1979 "Some Observations on Octane Contact Angles in Aqueous Media," J. Colloid & Interface Sci. 68, 387.

Bilinski, B. and Wojcik, W., 1987. "A Gas-Adsorption Study of the Influence of a Flotation Collector on the Polar/Nonpolar Surface Properties of Barite.," Colloids and Surfaces 25, 183:194.

Blake, T. D., 1975. "Investigation of Equilibrium Wetting Films of n-Alkanes on Alumina," J. Chem. Soc., Faraday Trans I, 71, 192:208.

Blake, T. D. and Kitchener, J. A., 1972. "Stability of Aqueous Films on Hydrophobic Methylated Silica," J. Chem. Soc., Faraday Trans I 68, 1435:1442.

Blake, P. and Ralston, J., 1985. "Controlled Methylation of Quartz Particles," Colloids and Surfaces. 15, 101:118.

Ball, B. and Fuerstenau, D.W., 1971. "Thermodynamics and Adsorption Behaviour in the Quartz/Aqueous Surfactant System," Disc. Faraday Soc. Vol. 52, pp. 361-371.

Campbell, J. A. L. and Sun, S. C., 1970. "Bituminous Electrokinetics" Trans. AIME 247:111.

Celick, M. S. and Somasundaran, P., 1980. "Effect of Pretreatment on Flotation and Electrokinetic Properties of Coal," Colloids and Surfaces, 1, 121:124.

Chander, S. and Fuerstenau, D. W., 1972. "On the Natural Floatability of Molybdenite," Trans. AIME 252:62.

Choi, W. Z., 1986. "Combined Size Reduction and Liberation Model of Grinding," Ph. D. Dissertation, Virginia Polytechnic Institute and State University.

Churaev, N. V. and Derjaguin, B. V., 1985. "Inclusion of Structural Forces in the Theory of Stability of Colloids and Films, " J. Colloid & Interface Sci. Vol. 103, pp. 542-553.

Chibowski, E. and Holysz, L., 1986. "Correlation of Surface Free Energy Changes and Flotability of Quartz," J. Colloid & Interface Sci. 112, 15:23.

Collins, G. L., Motarjemi, M. and Jameson, G. L., 1978. "A Method for Measuring The Charge on Small Gas Bubbles," J. Colloid & Interface Sci. 63(1):69-75.

Claesson, P. M., 1987. "Experimental Evidence for Repulsive and Attractive Forces not Accounted For by Conventional DLVO Theory," Progr Colloid & Polymer Sci. Vol 74, pp. 48-54.

Crawford, R. and Ralston, J., 1988. "The Influence of Particle Size and Contact Angle in Mineral Flotation," Int. J. Miner. Process. 23,1:24.

deBruin, P. L., 1955, "Flotation of Quartz by Cationic Collectors," Trans. AIME, 202:291-296.

Derjaguin, B. V. and Landau, 1941, "Theory of the Stability of Strongly Charged Lyophobic Sols and of the Adhesion of Strongly Charged Particles in Solutions of Electrolytes," Acta Physicochim. U.R.S.S., 14, 633-622.

Derjaguin, B. V., 1987. "Surfaces Forces," Consultants Bureau, New York.

Derjaguin, B. V. and Dukhin, S.S., 1961. "Theory of Flotation of Small and Medium Size Particles," Trans. IMM, Vol. 70, p. 221.

Derjaguin, B. V. and Kussakov, M., 1939. "Anomalous Properties of Thin Polymolecular Films," Acta Physicochimica U.R.S.S., 10(1):26-44.

Derjaguin, B. V. and Shukakidse, N. D., 1961. "Dependence of the Floatability of Antimonite on the Value of the Zeta-Potential," Trans. IMM, vol. 70, pp.569-600.

Dobby, G. S. and Finch, J. A., 1986. "A Model of Particle Sliding Time for Flotation Size Bubbles," J. Colloid & Interface Sci., 109(2), 493.

Evans, L. F. and Ewers, W. E., 1953. "The Process of Bubble-Mineral Attachment," in Proc. 1st International Mineral Processing Congress", London, IMM. pp.457-464.

Finch, J. A., and Smith, G. W., 1973. "Dynamic Surface Tension of Alkaline Dodecylamine Solutions," J. Colloid & Interface Science 45:81-91.

Finch, J. A., and Smith, G. W., 1979. "Contact Angle and Wetting," Miner. Sci. Eng., 11(1),36-63.

Fowkes, F., 1964. "Attractive Forces at Interfaces," Ind. Eng. Chem., 56(12), 40:52.

Fuerstenau, D. W., 1957. "Correlation of Contact Angles, Adsorption Density, Zeta Potentials and Flotation Rate," Trans. AIME, 208:1365.

Fuerstenau, D. W., Diao, J., and Hanson, J. S., 1988. "Characterization of Coal Particle Surfaces by Film Flotation," in the proceedings of the Symposium on Surface Chemistry of Coal at the 196th. ACS National Meeting, LA, Sept. Division of Fuel Chemistry, Vol 33, No.4, pp.748-755.

Fuerstenau, D. W., Rosenbaum, J. M. and Laskowski, J. 1983 "Effect of Surface Functional Groups on the Flotation of Coal," Colloids and Surfaces, 8:153-174.

Fuerstenau, D. W., Yang, G. C. C. and Laskowski, J. S., 1987 "Oxidation Phenomena in Coal Flotation, Part 1. Correlation Between Oxygen Functional Group Concentration, Immersion Wettability and Salt Flotation Response," Coal Preparation, Vol. 4, pp. 161-182.

Groszek, A. J. and Templer, C. E., 1987 "Flow adsorption calorimetry of coals before and after heat and oxidation treatment," Microscal Ltd., Publication 87-3, London, U.K.

Groszek, A. J., 1987 "Graphitic and Polar Surface Sites in Carbonaceous Solids," Carbon, No. 6, pp. 717-722.

Groszek, A.J., 1988 "Characterisation of Microporous Carbons by Flow Microcalorimetry," Microscal Ltd., Publication 88-4, London, U.K.

Gutierrez-Rodriguez, J. A., Purcell Jr, R.J. and Aplan, F. F., 1984 "Estimating the Hydrophobicity of Coal," Colloids and Surfaces 12:1-25.

Gutierrez-Rodriguez, J. A., Aplan, F. F., 1984 "The Effect of Oxygen on the Hydrophobicity and Floatability of Coal," Colloids and Surfaces, 12:25-51.

Hamaker, H. C., 1937. "The London-van der Walls Attraction Between Spherical Particles," Physica (Utrecht), 4,10, pp-1058-1072.

Hogg, R., Healy, T. W. and Fuerstenau, D. W., 1966. "Mutual Coagulation of Colloidal Dispersions," Trans. Faraday Society, Vol. 62, pp 1638:1651.

Israelachvili, J. N. and Adams, G. E., 1978. "Measurement of Forces Between Two Mica Surfaces in Aqueous Electrolyte Solutions in the Range 0-100 nm.,", J. Chem. Soc. Faraday Trans. 1, 74, p.975.

Israelachvili, J. N. and Pashley, R., 1982. "The Hydrophobic Interaction is Long Range, Decaying Exponentially with Distance", Nature, Vol. 300, 341:342.

Israelachvili, J. N., 1985, "Intermolecular and Surface Forces", Academic Press, London.

Gaudin, A. M. and Fuerstenau, D. W., 1955, "Streaming Potential studies, Quartz Flotation with Anionic Collectors," Trans. AIME 202, 66-72.

Glembotsky, V. A., 1953. "The Time of Attachment of Bubbles to Solid Particles in Flotation and its Measurement," Izv. Akad. Nauk USSR Otdel. Tekhn. Nauk, pp.1524-1531.

Jin, R., Ye, Y., Miller, J. D. and Hu, J. S., 1987. "Characterization of Coal Hydrophobicity by Contact Angle, Bubble Attachment Time, and FTIR Spectroscopy," Presented at the 116th AIME Annual Meeting, Denver, Colorado

Kitchener, J. A., 1984. "The Froth Flotation Process:Past,Present and Future-In Brief," in The Scientific Basis of Flotation, K.Ives (Editor), NATO ASI Series, Series E: Applied Sciences. No. 75, p.3.

Klassen, V. I. and Mokrousov, V. A., 1963. An Introduction to the Theory of Flotation. Butterworths, London.

Laskowski, J., 1966. "Flotation of Inherently Hydrophobic Minerals in Solutions with a Raised Concentration of Inorganic Salts", Transactions of Silesian Univ. of Technology, No. 16, Gliwice,

Laskowski, J., 1974. "Particle-Bubble Attachment in Flotation," Miner. Sci. Eng., 6(4):223.

Laskowski, J., 1986. "The Relationship Between floatability and Hydrophobicity," in Advances in Mineral Processing, P. Somasundaran (Editor), SME Publication, Chapter 11.

Laskowski, J. and Iskra, J., 1970. "Role of Capillary Effects in Bubble-Particle Collision in Flotation," Trans. IMM, C6.

Laskowski, J. and Kitchener, J. A., 1969. "The Hydrophilic-Hydrophobic Transition on Silica," J. Colloid & Interface Sci., 29(1):670.

Laskowski, J., Vurdela, R. M. and Lui, Q., 1988. "The Colloid Chemistry of Weak-Electrolyte Collector Flotation," in 16th. International Mineral Processing Congress, Stokholm, Sweden.

Laskowski, J., Yordan, J. L. and Yoon, R. H., 1988. "The Electrokinetic Potential of Micfobubbles Generated in Aqueous Solutions of Weak-Electrolyte Type Surfactants," Submitted to Lagmuir.

Luttrell, G. H., 1986. "Hydrodynamic Studies and Mathematical Modeling of Fine Coal Flotation," Ph. D. Dissertation, Virginia Polytechnic Institute and State University.

Mahanty, J. and Ninham, B. W., 1976. "Dispersion Forces," Academic Press, New York.

McShea, J. A. and Callaghan, I. C., 1983. "Electrokinetic Potentials at The Gas-Aqueous Interface by Spinning Cylinder Electrophoresis," Colloid & Polymer Sci., 261:757-766.

McTaggart, M. A., 1922. "On the Electrification at the Boundary between a Liquid and a Gas," Phil. Mag., 44:386

Melkus, T.G., Chiang, S. H. and Wen, W. W., 1987. "An Experimental Study of Heat of Immersion of Coal," Colloids and Surfaces 28:109-121

Miller, J. D., Laskowski, J. S. and Chang, S. S. 1983 "Dextrin Adsorption by oxidized coal," Colloids and Surfaces 8:137-151.

Mielczarski, J. A., Denca, A. and Strojek, J. W., 1986. "Application of Attenuated Total Reflection Infrared Spectroscopy to the Characterization of Coal," Appl. Spectroscopy., Vol 40, 7:998.

Painter, P. C., Starsinic, M., Coleman, M., 1985. "Determination of Functional Groups in Coal by Fourier Transform Interferometry," in Fourier Transform Infrared Spectroscopy, Applications to Chemical Systems, Volume 4. Ferraro, J.R. and Basile, L.J., Eds. Academic Press, N.Y.

Pashley, R. M., 1981. "Hydration Forces between Mica Surfaces in Aqueous Electrolyte Solutions," J. Colloid & Interface Sci., 80(1):153-162.

Pashley, R. M. and Israelachvili, J. N., 1981. "A Comparison of Surface Forces and Interfacial Properties of Mica in Purified Surfactant Solutions," Colloids and Surfaces, 2:169-187.

Pashley, R. M. and Israelachvili, J. N., 1984. "Molecular Layering of Water in Thin Films between Mica Surfaces and Its Relation to Hydration Forces," J. Colloid & Interface Sci., 101(2):511-523.

Pashley, R. M. and Kitchener, J. A., 1979. "Surface Forces in Adsorbed Multilayer of Water on Quartz," J. Colloid & Interface Sci., 71(3):491-500.

Partridge, A. C. and Smith, G. W., 1971. "Small-Sample Flotation Testing," Trans. IMM, Vol.80, C199.

Phillips, K. M., Glanville, J. O. and Wightman, J. P., 1986. "Heat of Immersion of Virginia-C Coal in Water as a Function of Surface Oxidation," Colloids and Surfaces, 21:1-8.

Rabinovich, Ya. I., Derjaguin, B. V., 1988 "Interaction of Hydrophobized Filaments in Aqueous Electrolyte Solutions," Colloids and Surfaces, 30:243-251.

Rao, S. R., 1974. "Surface Forces in Flotation," Miner. Sci. Eng, 6(1):45.

Read, A. D. and Kitchener, J. A., 1969. "Wetting Film on Silica," J. Colloid & Interface Sci., 30(3),391.

Scales, P. J., Healy, T. W. and Evans, D. F., 1988. "The Zeta Potential of Muscovite Mica: Counterion Complexation by a Macrocyclic Ligand," J. Colloid & Interface Sci, Vol. 124(2), pp.391-395.

Schulze, H. J., 1984. Physico-chemical Elementary Processes in Flotation, p.100, Elsevier, New York.

Smith, R. W., 1963. "Coadsorption of Dodecylamine Ion and Molecule on Quartz," Trans. AIME 229:427.

Somasundaran, P., 1976. "The Role of Ionomolecular Surfactant Complexes in Flotation," Int. J. Mineral Processing, Vol. 3, pp.35-40.

Sutherland, K. L., 1948. "Kinetics of the Flotation Process," J. Phys. Chem., Vol. 52, p. 394.

Sun, S. C., 1954. "Effect of oxidation of Coals on their Flotation Properties," Trans. AIME, vol. 6, no. 4, p.427.

Sven-Nillson, I., 1934. "Effect of Contact Time Between Mineral and Air Bubbles on Flotation," Kolloid Z., 69:230.

Tamai, Y., Makuuchi, K, and Suzuki, M., 1967. "Experimental Analysis of Interfacial Forces at the Plane Surface of Solids," J. Phys. Chem., 71, 13, 4176:4179.

Verwey, E. J. W. and Overbeek, J. Th. G., 1948. "Theory of Stability of Lyophobic Colloids," Elsevier, Amsterdam.

Visser, J., 1972. "On Hamaker Constants, Comparison between Hamaker Constant and Lifshitz-Vander Walls Constant,", in Advances in Colloid and Interface Science, Vol. 3, 331-363.

Wakamatsu, T and Fuerstenau, D. W., 1973. "Effect of Alkyl Sulfonates on the Wettability of Alumina, " Trans. AIME, Vol. 254, 123-126.

Wark, I. W. and Cox, A. B., 1934. "Principles of Flotation I. An Experimental Study of the Effect of Xanthates on the Contact Angles at Mineral Surfaces:, Trans. AIME, 112:189-244.

Wen, W. W. and Sun, S. C., 1977 " An Electrokinetic Study on the Amine Flotation of Oxidized Coal," Trans. AIME, 262, 174.

Xu, Z. and Yoon, R. H., 1989 " The Role of Hydrophobic Interaction in Coagulation," J. Colloid & Interface Sci., in press.

Yoon, R. H, 1988 "Advanced Mineral Processing", classnotes.

Yoon, R. H., Adel, G. T. and Luttrell, G. H., 1987 "Development of the Microbubble Column Flotation Process," in Processing and Utilization of High Sulfur Coals II, Chugh, Y. P. and Caudle, R. D. editors, Elsevier Science Publishers, Amsterdam, pp. 533-543.

Yoon, R. H. and Luttrell, G. H., 1988. The Effect of Bubble Size on Fine Particle Flotation," in press.

Yoon, R. H. and Yordan, J. L., 1986. "Zeta Potential Measurements on Microbubbles Generated Using Various Surfactants," J. Colloid & Interface Science., 113(2):430-438.

Yordan, J. L. and Yoon, R. H., 1986. "Induction Time Measurements for the Quartz-Amine Flotation System," presented at the 115th. Annual Meeting of the AIME, New Orleans, Louisiana.

Yordan, J. L. and Yoon, R. H., 1988. "Induction Time Measurements for a Coal Flotation System," in Interfacial Phenomena in Biotechnology and Materials Processing, Attia, Y.A., Moudgil, B.M. and Chander, S. Editors, Elsevier Science Publishers, Amsterdam, pp. 333-343.

Zisman, A., 1964. "Relation of Equilibrium Contact Angle to Liquid and Solid Constitution," in Contact Angle, Wettability and Adhesion, Gould, R. F., Ed., Advances in Chemistry Series No. 43 American Chemical Society, Washington, D.C., pp 1-51.

APPENDIX I

OPERATING MANUAL AND COMPUTER PROGRAMS FOR BUBBLE-PARTICLE INTERACTION ENERGY CALCULATIONS

Operating Manual and Computer Programs for Bubble-Particle Interaction Energy Calculations

This section describes the use of a series of computer programs developed for the estimation of the parameters C, Do, E and the isotherms of V_E, V_D, V_S and V_T. The programs which have been written in compiled basic are the following:

a) DLVO1 : This programs allows the estimation of the minimum value of E that makes $dV_T^2/dH^2 < 0$.

b) DLVO2 : This program allows the estimation of C and Do using the value of E obtained from DLVO1.

c) DLVO3 : This program allows the evaluation of the isotherms of of V_E, V_D, V_S and V_T using the output from DLVO2.

The procedure for running the compiled version of the programs is outlined in the following sections:

1. Insert program disk containing the compiled version of the programs into drive A.
2. Turn the computer power switch to the ON position.
3. After the system prompt, type DLVO1 and press return
4. The input data required by the program is entered as prompted by the program. This data will include:
   a) CRITICAL RUPTURE THICKNESS (H_c)- Input the value of H_c for the solid investigated in units of meters.
   b) HAMAKER CONSTANT (A_{123})- Input the complex Hamaker constant for the flotation system investigated in units of Joules.
   c) ELECTROLYTE CONCENTRATION - Input the electrolyte concnetration

in aquoeus solution in units of moles/l.

d) BUBBLE SIZE - Input the size of bubbles used in the experiment in units of meters.

e) ZETA POTENTIALS OF BUBBLE AND PARTICLES - Input the zeta potentials of the bubbles and the particles in units of volts.

f) RANGE OF ACTIVATION ENERGY TO BE CALCULATED - Input the minimum, maximum values of E and the step that you wish to investigate. Values of 1, 100 and 1 are recomended as initial guess.

6) After all the data have been entered, press return and the output will be sent to the screen. A printed copy of the output can be obtained by simultaneously depressing SHIFT and PRTSC.]

6. Examine the output and find the minimum value of E that makes the second derivative of $V_T < 0$. That is the value of E at the point where dvtt changes from positive to negative.

7. Return to the operating system by simultaneously depressing CTRL ALT and DEL.

8. After the system prompt type DLVO2 and press return. This new program will allow you to obtain the values of C, Do and E

9. Input the data required as prompted by the computer. Note that the only new data required is the value of the fraction E that you obtained from DLVO1.

10. The output of DLVO2 will display the values of C, Do and E. Annotate these values and use them as input data for DLVO3.

11. Return to the system by simultaneously pressing CTRL, ALT and DEL

12. Insert a blank, formatted data disk in drive B.
13. After the system prompt, type DLVO3 and press return. This program will allow you to obtain the isotherms of disjoining pressure.
14. Input the required data as prompted by the computer. Besides the data required in step 4, the following data must also be entered:
    a)RANGE OF SEPARATION DISTANCE (H)- Input the values of the minimum and maximum values of H and the step required. The following values are recomended : 2,200,2.
15. The output of DLVO3 is sent to a data file named DATA1.DAT in drive B. This file can be displayed on the screen by typing B:TYPE DATA1.DAT or a printed copy of the output can be obtained by typing B:COPY DATA1.DAT PRN. The output will contain 5 columns with the following distribution:
    a)column 1- separation distance (H)
    b)column 2- V_E
    c)column 3- V_D
    d)column 4- V_S
    e)column 5- V_T
16. The file DATA1.DAT can be directly read by GRAPHER, LOTUS or SUPERCALC if a plot is desired.

```
'                        PROGRAM DLVO1
'
'
'        THIS PROGRAM DETERMINES THE VALUE OF ACTIVATION ENERGY
'          FOR WHICH THE SECOND DERIVATIVE OF VT IS NEGATIVE
'
cls
locate 5,5
input"Enter the critical rupture thickness Hc in meters",hc#
print"
locate 6,5
input"Enter the complex Hamaker constant A123 in joules,"a123#
locate 7,5
'
'IN THIS PART THE PROGRAM FIND THE MINIMUM VALUE OF E THAT MAKES
'dvt2/dh2 <0.  NOTE THAT THE ACCURACY DEPENDS ON THE INTERVAL OR
'STEP THAT YOU SELECT, I SUGGEST TO START WITH Einitial = 1;
'E final = 100; AND A STEP OF 1, THEN OBSERVE IN THE OUTPUT WHEN
'THE DERIVATIVE CHANGES SIGN AND THEN SEARCH MORE CAREFULLY AROUND
'THAT VALUE BY DECREASING THE STEP.  GOOD LUCK
'
input"Enter the initial, final and step fraction E(J)",ee#,ee1#,st#
print"
locate 8,5
input"Enter electrolyte concentration in Moles/l",EC#
print"
locate 9,5
input"Enter radius of bubble (m)",rb#
print"
locate 10,5
input"Enter zeta potential of particle (volts)",zps#
print"
locate 11,5
input"Enter zeta potential of bubble (volts)",zpb#
do until ee#=ee1#
'
' THIS PART CALCULATES VE
'
b#=(3.1416*8.854e-12*78.5*rb#*(zpb#^2+zps#^2))
c#=((2*zpb#*zps#)/(zpb#^2+zps#^2))
k#=((sqr(ec#)/0.304)*1e9)
kk#=(1/k#)
d#=(log((1+exp(-k#*hc#))/(1-exp(-k#*hc#))))
dd#=(log(1-exp(-2*k#*hc#)))
ve#=b#*(c#*d#+dd#)
'
'
'
'
'
```

```
'
'THIS PART CALCULATES VD
'
vd#=-(a123#*rb#)/(6*hc#)
'
'THIS PART EVALUATES VS
e#=ee#/100*(abs(ve#)+vd#)
print"fraction=",ee#
print"E=",e#
vs#=(e#-ve#-vd#)
'
'THIS PART EVALUATES THE DERIVATIVES OF VE AND VD
'
dve#=(2*k#*b#/(1-exp(-2*k#*hc#)))*(exp(-2*k#*hc#)-(c#*exp(-k#*hc#)))
dvee#=(2*k#*b#/(1-exp(-2*k#*hcc#)))*(exp(-2*k#*hcc#)-(c#*exp(-k#*hcc#)))
dvd#=(a123#*rb#)/(6*(hc#^2))
'
'THIS PART EVALUATES THE DERIVATIVE OF VS
'
dvs#=-dve#-dvd#
'
'THIS PART EVALUATES THE CONSTANTS C1 AND D1
'
d1#=-vs#/dvs#
c1#=-vs#/(rb#*d1#*exp(-hc#/d1#))
'
'
'THIS PART EVALUATES THE SECOND DERIVATIVE OF VT TO CHECK
'ITS SIGN, IT MUST BE NEGATIVE
'
'THIS PART EVALUATES THE SECOND DERIVATIVE OF VS
dvs2#=-(c1#*rb#/d1#)*exp(-hc#/d1#)
'
'THIS PART EVALUATES THE SECOND DERIVATIVE OF VD
dvd2#=-(a123#*rb#)/(3*hc#^3)
'
'THIS PART EVALUATES THE SECOND DERIVATIVE OF VE
ddd#=(1-exp(-2*k#*hc#))^2
dve2#=(2*k#^2*b#*(c#-2*exp(-k#*hc#) - c#*exp(-2*k#*hc#)))/(ddd#)
'
'THIS PART EVALUATES DVT2
dvtt#=dve2#+dvs2#+dvd2#
ee#=ee#+st#
print"dvtt=",dvtt#
loop
end
```

```
'                              PROGRAM DLVO2
'
'
'THIS PROGRAM DETERMINES THE VALUE OF ACTIVATION ENERGY (E),C and Do
'             FOR WHICH ALL CONSTRAINS ARE SATISFIED, I.E.
'
'               a) THE SUM OF VT = E
'               b) THE DERIVATIVE OF VT= 0
'               c) THE SECOND DERIVATIVE IS NEGATIVE
'
'THIS PART READS THE INPUT DATA
'
'
cls
locate 5,5
input"Enter the critical rupture thickness Hc in meters",hc#
print"
locate 6,5
input"Enter the complex Hamaker constant A123 in joules,"a123#
locate 7,5
'
' IN THIS PART, THE VALUE OF E OBTAINED FROM DLVO1 IS ENTERED
'            THE VALUE E SHOULD BE BETWEEN 1 TO 100
'
'
input"Enter the fraction of activation energy E in joules",ee#
print"
locate 8,5
input"Enter electrolyte concentration in Moles/l",EC#
print"
locate 9,5
input"Enter radius of bubble (m)",rb#
print"
locate 10,5
input"Enter zeta potential of particle (volts)",zps#
print"
locate 11,5
input"Enter zeta potential of bubble (volts)",zpb#
'
' THIS PART CALCULATES VE
'
b#=(3.1416*8.854e-12*78.5*rb#*(zpb#^2+zps#^2))
c#=((2*zpb#*zps#)/(zpb#^2+zps#^2))
k#=((sqr(ec#)/0.304)*1e9)
kk#=(1/k#)
d#=(log((1+exp(-k#*hc#))/(1-exp(-k#*hc#))))
dd#=(log(1-exp(-2*k#*hc#)))
ve#=b#*(c#*d#+dd#)
'
'THIS PART CALCULATES VD
```

```
'
vd#=-(a123#*rb#)/(6*hc#)
'
'THIS PART EVALUATES VS
e#=(ee#/100)*(ABS(ve#)+vd#)
print"E=",e#
vs#=(e#-ve#-vd#)
'
'THIS PART EVALUATES THE DERIVATIVES OF VE AND VD
'
dve#=(2*k#*b#/(1-exp(-2*k#*hc#)))*(exp(-2*k#*hc#)-(c#*exp(-k#*hc#)))
dvee#=(2*k#*b#/(1-exp(-2*k#*hcc#)))*(exp(-2*k#*hcc#)-(c#*exp(-k#*hcc#)))
dvd#=(a123#*rb#)/(6*(hc#^2))
'
'THIS PART EVALUATES THE DERIVATIVE OF VS
'
dvs#=-dve#-dvd#
'
'THIS PART EVALUATES THE CONSTANTS C1 AND D1
'
d1#=-vs#/dvs#
print"Do=",d1#
c1#=-vs#/(rb#*d1#*exp(-hc#/d1#))
print"C=",c1#
END
```

```
'                                PROGRAM DLVO3
'
'  THIS  PROGRAM CALCULATES THE ISOTHERMS OF INDIVIDUAL COMPONENTS
'        OF THE INTERACTION ENERGY AND THE TOTAL ENERGY
'
'
open "b:DATA1.dat" for output as #3
cls
locate 3,5
input"Enter the initial, final thickness H and step in nm",h1#,h2#,h3#
print"
locate 4,5
input"Enter the complex Hamaker constant A123 in joules,"a123#
locate 5,5
input"Enter electrolyte concentration in Moles/l",EC#
print"
locate 6,5
input"Enter radius of bubble (m)",rb#
print"
locate 7,5
input"Enter zeta potential of particle (volts)",zps#
print"
locate 8,5
input"Enter zeta potential of bubble (volts)",zpb#
print"
locate 9,5
input"Enter C (J/m2) and Do in nm",c1#,d1#
'
'LOOP STARTS HERE
hc#=h1#
do until hc#=h2#
'
' THIS PART CALCULATES VE
'
b#=3.1416*8.854e-12*78.5*rb#*(zpb#^2+zps#^2)

c#=(2*zpb#*zps#)/(zpb#^2+zps#^2)
k#=(sqr(ec#)/0.304)*1e9
d#=log((1+exp(-k#*hc#*1e-9))/(1-exp(-k#*hc#*1e-9)))
dd#=log(1-exp(-2*k#*hc#*1e-9))
ve#=b#*(c#*d#+dd#)
'
'THIS PART CALCULATES VD
'
vd#=-(a123#*rb#)/(6*hc#*1e-9)
'
'THIS PART CALCULATES VS
'
vs#=-c1#*rb#*d1#*1e-9*exp(-hc#/d1#)
'
```

```
'THIS PART CALCULATES VT
'
vt#=ve#+vd#+vs#
'
'
hc#=h1#+h3#
h1#=h1#+h3#
write #3,hc#;ve#;vd#;vs#;vt#
loop
END
```

The vita has been removed from the scanned document